

## **INFORMATION TO USERS**

This reproduction was made from a copy of a manuscript sent to us for publication and microfilming. While the most advanced technology has been used to photograph and reproduce this manuscript, the quality of the reproduction is heavily dependent upon the quality of the material submitted. Pages in any manuscript may have indistinct print. In all cases the best available copy has been filmed.

The following explanation of techniques is provided to help clarify notations which may appear on this reproduction.

1. Manuscripts may not always be complete. When it is not possible to obtain missing pages, a note appears to indicate this.
2. When copyrighted materials are removed from the manuscript, a note appears to indicate this.
3. Oversize materials (maps, drawings, and charts) are photographed by sectioning the original, beginning at the upper left hand corner and continuing from left to right in equal sections with small overlaps. Each oversize page is also filmed as one exposure and is available, for an additional charge, as a standard 35mm slide or in black and white paper format.\*
4. Most photographs reproduce acceptably on positive microfilm or microfiche but lack clarity on xerographic copies made from the microfilm. For an additional charge, all photographs are available in black and white standard 35mm slide format.\*

**\*For more information about black and white slides or enlarged paper reproductions, please contact the Dissertations Customer Services Department.**

**U·M·I** Dissertation  
Information Service

University Microfilms International  
A Bell & Howell Information Company  
300 N. Zeeb Road, Ann Arbor, Michigan 48106



1328271

**Moss, Robert Michael**

STUDY OF A LOW ENERGY ANTINEUTRON SOURCE

*Rice University*

M.A. 1986

University  
Microfilms  
International 300 N. Zeeb Road, Ann Arbor, MI 48106

Copyright 1985

by

Moss, Robert Michael

All Rights Reserved



## PLEASE NOTE:

In all cases this material has been filmed in the best possible way from the available copy. Problems encountered with this document have been identified here with a check mark ☒.

1. Glossy photographs or pages \_\_\_\_\_
2. Colored illustrations, paper or print \_\_\_\_\_
3. Photographs with dark background \_\_\_\_\_
4. Illustrations are poor copy \_\_\_\_\_
5. Pages with black marks, not original copy \_\_\_\_\_
6. Print shows through as there is text on both sides of page \_\_\_\_\_
7. Indistinct, broken or small print on several pages ☒
8. Print exceeds margin requirements \_\_\_\_\_
9. Tightly bound copy with print lost in spine \_\_\_\_\_
10. Computer printout pages with indistinct print \_\_\_\_\_
11. Page(s) \_\_\_\_\_ lacking when material received, and not available from school or author.
12. Page(s) \_\_\_\_\_ seem to be missing in numbering only as text follows.
13. Two pages numbered \_\_\_\_\_. Text follows.
14. Curling and wrinkled pages \_\_\_\_\_
15. Dissertation contains pages with print at a slant, filmed as received \_\_\_\_\_
16. Other \_\_\_\_\_  
\_\_\_\_\_  
\_\_\_\_\_

University  
Microfilms  
International



RICE UNIVERSITY

STUDY OF A LOW ENERGY  
ANTINEUTRON SOURCE

by


ROBERT MICHAEL MOSS

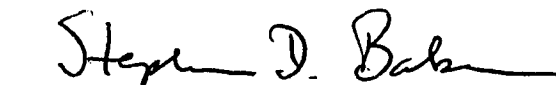
A THESIS SUBMITTED  
IN PARTIAL FULFILLMENT OF THE  
REQUIREMENTS FOR THE DEGREE

MASTER OF ARTS

APPROVED, THESIS COMMITTEE:

  
Gordon S. Mutchler, Professor  
of Physics, Chairman

  
Gerald C. Phillips, Professor  
of Physics and Director of  
Bonner Nuclear Lab

  
Stephen D. Baker, Professor  
of Physics

Houston, Texas

August 1985

Copyright  
Robert Michael Moss  
1985

## ABSTRACT

### Study of a Low Energy

### Antineutron Source

by

Robert Michael Moss

The low energy antineutron source used during E767 at BNL is studied in detail. The active source volume consisted of a stack of 20 thin scintillators. Antineutrons were produced via charge-exchange of the incident antiprotons. The source volume was surrounded by a lead-scintillator vetobox. Events with zero or one counter hit in the vetobox were considered possible charge-exchanges. The apparatus is studied by comparing a Monte-Carlo simulation with data taken from an unbiased  $\bar{p}$  trigger.

The apparatus is found to be insensitive to many details of the expected interactions, and the Monte-Carlo assumptions are sufficient to understand the source operation and output. At 515 MeV/c about ¼% of the total number of events produce useful antineutrons. The vetobox has over 99% efficiency for vetoing annihilations. The results suggest using a segmented liquid hydrogen target with an improved trigger to both increase  $\bar{n}$  flux and increase data taking efficiency.

## ACKNOWLEDGEMENTS

This study is part of an experiment made possible through the cooperation and dedication of many people. Each member of the E-767 collaboration has played an essential role in making the experiment happen. It is not possible to single out any one person's efforts in particular, because without each individual part the experiment as a whole would not have existed. I would like to thank each member of the collaboration for a very successful learning experience.

Of course, my participation in this particular experiment is due to my thesis advisor, Dr. Mutchler. Dr. Mutchler gave me complete freedom to work as I pleased, and always came through in a calm manner when problems arose. I consider this an excellent position to be in, and I am glad for the opportunity. I would also like to thank the other members of my committee, Dr. Phillips and Dr. Baker, for their support and encouragement.

Special thanks go to Mary Comerford for typing the draft for the oral examination and to Anita Poley for typing the final draft of this thesis.

I would sincerely like to thank my family for their loving support throughout this entire project. In particular I would like to thank my mother and father for being

the two people ultimately responsible for giving me the opportunities I have today.

Finally, and most importantly, I would like to thank my loving wife, Ann, for making my life as happy as it could possibly be.

## TABLE OF CONTENTS

	Page
Abstract . . . . .	ii
Acknowledgments . . . . .	iii
List of Figures . . . . .	vii
List of Tables . . . . .	ix
I. Introduction . . . . .	1
II. E-767 Experimental Setup . . . . .	10
III. Antineutron Source . . . . .	17
A. Antineutron Source Apparatus . . . . .	17
B. Interactions Expected . . . . .	21
C. Trigger Logic . . . . .	26
IV. Data Analysis . . . . .	33
V. Monte-Carlo Analysis . . . . .	47
A. Cross Sections . . . . .	47
B. Annihilation Multiplicities . . . . .	57
C. Monte-Carlo Flow Chart . . . . .	60
D. Energy Loss . . . . .	74
VI. Comparison of Data and Monte-Carlo Results . . . . .	77
A. Antiproton Momenta . . . . .	77
B. Annihilation Point . . . . .	78
C. Charge-Exchange Point . . . . .	86
D. Event Classification . . . . .	105
E. Annihilation Multiplicities . . . . .	111
F. Efficiency of Antineutron Source . . . . .	118

VII. Conclusions . . . . .	122
Appendix I. Monte-Carlo Annihilation Branching	
Ratios . . . . .	127
Bibliography . . . . .	135

## LIST OF FIGURES

	Page
1. E-767 Experimental Layout . . . . .	11
2. Top View of T-Counters . . . . .	19
3. Vetobox Cross Section . . . . .	20
4. Source and Vetobox . . . . .	22
5. Antiproton Trigger Logic . . . . .	28
6. Antineutron Trigger Logic . . . . .	30
7. Data Analysis Main Program Flow Chart . . . . .	35
8a-e. Source Analysis Flow Chart . . . . .	37-41
9. $\bar{p}p$ Total Cross Section . . . . .	48
10. $\bar{p}p$ Charge-Exchange Cross Section . . . . .	51
11. $\bar{p}p$ Annihilation Cross Section . . . . .	53
12. $\bar{p}p$ Elastic Scattering Cross Section . . . . .	55
13a-j. Monte-Carlo Program Flow Chart . . . . .	61-70
14. Annihilation Point 475 MeV/c . . . . .	79
15. Annihilation Point 515 MeV/c . . . . .	80
16. Annihilation Point 550 MeV/c . . . . .	81
17. Annihilation Point 578 MeV/c . . . . .	82
18. Monte-Carlo Charge-Exchange Results 475 MeV/c .	90
19. Events with No Hits in the Vetobox 475 MeV/c. .	91
20. "Possible" Charge-Exchange Events 475 MeV/c . .	92
21. Monte-Carlo Charge-Exchange Results 515 MeV/c .	95
22. Events with No Hits in the Vetobox 515 MeV/c. .	96

23.	"Possible" Charge-Exchange Events 515 MeV/c . . .	97
24.	Monte-Carlo Charge-Exchange Results 550 MeV/c . .	98
25.	Events with No Hits in the Vetobox 550 MeV/c. . .	99
26.	"Possible" Charge-Exchange Events 550 MeV/c . . .	100
27.	Monte-Carlo Charge-Exchange Results 578 MeV/c . .	102
28.	Events with No Hits in the Vetobox 578 MeV/c. . .	103
29.	"Possible" Charge-Exchange Events 578 MeV/c . . .	104
30.	Annihilation Multiplicities 475 MeV/c . . . . .	117

# LIST OF TABLES

	Page
1. Dimensions for E-767 . . . . .	23
2. Breakdown of $\bar{p}$ Events . . . . .	106
3. Classification of Data . . . . .	108
4. Classification of Monte-Carlo Events . . . . .	109
5. Annihilation Multiplicities 475 MeV/c . . . . .	112
6. Annihilation Multiplicities 515 MeV/c . . . . .	113
7. Annihilation Multiplicities 550 MeV/c . . . . .	114
8. Annihilation Multiplicities 578 MeV/c . . . . .	115
9. Percentage of Possible Charge-Exchanges that Have Only One Hit in the Vetobox . . . . .	120

## CHAPTER I

### INTRODUCTION

The antinucleon-nucleon interaction is a rich and interesting area of physics that is useful for studying the strong interaction. This system has two distinct final states: the  $\bar{N}N$  final state (elastic scattering or charge-exchange) and the multiple meson final state (annihilation). The first case can be described by the G-parity transform of the  $NN$  potential, where the intermediate and long range parts are dominated by meson exchange. On the other hand, annihilation is an additional channel not available in the  $NN$  system. Annihilation occurs if the quark "bags" overlap and the quarks rearrange to form mesons, hence it is a short range interaction. Study of the  $\bar{N}N$  interaction can, therefore, provide information on the range of  $\bar{N}N$  forces, and consequently on the confinement radius for the quark bags. Because of the additional annihilation channel, study of the  $\bar{N}N$  interaction can help distinguish between which interactions involve meson exchanges and which arise from quark-gluon interactions.

The first successful calculation of the  $\bar{N}N$  potential was made by Bryan and Phillips [BP68]. They used a G-parity

transformed One Boson Exchange (OBE) potential of Bryan and Scott [BS69] for the real part, and approximated the short range annihilation potential by a purely imaginary Woods-Saxon potential which was independent of spin, isospin, and energy:

$$-iW(r) = \frac{-iW_0}{1 + \exp(br)} .$$

By fitting  $W_0$  and  $b$  to the total and elastic cross sections at 100 MeV/c, good fits to the (poor) existing data were achieved.

The ten years following the work of Bryan and Phillips brought better data and more sophisticated NN potential models. In particular, the NN Paris potential was developed, [LA80], in which the intermediate range part, described by the  $\rho$  meson and the non-physical  $\sigma$  mesons in the OBE model, were replaced by two pion exchange. Dover and Richard [DR80] used a simplified static version of the G-parity transformed Paris potential, to which they added a phenomenological spin, isospin and energy independent annihilation potential of the Woods-Saxon form similar to that of Bryan and Phillips. However, Dover and Richard allowed an additional real part, i.e.

$$-iW_0 \rightarrow -V_0 - iW_0.$$

The addition of the real part resulted in a significant

improvement in the fit to the total cross sections, but the backward angle scattering was grossly underestimated.

There are several objections to the preceding models [GR83]. First, these models are inconsistent with narrow nuclear bound states in the  $\bar{N}N$  system (if they exist) since they produce widths on the order of hundreds of MeV. One solution to this problem could be to incorporate an explicit energy dependence. This means that an energy independent potential fitted in the scattering region cannot describe bound states possibly several hundreds of MeV below  $\bar{N}N$  threshold. Second, these phenomenological theories are inconsistent with models based on meson emission or quarks, because of the independence of the annihilation on spin and isospin.

These objectives were partly met by the  $\bar{N}N$  potential of the Paris group [C082]. Their model for the  $\bar{N}N$  optical potential used the G-parity transform of the  $NN$  Paris potential [LA80] for the long and intermediate range parts (the real part of the potential), together with a phenomenological description for the short range part. For the absorptive part of the potential (the imaginary annihilation part) they used an energy dependent general scalar operator of the form

$$W(\vec{r}, T_{\text{LAB}}) = [g_C(1+f_C T_{\text{LAB}}) + g_{SS}(1+f_{SS} T_{\text{LAB}}) \vec{\sigma}_1 \cdot \vec{\sigma}_2 \\ + g_T S_{12} + \frac{g_{LS}}{4M^2} \vec{L} \cdot \vec{S} \frac{1}{r} \frac{d}{dr}] \frac{\kappa_0(2Mr)}{r}$$

This form is suggested by detailed calculations of annihilation diagrams with two meson intermediate states.

With this Paris potential, a very good fit to current data is achieved, but at the cost of twelve parameters. The treatment of the phenomenological core region introduces more parameters, but these are probably unimportant because of the enormous annihilation potential in this region. Because of the large number of free parameters, the Paris potential must be treated as a phenomenological fit to data, rather than a form derived from a more fundamental theory. Nevertheless, this potential appears to be the best description of  $\bar{N}N$  scattering available today. It should be noted, however, that none of the above potentials has a realistic energy dependence which allows calculation of bound states far below  $\bar{N}N$  threshold, and in addition, none of these phenomenological approaches can give any help in calculating branching ratios for annihilation into specific meson channels [GR83].

The description of the annihilation process and other short range phenomena in the  $\bar{N}N$  interaction by microscopic quark models is still in its infancy. The simplest assumption at the quark level is that the three quarks and three antiquarks of the nucleon and antinucleon rearrange themselves into three  $q\bar{q}$  pairs, forming three mesons. This is the so-called quark rearrangement model [QRM]. After some early work in the sixties and seventies which was essentially discarded [GR83], Maruyama and Ueda [MU91], [MU94] have

recently used the QRM to fit the annihilation branching ratios. They did this by introducing parameters to account for the initial state interactions in the spin and isospin states, and the effective coupling of a  $q\bar{q}$  pair into a meson [GB83]. This method had reasonable success. Maruyama has also attempted an alternative approach using a junction model [MA83]. In this model the quarks of the nucleon and antinucleon are joined by "strings" to a junction and an antijunction, which may annihilate. However, Maruyama and Ueda [MU83] admit problems with the model, and prefer the previous approach. In addition to the quark rearrangement model, it has been suggested that a  $q\bar{q}$  pair can annihilate to form the two meson final states. It should be pointed out that all of the QRM theories still require a phenomenological repulsive potential at short distances, and that the spin and isospin dependencies predicted by the models often conflict with the sparse existing data. A comprehensive review of theoretical descriptions of  $\bar{N}N$  annihilation can be found in the paper by Green and Niskanen [GR83].

Experimentally, little is known of the  $\bar{N}N$  interaction between zero and  $\sim 400$  MeV/c, the momentum range in which much of what is known about the  $NN$  interaction was learned. Early experiments were limited to either higher energies or reactions at rest. In addition, these experiments were limited by poor quality  $\bar{p}$  beams, which suffered from low intensity, large momentum spread, large phase space and

severe pion contamination. Some of the earliest data on  $\bar{p}p$  elastic, charge-exchange, annihilation, and total cross sections as well as annihilation multiplicities were from bubble chamber work by Baltay [BA66] and Agnew [AG60], as well as work by Chamberlain [OC57]. Some of the most recent  $\bar{p}p$  cross sections are presented at the beginning of Chapter V.

A characteristic of the many  $\bar{N}N$  models discussed earlier is that they all predict a rich  $\bar{N}N$  spectrum, with many narrow resonances and bound states clustering near threshold. The intense interest in these theories was generated by the experimental evidence of possible narrow states near threshold, generally named baryonium. There are at least two baryonium candidates in the  $\bar{p}p$  system and perhaps one in the  $\bar{n}p$  system.

The most likely baryonium candidate is the so called S(1936) meson. In the mid-seventies, at least three different experiments [CA74], [CH76], and [BR77] reported narrow structure in the  $\bar{p}p$  total cross section near 500 MeV/c. Later experiments, however, failed to confirm the existence of the S meson [EJ81], [NA84d], [HA80b]. In 1982, Amsler et al. claimed to see structure in the S meson region [AM82]. Recent results at LEAR (the Low Energy Antiproton Ring at CERN) show no structure on the total cross section [BE84], but a different experiment does report structure in the charge annihilation cross section near the S meson region [TW84]. More evidence for baryonium is the evidence of high energy  $\gamma$  lines from a possible  $\bar{p}p$  bound state [PA78]. On the

other hand, some recent LEAR data could not find evidence of any structure with much better statistics [TW84]. Finally, there has been one report of a structure at 840 MeV in the  $\bar{p}n$  (actually the  $\bar{p}d$ ) system [KA75]. This result has never been confirmed nor denied. It is clear that even today the situation is somewhat confused.

Another interesting experimental result is the evidence against S-wave dominance in  $\bar{p}p$  annihilation at rest presented by Devons et al. [DE71]. It should be noted that this idea is not so surprising in view of some recent calculations in the quark rearrangement model [GR83].

In order to resolve the ambiguities in the experimental data and to discriminate between the different theoretical models for the  $\bar{N}N$  interaction, much more high precision data is needed with particular emphasis in low momenta near threshold (less than 400 MeV/c). It is difficult to address these questions using existing low energy antiproton beams because of the rapidly rising energy loss as the momentum goes to zero. Because of finite momentum and vertex resolution, the in-flight data becomes highly contaminated with stopping interactions. However, use of a neutral antineutron beam would eliminate all of the above energy-loss related problems, provided enough antineutrons can be produced. With the above in mind, experiment 767 was proposed at Brookhaven National Laboratory with two main purposes: (1) development

of a low energy active antineutron source and (2) measurement of the  $\bar{n}p$  annihilation cross section near  $\bar{N}N$  threshold. Note that this is a pure ( $I=1$ ) isospin channel, so that the isospin dependence of the  $\bar{N}N$  interaction can be studied directly, without the ambiguities inherent in a  $\bar{p}d$  experiment.

It is the purpose of this thesis to study the behavior and performance of the antineutron source apparatus used for experiment 767. This study requires the following: (a) acquisition of data from the apparatus with a properly unbiased trigger, (b) analysis of the data from the source apparatus, (c) Monte-Carlo analysis of the source apparatus performance, and (d) comparison of Monte-Carlo and data analysis results to determine annihilation veto efficiency and antineutron production efficiency.

In Chapter II, the layout of experiment 767 is presented, along with brief descriptions of the various apparatus involved. Description of the antineutron source is deferred to Chapter III, where the physics involved and the method of study is described. Chapter IV concerns itself with the details of the data analysis, while in Chapter V the philosophy and details of the Monte-Carlo analysis are discussed. A brief review of current data and theories relevant to the Monte-Carlo is also given. The results of the data analysis and the Monte-Carlo calculations are presented and compared

in Chapter VI. Chapter VII concludes with discussions on the effectiveness of the Monte-Carlo and the parameters of the antineutron source.

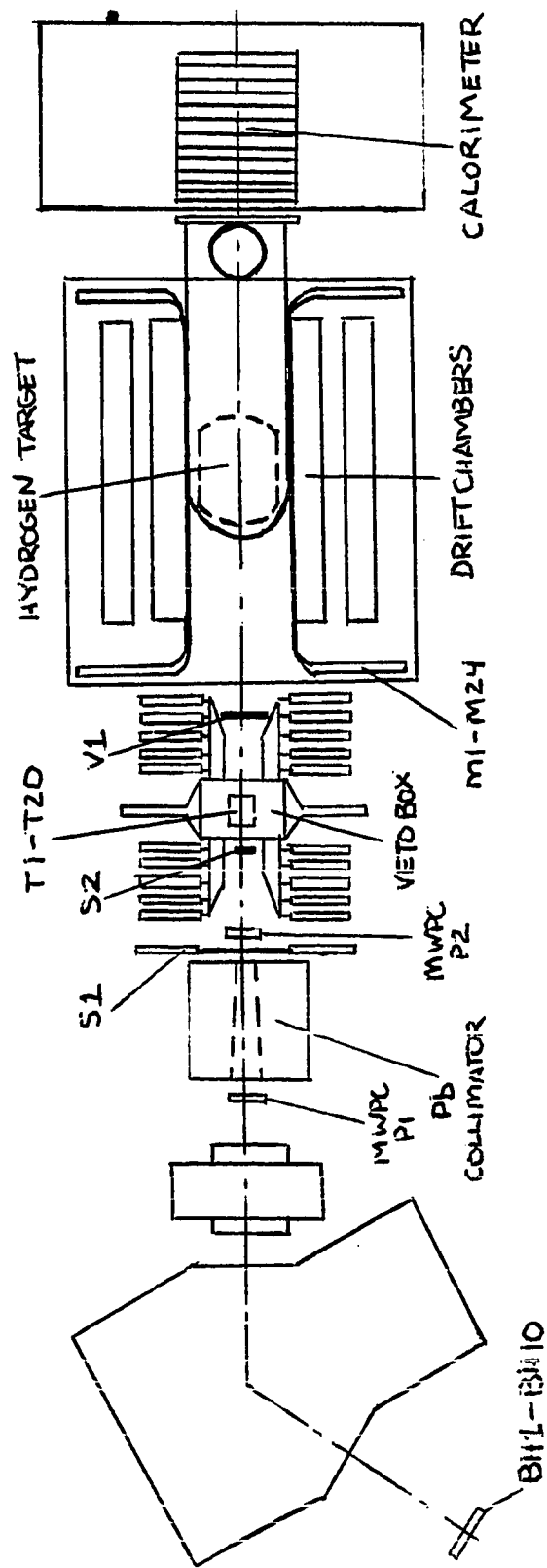
## CHAPTER II

### E-767 EXPERIMENTAL SETUP

Experiment 767 was set up in the experimental area at the end of the C8 line of the Low Energy Separated Beam II (LESB II) of the Alternating Gradient Synchrotron (AGS) at Brookhaven National Laboratory (BNL). For the purpose of this experiment, this beam line was tuned to provide ~ 400-800 MeV/c antiprotons at a rate of ~ 1000-3000 per spill. Details on this beam line and those associated with it are available from [XU85].

The experimental layout for E-767 is shown in Figure 1. This detector system consists of four parts: (1) a scintillator and multiwire proportional chamber system to identify and locate antiprotons; (2) an active antineutron source and its associated veto counters; (3) a hydrogen target surrounded by drift chambers for identifying and reconstructing  $\bar{p}p$  annihilations; and (4) a segmented calorimeter for determining the antineutron flux. Brief descriptions of these apparatus are given in this chapter with the exception of the antineutron source, which is discussed in detail in Chapter III. More detailed information about the construction and performance of the other apparatus is available from other sources [AH84], [CE84], [XU85].

**FIGURE 1**  
E-767 DETECTOR LAYOUT



The beam in the C8 line is heavily contaminated with pions, with a ratio of antiprotons to pions of  $\sim 1/200$ . Clearly it is important to distinguish the desired antiprotons from the background pions. To this end, a system of detectors was constructed to tag and locate the antiprotons in the beam. This system consisted of a beam hodoscope (BH), two multiwire proportional chambers (P1 and P2), and two antiproton identifying scintillators (S1 and S2). The antiprotons must pass through the hodoscope, the beam chambers, and S1 and S2 before entering the antineutron source.

The antiprotons can be distinguished from the pions in two ways, namely by time-of-flight (TOF) between the hodoscope and S1 or by energy loss in S1 and S2. The flight path between BH and S1 is  $\sim 377$  cm, so that the TOF for 505 MeV/c antiprotons is  $\sim 26.5$  ns, while for pions with the same momentum the TOF is  $\sim 13$  ns. The energy deposited by the antiproton in S1 and S2 is 2-3 times that deposited by the minimum ionizing pion at this momentum. Both of these methods were used in the fast triggering to remove as many pions as possible from the sample.

The two multiwire proportional chambers each had one X and one Y coordinate, and were used online to tune the beam into the antineutron source. Information from these chambers was also used in the off line analysis to be discussed in Chapter IV.

The beam hodoscope (BH) consists of ten thin scintillators 3.81 cm wide by 7.62 cm high arrayed side by side in the C8 beam line. It should be noted that the time resolution of these scintillators was poor ( $\sim 2-3$  ns), and that pulse-height information was not available. These scintillators are part of the beam line facility and were not constructed by the E-767 collaboration. It would be advisable to replace these scintillators in any future work.

An antiproton was tagged (triggered) when there was a proper time coincidence between BH, S1, and S2, as well as satisfying pulse-height requirements in S1 and S2. It was discovered that multiple pions in the system could mimic a valid  $\bar{p}$  trigger. For this reason a multiplicity unit was designed for the BH so that only events which had only one particle in the hodoscope and no other particles within 10 ns were triggered. It should also be noted that S1 defined the time, i.e. the TDC for S1 was defined to be zero, and all other times were relative to S1.

The purpose of E-767 being to determine the  $\bar{n}p$  annihilation cross section, it is necessary to measure the annihilation rate as a function of the antineutron momentum. For this purpose, a liquid hydrogen target was placed downstream of the antineutron source and surrounded with scintillators (M-counters) and drift chambers. The antineutron velocity was calculated from the measured TOF from the source to the annihilation point and the distance travelled. The

antineutron annihilates with a proton in the target to produce several pions, which proceed out through the scintillator-drift chamber system. The annihilation point is determined by vertex reconstruction from the drift chamber data, and the interaction time is determined from the TDC information in the M-counters surrounding the target.

The liquid hydrogen target was an aluminum cylinder of length 50 cm and radius 20 cm in a vacuum jacket 50.8 cm in diameter. Its size and location downstream of the source were determined by event rate and TOF considerations [LO81]. The target was constructed and maintained by BNL.

The twelve M-counters were placed in a "barrel-slat" configuration around the target, between the target and the drift chambers. The solid angle subtended by these counters was about 74% of  $4\pi$  steradians. Each counter consisted of a  $\sim 1$  m long quarter-inch thick scintillator with a photomultiplier tube on each end. The construction and installation of the M-counters were the responsibility of the Rice collaborators.

The drift chambers surrounded the target and M-counters, and subtended a solid angle of about 50% of  $4\pi$  steradians. They were arrayed into four identical quadrants, each consisting of a smaller inner chamber and a larger outer chamber. The active volume of an inner chamber was  $55.88 \times 151.13 \times 10.16$  centimeters, and that of an outer chamber was  $106.68 \times 151.13 \times 10.16$

centimeters. Each chamber had four coordinate planes. From the target out, each chamber had a U-coordinate (sense wires at  $45^\circ$  with respect to the target axis), two X-coordinates (sense wires perpendicular to target axis), and a Y-coordinate (sense wires parallel to target axis). A basic drift cell consisted of alternating field and sense wires placed 2.54 cm (1") apart and centered between two high-voltage foils that were also 2.54 cm (1") apart. Outside each quadrant was a large scintillator (E). A coincidence between an M and an E counter was evidence that a charged particle had passed through the intervening drift chambers. This was used to monitor the drift chamber efficiency while on line. The design, construction, and analysis of the drift chambers were the responsibility of our collaborators from the University of Houston [XU85].

In order to calculate the  $\bar{n}p$  annihilation rate, it is also necessary to know the incident flux of antineutrons. For this reason a modular calorimeter was placed downstream of the target-drift chamber system as an antineutron detector. A typical module had three layers: a 2.54 cm (1") thick aluminum plate, a layer of parallel 1.27 cm ( $\frac{1}{2}$ ") diameter drift tubes, and a layer of 4 parallel 0.635 cm ( $\frac{1}{4}$ ") thick scintillators. The drift tubes and scintillators were parallel within a module, but the orientation of each module was alternated by  $90^\circ$ . The first three (upstream) modules

had no aluminum plates to allow low momentum antineutrons to penetrate deeper into the calorimeter. The rest of the modules were as described above, for a total of 12 modules. The principle of operation is to detect the antineutrons by the large amount of energy ( $\sim 2$  GeV/c) deposited upon annihilation in the calorimeter and the high average multiplicity of annihilation products. Vertex reconstruction is accomplished using the drift tube information, and information about energy deposition is extracted from the scintillators. The design, construction, and analysis of the calorimeter were the responsibility of our collaborators from Pennsylvania State University [AH84], [CE84].

## CHAPTER III

### ANTINEUTRON SOURCE

Key to the success of the experiment is the production of antineutrons. The method of production used in this experiment was via charge-exchange: the incident antiproton "exchanges its charge" with a proton in the source medium and becomes an antineutron and a neutron. A simple calculation shows that the threshold for this reaction for the proton at rest is  $\sim 98$  MeV/c incident  $\bar{p}$  momentum.

#### A. Antineutron Source Apparatus

The source apparatus must be able to locate the point where the antineutron was produced. Location of the charge-exchange point was achieved by using a segmented, active source volume consisting of plastic scintillators individually wrapped and placed in a stack. The antiproton enters the stack, giving hits in consecutive counters as it loses energy. After the charge-exchange takes place, the resulting particles are uncharged, and no subsequent counters register hits. The approximate location of the interaction is given by the last counter hit. Our source consisted of 20 0.635 cm ( $\frac{1}{4}$ ") thick scintillators (T-counters). Each was

12.7 cm (5") wide and 5.08 cm (2") high, centered in the beam line. They were composed of polyvinyltoluene, with a hydrogen-carbon ratio  $H/C \sim 1.1$ . This ratio is typical of NE102A, the type of plastic used in all scintillators in this experiment. A view of the T-counters from above is shown in Figure 2.

The charge-exchange interaction occurs only a small percentage of the time. Most often the antiprotons annihilate on a proton or neutron in the source and produce several pions. Clearly such an interaction will produce a signal in the T-counters much like that for charge-exchange. In order to identify the charge-exchange events from the annihilations, the T-counters were surrounded by a set of anticoincidence counters (B-counters) called the vetobox. The vetobox consists of 12 scintillators arrayed around the T-counters, 3 to a side. The scintillators are sandwiched between lead and aluminum sheets to increase the detection efficiency for  $\gamma$ -rays that may be produced in the annihilation. A cross section of the vetobox and source with relevant dimensions is shown in Figure 3. It should be mentioned that the counters B4-B6 and B10-B12 (on the top and bottom of the source) are  $30.48 \times 30.48$  cm ( $12" \times 12"$ ) scintillators, and therefore subtend a much larger solid angle than do counters B1-B3 and B7-B9 (on the sides of the source), which are only  $11.43 \times 30.48$  cm ( $4.5" \times 12"$ ). In

FIGURE 2  
T-COUNTERS

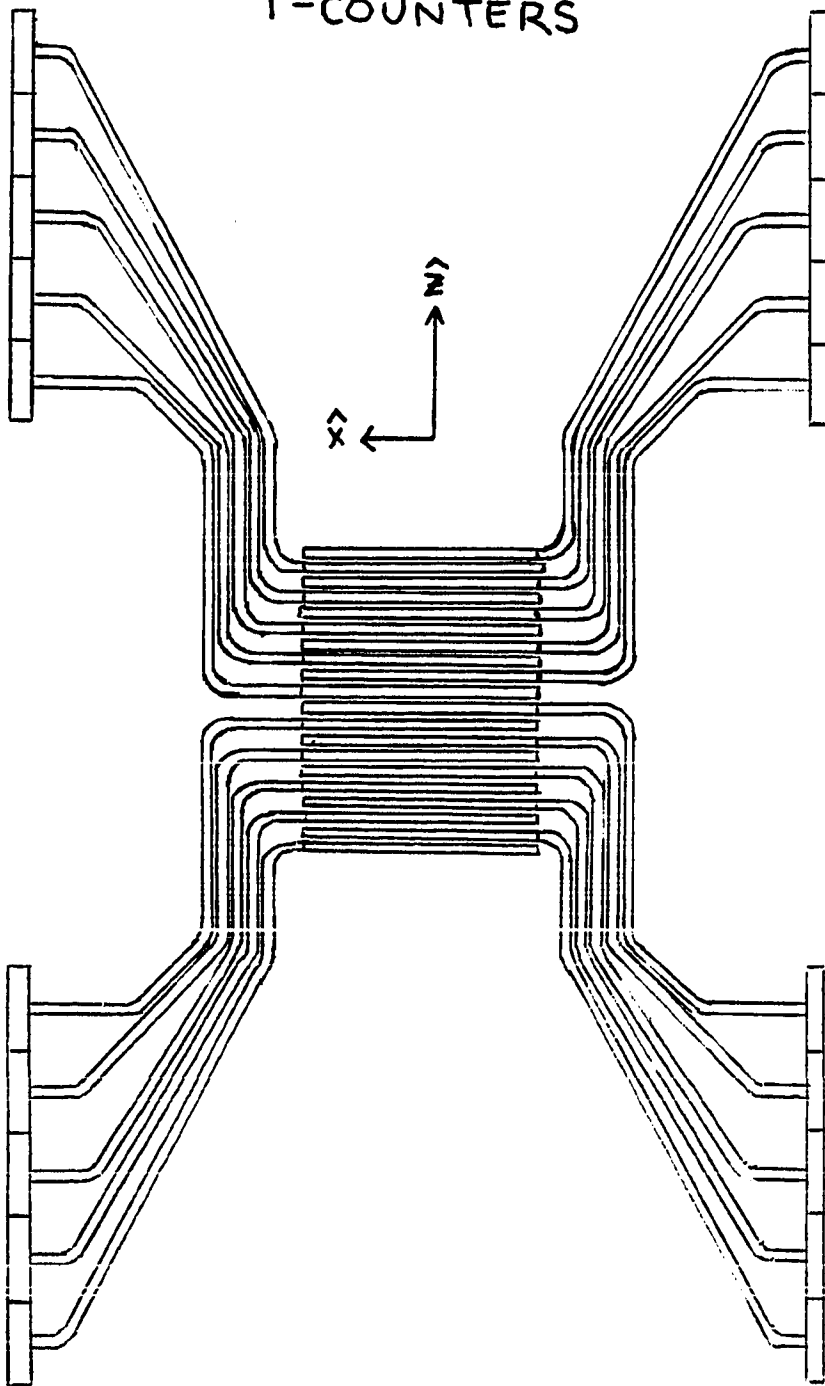
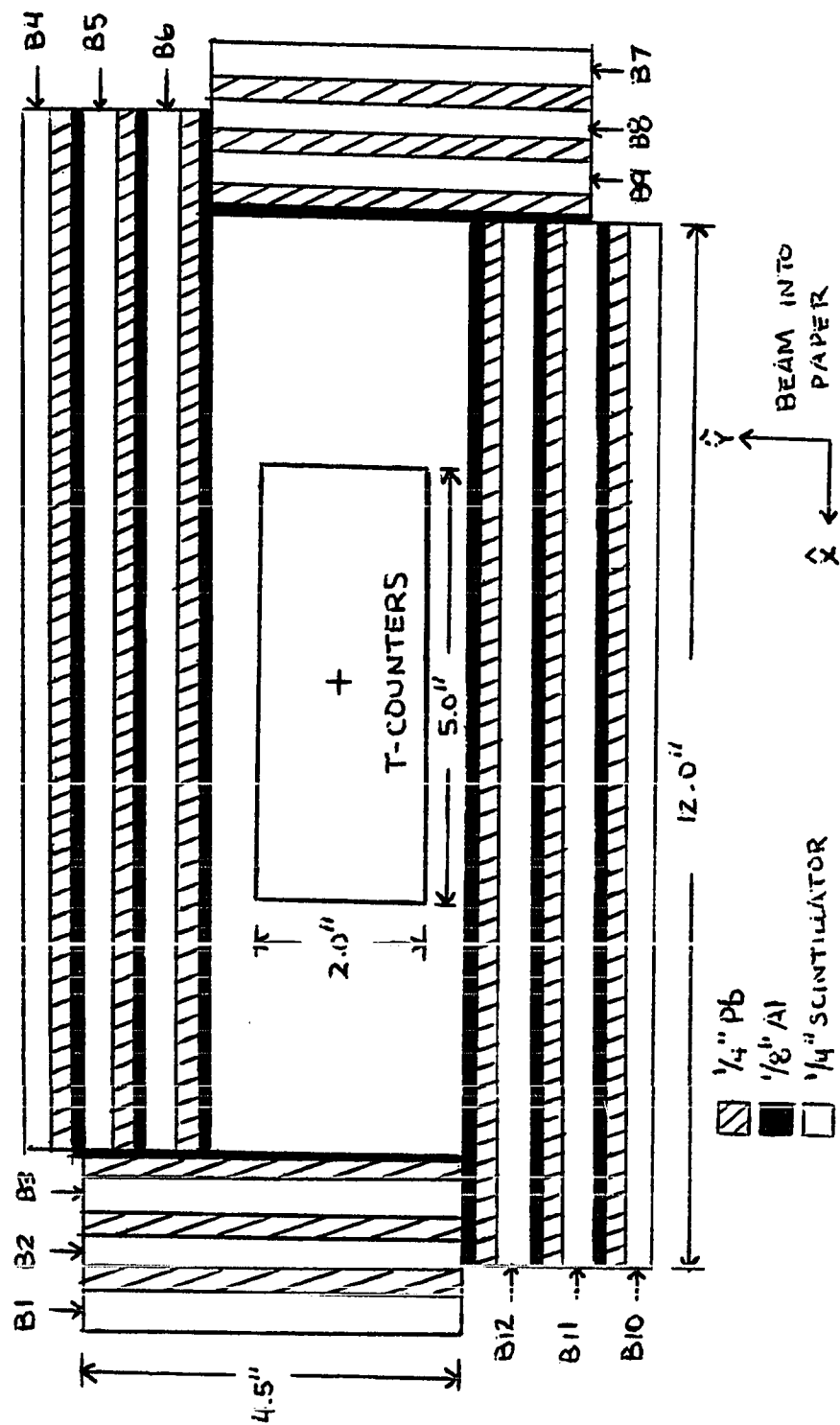


**FIGURE 3**  
CROSS SECTION OF SOURCE AND VETOBOX



addition to the vetobox, a large  $30.48 \times 30.48$  cm anti-coincidence scintillator (V1) was placed just downstream of the source, centered in the beam. This counter will detect annihilation and beam pions, as well as antiprotons which penetrate through the source.

Each of the counters described above (T1-T20, B1-B12, V1) was connected to a single photomultiplier tube from which timing and pulse-height information was gathered. Constant-fraction discriminators were not used. A view of the source and vetobox looking downstream is shown in Figure 4. Table 1 gives relevant distances between various counters and apparatus, as well as individual scintillator dimensions.

#### B. Interactions Expected

The physics that can occur in the source and surrounding veto counters is rich, and many different interactions can be expected. As the antiproton traverses the source material, it loses energy (primarily by ionization) at a known rate. Being a heavy charged particle, an antiproton has a range, parameterized as

$$R = (138.79 - 45.2p^2)p^{3.55}$$

where  $p$  is in GeV/c and  $R$  is in cm [RL83]. This formula is valid for plastic scintillators such as the one used here (NE102A). Those antiprotons which do not interact in flight

**FIGURE 4**  
SOURCE AND VETO BOX

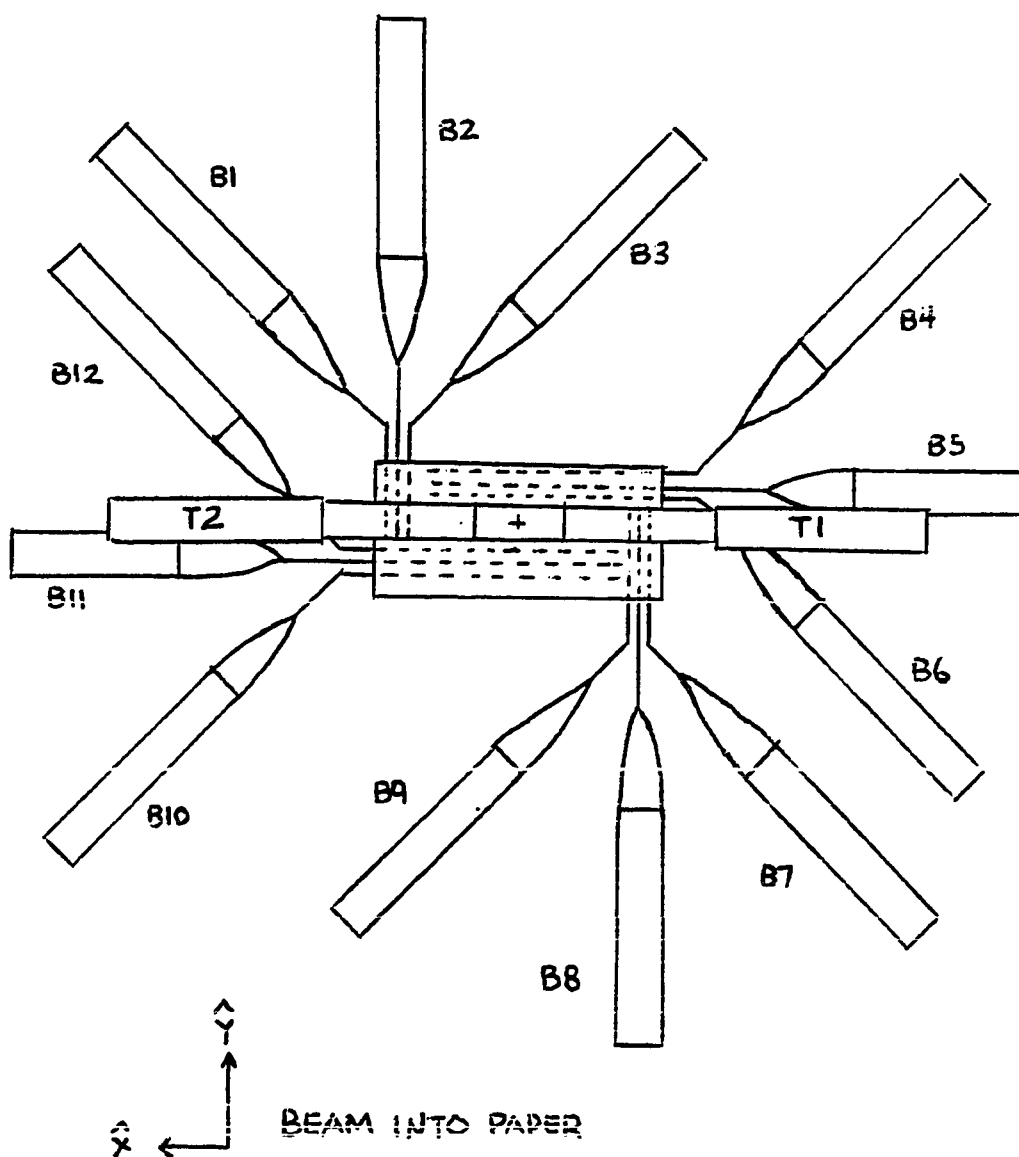


TABLE 1  
DIMENSIONS FOR E-767  
(centimeters)

BH - S1	377.2 (nominal)
P1X - S1	72.7075
P1X - P2X	82.55
P1Y - P2Y	80.01
S1 - S2	59.69
S1 - T1	67.691
S1 - T20	82.169
T1 - T20	14.478
S1 - tgt.center	245.11
S1 - cal.center	415.29
BH-counters	3.81 X 7.62
T-counters	5.08 X 12.7
S1	7.62 X 15.24
S2	4.445 X 12.065
B1-B3,B7-B9	11.43 X 30.48
B4-B6,B10-B12,V1	30.48 X 30.48

come to the end of their range and annihilate, either on a free proton in a hydrogen nucleus, or on a nucleon in a carbon nucleus. The annihilation products consist primarily of pions, which are emitted more or less isotropically. On the average, the total pion multiplicity per annihilation is  $\sim 4-5$ , with  $\sim 3-4$  charged pions and  $\sim 1-2$  neutral pions [AG60], [AE60].

At these relatively low momenta (below  $\sim 600$  MeV/c), about 40% of the antiprotons interact in flight. There are three primary interactions: elastic scattering, annihilation, and charge-exchange. Each of these interactions can occur on either a hydrogen or carbon nucleus. The charge-exchange process on hydrogen was discussed earlier:

$$\bar{p} + p \rightarrow \bar{n} + n .$$

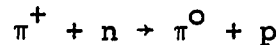
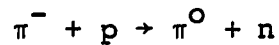
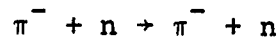
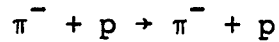
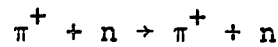
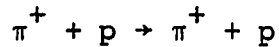
Charge-exchange on carbon is somewhat more complicated. One likely mechanism is

$$\bar{p} + C^{12} \rightarrow \bar{n} + n + B^{11} .$$

Note the added possibility of  $\gamma$  emission from an excited state of the residual nucleus. Annihilation on hydrogen results mainly in pions, with about 4% kaons in the annihilation products [AG60]. Annihilations on carbon are complicated by the fact that the annihilation can also result in protons being emitted, as well as possible  $\gamma$ -rays from the residual nucleus, whose exact state is difficult to determine.

Elastic scattering changes the path length of the antiproton in the source, thus introducing uncertainty in the energy of the antiproton at the interaction point. It can also result in the antiproton leaving the source volume before it interacts again. The antiproton can then either interact in the vetobox or be scattered back into the source volume.

The particles that result from either the annihilation or charge-exchange of the antiproton will also interact in the source and vetobox. The charged pions can scatter or charge-exchange:



They have a mean life  $\tau \sim 26$  ns, and should not decay before leaving the vicinity of the vetobox. The neutral pions will decay almost instantly ( $\tau \sim 10^{-7}$  ns) by



The kaons resulting from annihilations are produced in pairs (associated production). Since the strangeness of the  $\bar{p}p$  or  $\bar{p}n$  system is zero, the kaons will be produced as  $K^+K^-$ ,  $K^0\bar{K}^0$ , or  $K^-K^0$  pairs. Furthermore, the  $K^0$  and the  $\bar{K}^0$  are linear combinations of the  $K_L^0$  and  $K_S^0$ , where the L and S refer to long and short decay times. The charged

kaons gave a mean life  $\tau \sim 12.4$  ns, and thus should pass through the vetobox before any decays take place. Half of the neutral kaons produced are  $K_L^0$ , with  $\tau \sim 51.8$  ns, and should pass through the vetobox unobserved. The other half of the neutral kaons are  $K_S^0$ , with  $\tau < 1$  ns, which will decay mainly by

$$\begin{array}{ll} K_S^0 \rightarrow \pi^+ \pi^- & 65.6\% \\ K_S^0 \rightarrow \pi^0 \pi^0 \rightarrow 4\gamma & 31.4\% \end{array}$$

The antineutrons produced via charge-exchange can subsequently annihilate either in the source or the vetobox, as well as scatter. The neutrons that are produced can scatter, and even though neutral, they can produce a hit in the source or vetobox due to energy loss from collisions. Interactions on carbon also give the possibility of  $\gamma$ -ray emission from an excited state of the residual nucleus. Finally, any  $\gamma$ -rays can produce showers in the vetobox, which are complicated events where many particles (mostly electrons, positrons, and photons) are involved.

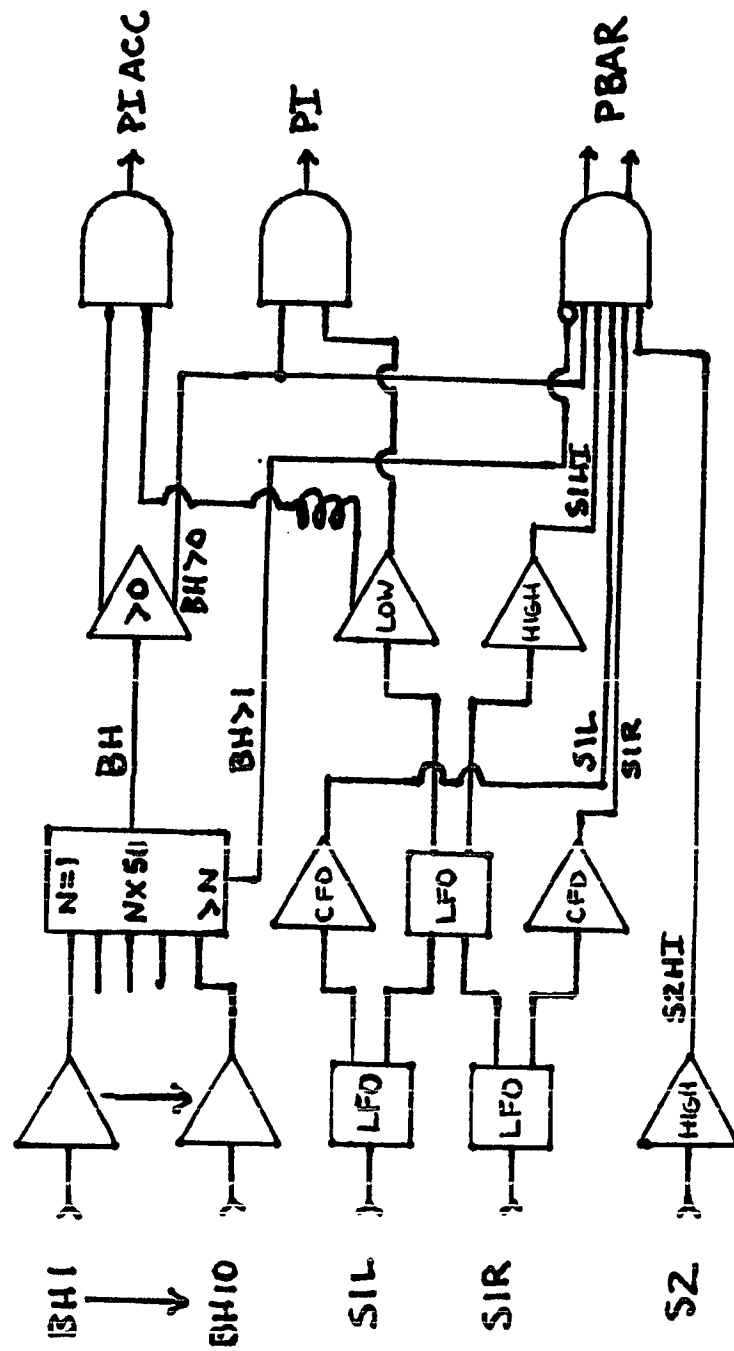
### C. Trigger Logic

With so many possible reactions taking place, together with a large background ( $\pi^-/\bar{p} \sim 200$ ), it is clear that a fast triggering system is needed to minimize background contamination and to select events of interest. For E-767 the

trigger logic must be able (a) to discriminate between pions and antiprotons, (b) to determine when an antineutron was produced in the source, and (c) to strobe the recording of data from the drift chambers and calorimeter properly. The discussion of (c) and its associated trigger logic is not necessary for a study of the antineutron source, and is omitted here (see [XU85]).

The logic diagram for the electronics associated with the triggering of antiprotons is shown in Figure 5. The ten hodoscope counters (BH1-BH10) go into a multiplicity unit which has two outputs into the PBAR AND gate. One output requires that at least one particle passed through the hodoscope ( $BH > 0$ ), while the other output requires that more than one particle passed through the hodoscope within a 10 ns window of the first ( $BH > 1$ ). The scintillator S1 is actually a double-ended counter, designated S1L and S1R. The signal from each goes into a linear fan-out (LFO) which has two outputs. One is input to a constant-fraction discriminator (CFD) for timing purposes. The outputs of the CFD's go into the PBAR AND gate. The other output is summed via another LFO and input into two different discriminators. One discriminator is set "low" to give an output for pions in S1 (S1Lo), and the other is set "high" to give an output for antiprotons in S1 (S1HI). The signal from S1HI is input to the PBAR AND gate. The signal from S1Lo, together with  $BH > 0$ , determine pions (PI) and out-of-time ("accidental") pions

FIGURE 5  
PBAR TRIGGER



(PIACC). Finally, the signal from counter S2 is discriminated for antiprotons (S2HI) and input into the PBAR AND gate. Thus, the trigger requirements for an antiproton can be written

$$\text{PBAR} \equiv (\overline{\text{BH} > 1}) \cdot (\text{BH} > 0) \cdot \text{S1HI} \cdot \text{S1L} \cdot \text{S1R} \cdot \text{S2HI}$$

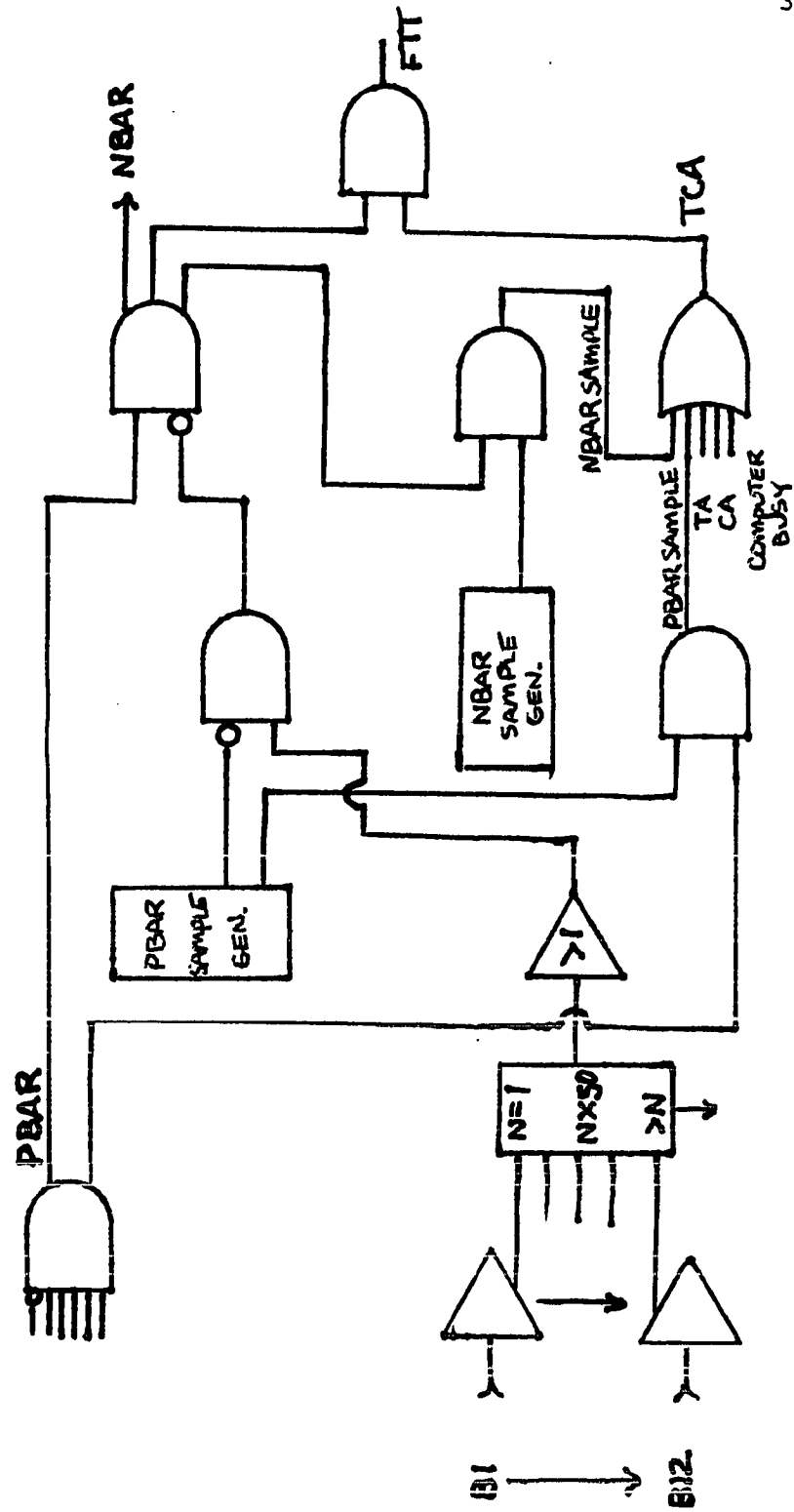
where the bar means anticoincidence. Note that the relative timing is such that S1L strobes the gate.

The logic diagram for the electronics associated with tagging the antineutrons is shown in Figure 6. The inputs from the vetobox (B1-B12) are fed into a multiplicity unit in a manner similar to the hodoscope. The output is discriminated, and events which have more than one hit in the vetobox are vetoed. One hit in the vetobox is permitted to avoid vetoing events which are valid charge-exchanges where the neutron is seen in the vetobox. The trigger requirement for an antineutron is then simply

$$\text{NBAR} \equiv \text{PBAR} \cdot (\overline{\text{B} > 1})$$

Also shown in Figure 6 is the logic required to sample the inputs at PBAR and NBAR for normalization purposes (PBAR SAMPLE, NBAR SAMPLE). The signal FTN strobes the TDC's and data readout cycle. It requires a coincidence between NBAR and TCA. TCA is the output of an OR gate, with PBAR SAMPLE,

FIGURE 6  
NBAR TRIGGER



NBAR SAMPLE, Computer Busy, TA, and CA as inputs. TA and CA refer to valid target or calorimeter events.

The normal trigger used in the data taking of E-767 (NBAR), described above, clearly is inappropriate for a study of the antineutron source. A trigger was needed that would allow recording of data in the source apparatus for any antiproton interactions, irrespective of the state of the rest of the system. For this purpose, the trigger described above was modified in the following way: first, the vetobox requirement for NBAR was removed, i.e.

$$\text{NBAR} \equiv \text{PBAR} .$$

Second, the NBAR SAMPLE generator was set to 50%. Thus, events which showed an antiproton in the source were recorded, with no other requirements. The event ratio was such that a 50% NBAR SAMPLE allowed data taking at a speed limited only by the computer busy time.

Using the modified trigger just described, the antineutron source apparatus was studied with two main purposes in mind: (a) to understand the source operation and output, and (b) to determine various efficiencies, such as antineutron production rate vs. T-counter,  $\bar{p}$  annihilation rate vs. T-counter, and veto efficiency vs. annihilation point. These things are expected to be functions of momentum and beam phase space. The method of study has three major steps:

(1) Analysis of raw data - Here annihilation multiplicities, charge-exchange rate, etc. are determined from the actual data. The details of this analysis are given in Chapter IV.

(2) Monte-Carlo simulation of source apparatus - Here all of the "known" physics involved in the source is used to simulate the experiment in the computer. This aspect of the study is discussed in Chapter V.

(3) Comparison - Finally, the Monte-Carlo simulated data are compared to the actual data, and conclusions are drawn on validity of the Monte-Carlo, corrections to data values, etc. This step in the study comprises Chapters VI and VII.

## CHAPTER IV

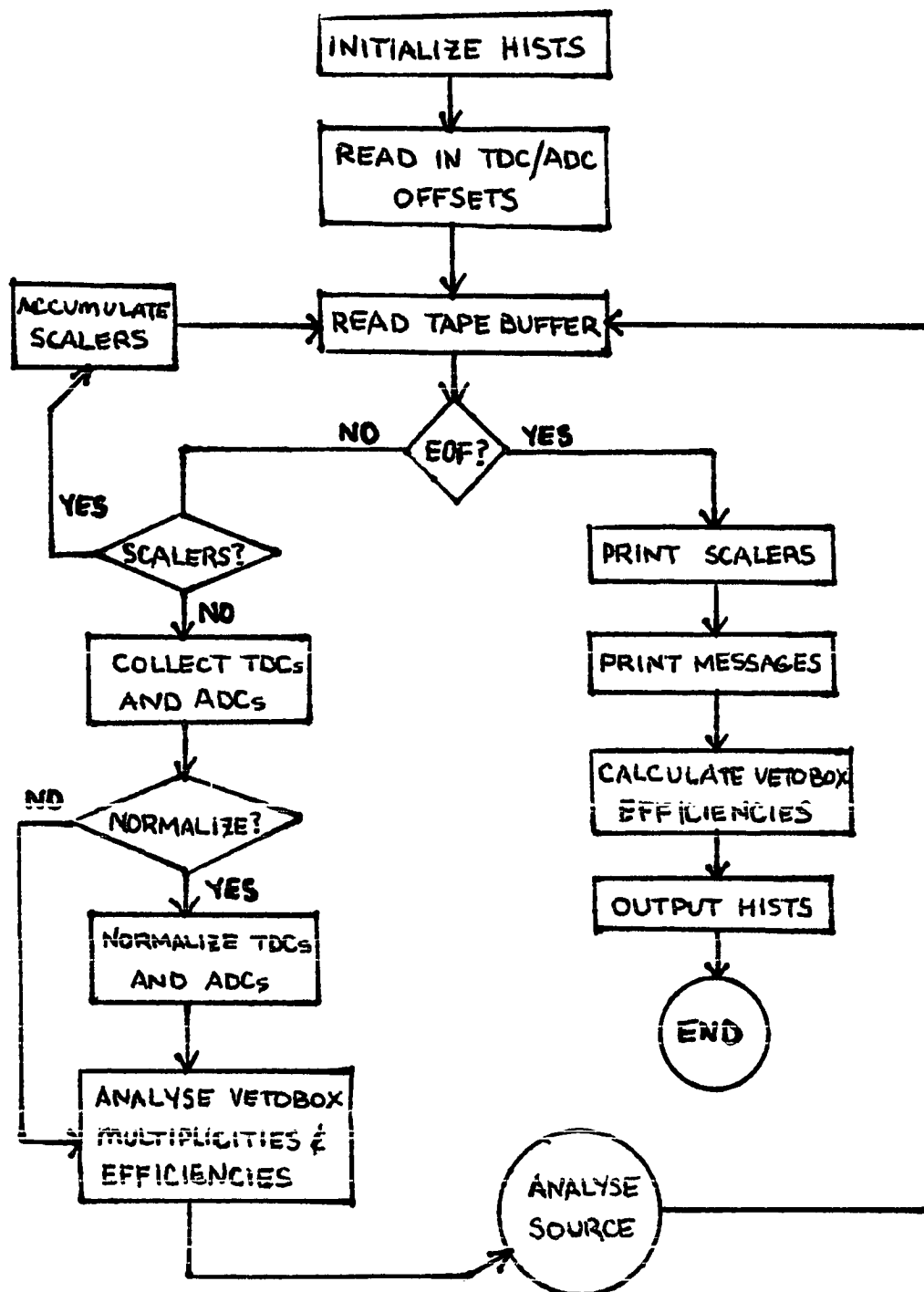
### DATA ANALYSIS

Analysis of the data taken from the source apparatus basically consists of identifying and cataloguing the different events which occur. In order to understand the source operation and to determine the usefulness of the apparatus as an antineutron source, three primary results are sought: [1] annihilation multiplicities, [2] verification of antiproton interaction cross sections, and [3] various efficiencies. The annihilation multiplicities are determined by analysis of the vetobox. Once the annihilation is identified, it is catalogued by the number of vetobox quadrants that were hit. Clearly this is a function of the geometry of the source as well as the angular distribution of the annihilation products. The antiproton interaction cross sections are determined by identifying the T-counter where the particular interaction took place [TLAST]. A histogram of TLAST for a particular interaction gives information in the cross section for that interaction as a function of energy for a particular incident  $\bar{p}$  momentum. The efficiencies of interest to E-767 are the veto efficiency for annihilations and the antineutron production rate. These are both expected to be functions of momentum and the geometry of the source configuration. Analysis of the data

alone, of course, is not sufficient to determine these results. The results of the data analysis must be compared to Monte-Carlo results so that corrections can be made due to the event selection criteria; e.g. an event where the  $\bar{p}$  scatters out of the source volume and then subsequently annihilates in the vetobox cannot be distinguished from an annihilation that took place in the source at the location of the  $\bar{p}$ 's exit. Corrections for such effects can only be made by Monte-Carlo analysis.

The flow chart for the main program of the data analysis of the source apparatus is shown in Figure 7. The data are formatted on tape into 450 word event buffers interspaced with 450 word scalar buffers. After an event buffer is identified, the raw TDC and ADC values for all of the counters are collected. The next step is to "normalize" these raw values such that (1) S1 TDC = 0, and (2) ADC for minimum ionizing particles = 100. This is accomplished by applying an additive offset to the TDC values and a multiplicative factor to the ADC values on a counter-by-counter basis. These offsets were calculated using data from a PI triggered calibration run. After normalization, the vetobox is analyzed. This consists primarily of determining which B-counters were hit and the various multiplicities for the event; e.g. vetobox quadrant multiplicity per event, total number of B-counters hit per event, etc. The source analysis follows after the vetobox

**FIGURE 7**  
DATA ANALYSIS  
MAIN PROGRAM



analysis is complete. This is where the  $\bar{p}$ 's are identified, the T-counters are examined, and the various events are classified. Upon completion, the next tape buffer is read in and the sequence starts over for the next event. The results are output after the end of the tape is reached.

The flow chart for the source analysis is given in Figures 8a-8e. First, the time for S1 is defined, and then the hodoscope is examined for antiprotons. Events which do not have 1 and only 1  $\bar{p}$  in the hodoscope are discarded [event cut 1]. Next S1L, S1R, and S2 ADC's are examined for evidence of an antiproton. Events which do not show a  $\bar{p}$  in all three of these counters are discarded [event cuts 2-4, respectively] [Figure 8a]. Following this, the MWPC's P1 and P2 are examined. Those events where there is not 1 and only 1 hit in each coordinate are discarded [event cut 5]. In addition, those events where a straight-line projection of the antiprotons track showed that the  $\bar{p}$  may leave the source volume before interacting were discarded [event cut 5]. These cuts serve to reduce background from out-of-time beam pions and to reduce the number of events where the  $\bar{p}$  scatters out of the source volume before interacting. Clearly, the number of events which survive these cuts is a function of the efficiency of the MWPC's. Next the  $\bar{p}$  momentum is calculated from the TOF between the hodoscope and S1. Those events with a calculated  $\bar{p}$  momentum less than 450 MeV/c or greater than 750

FIGURE 8a  
SOURCE ANALYSIS

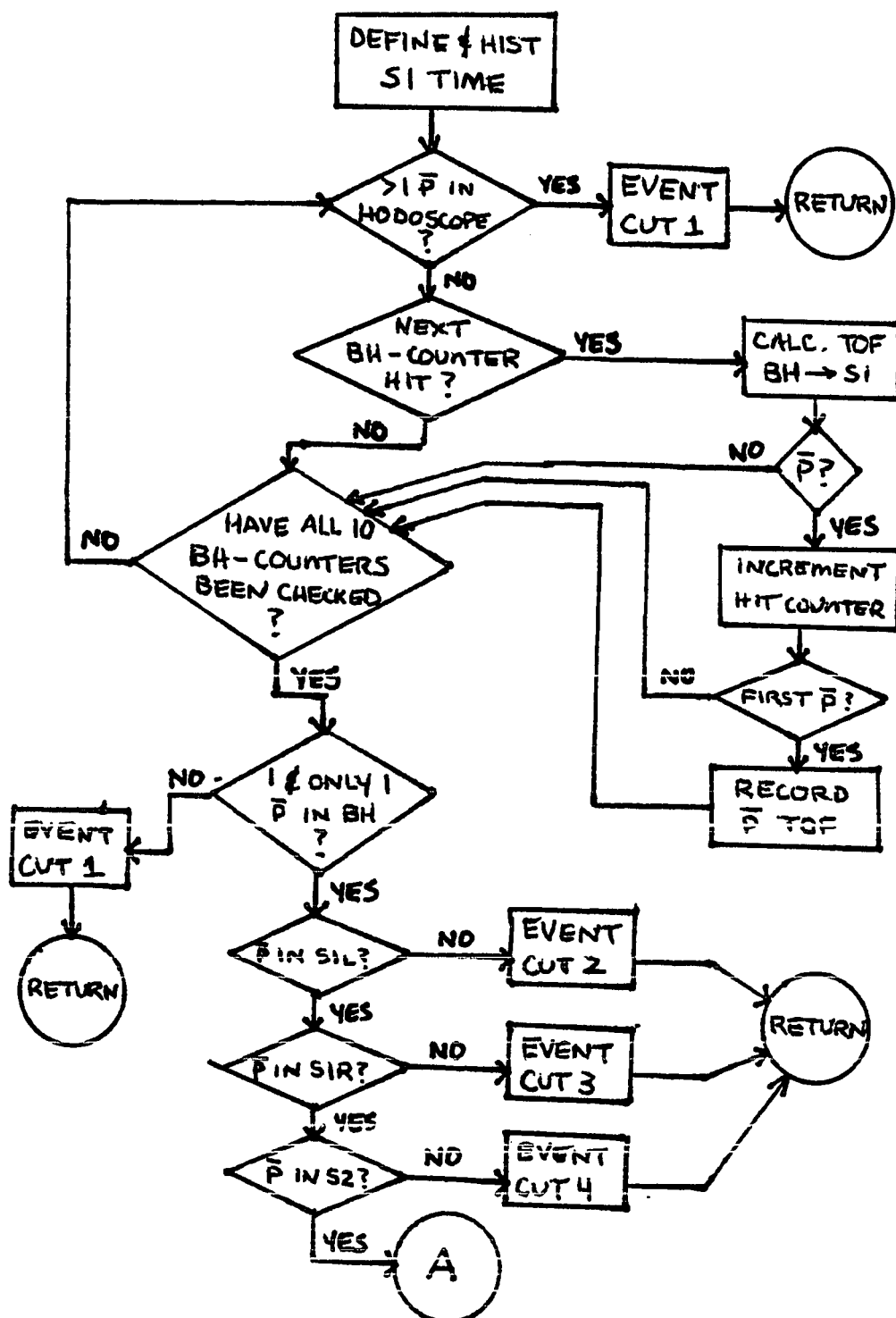


FIGURE 8b

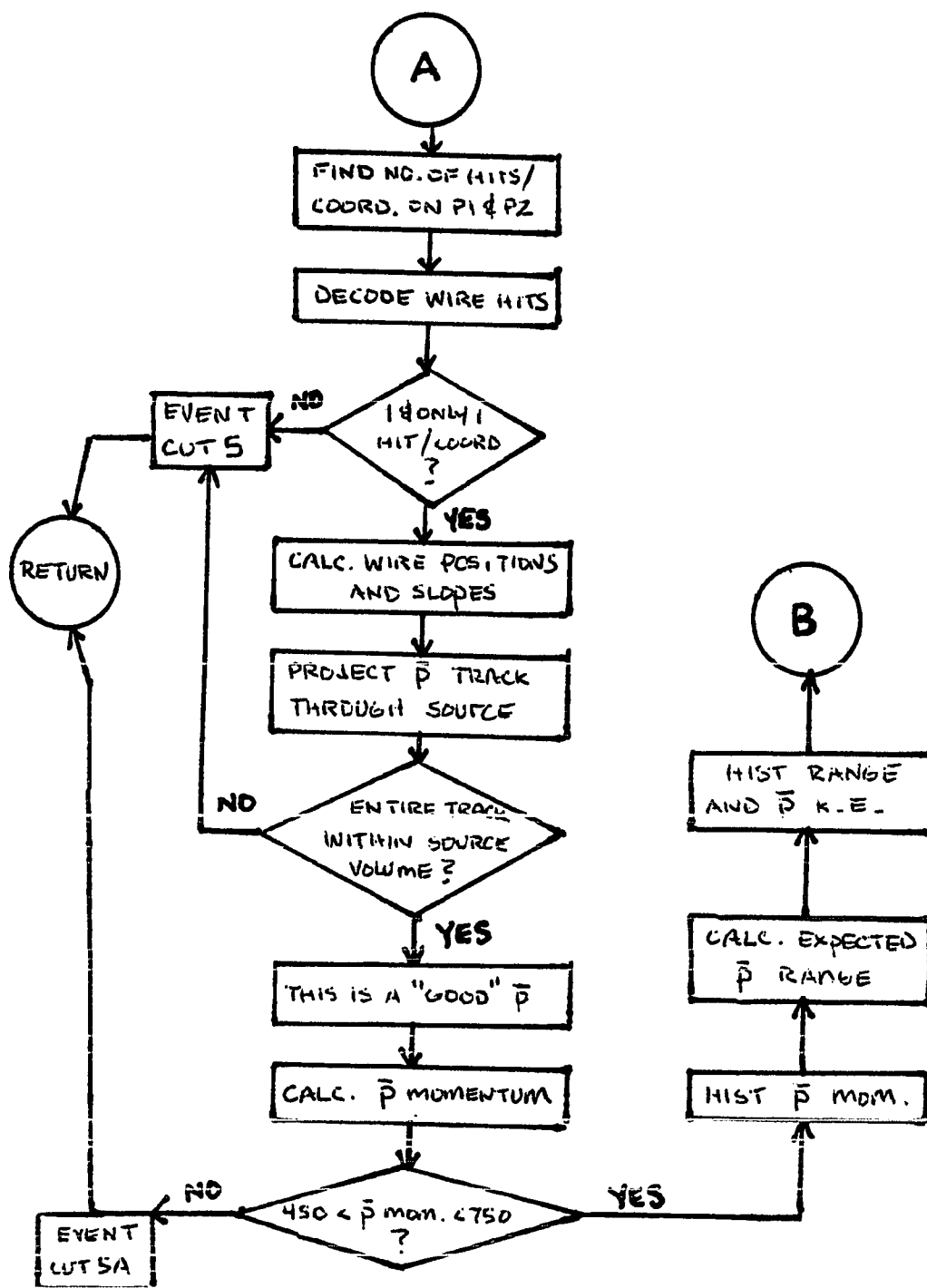


FIGURE 8c

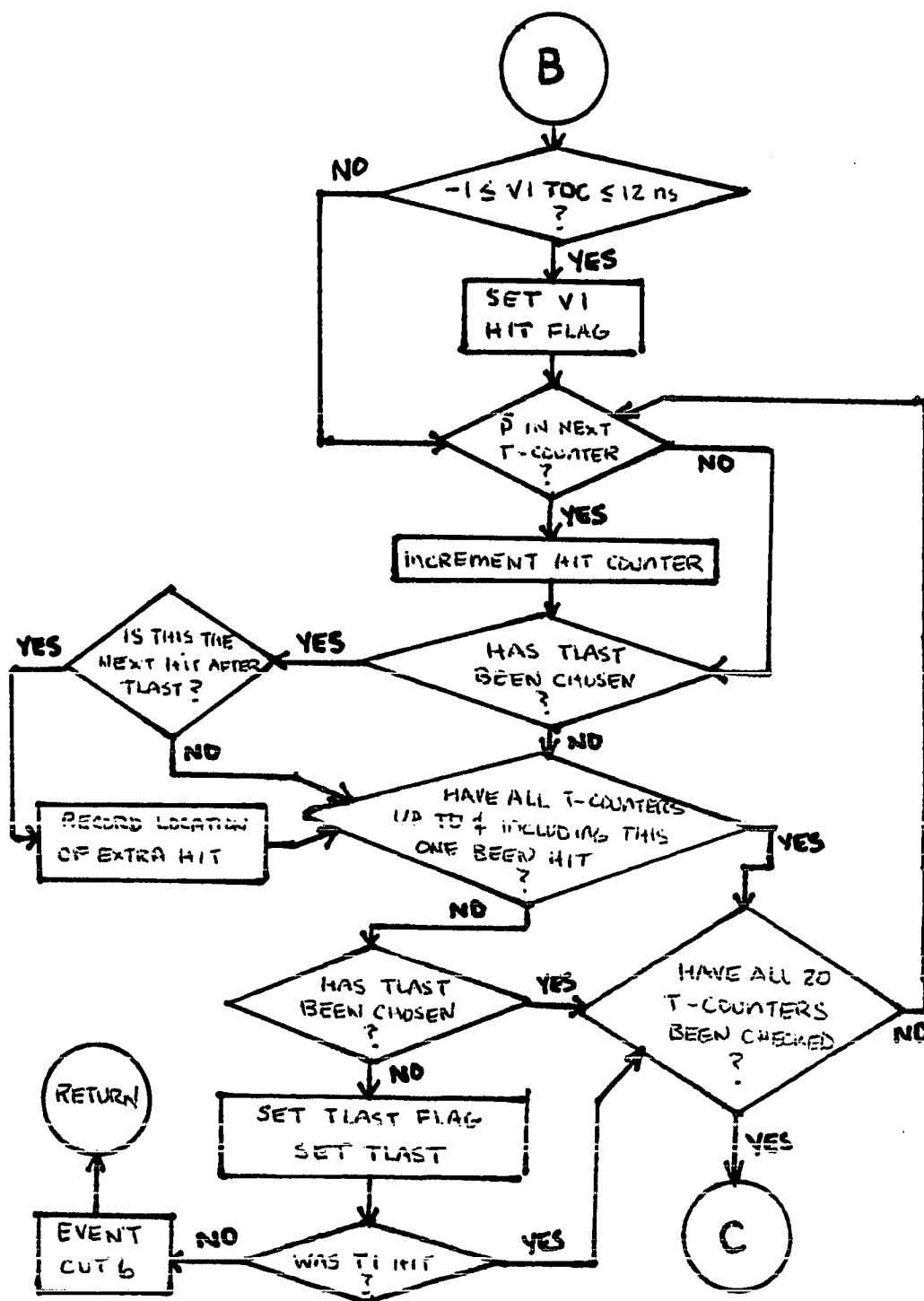


FIGURE 8d

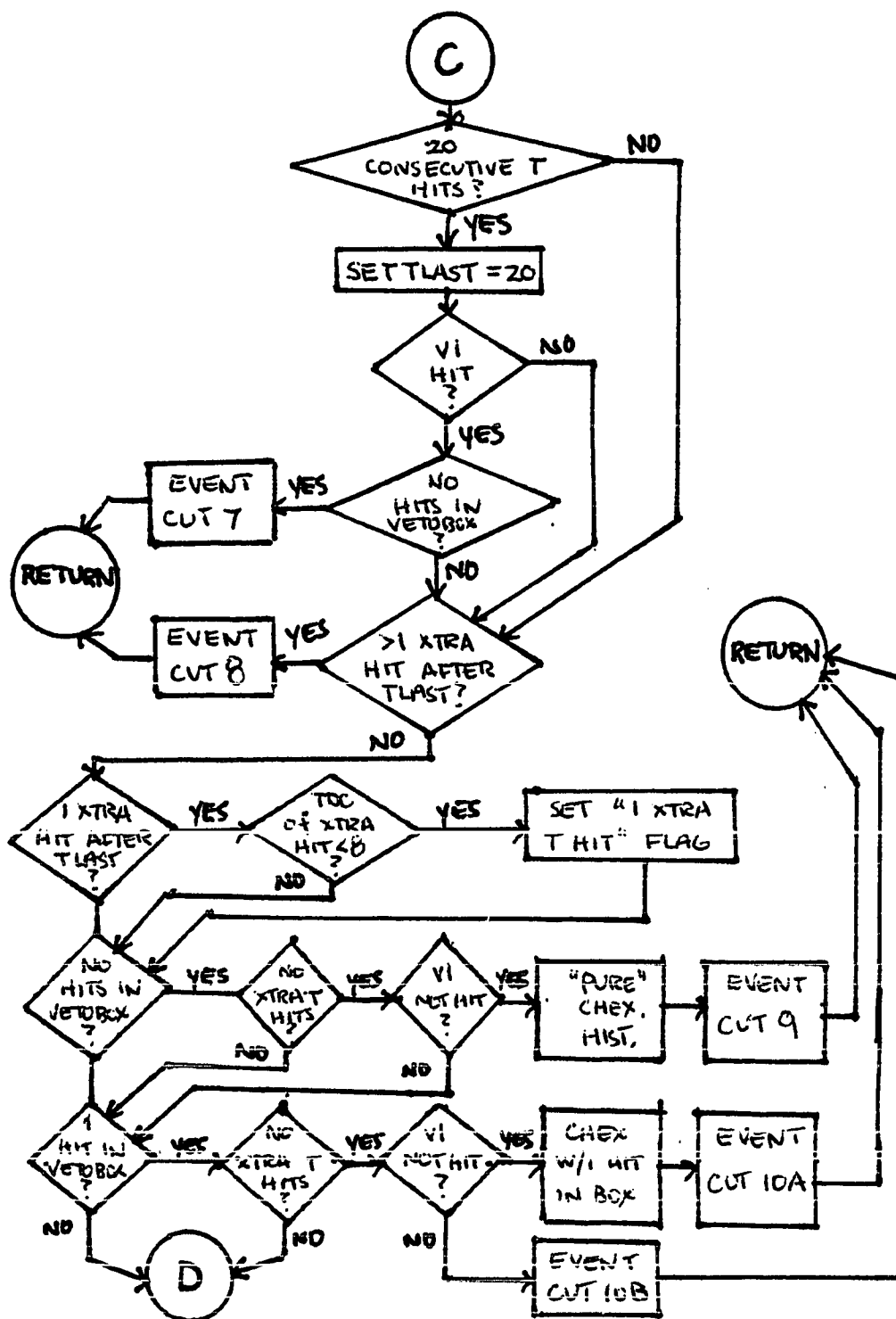
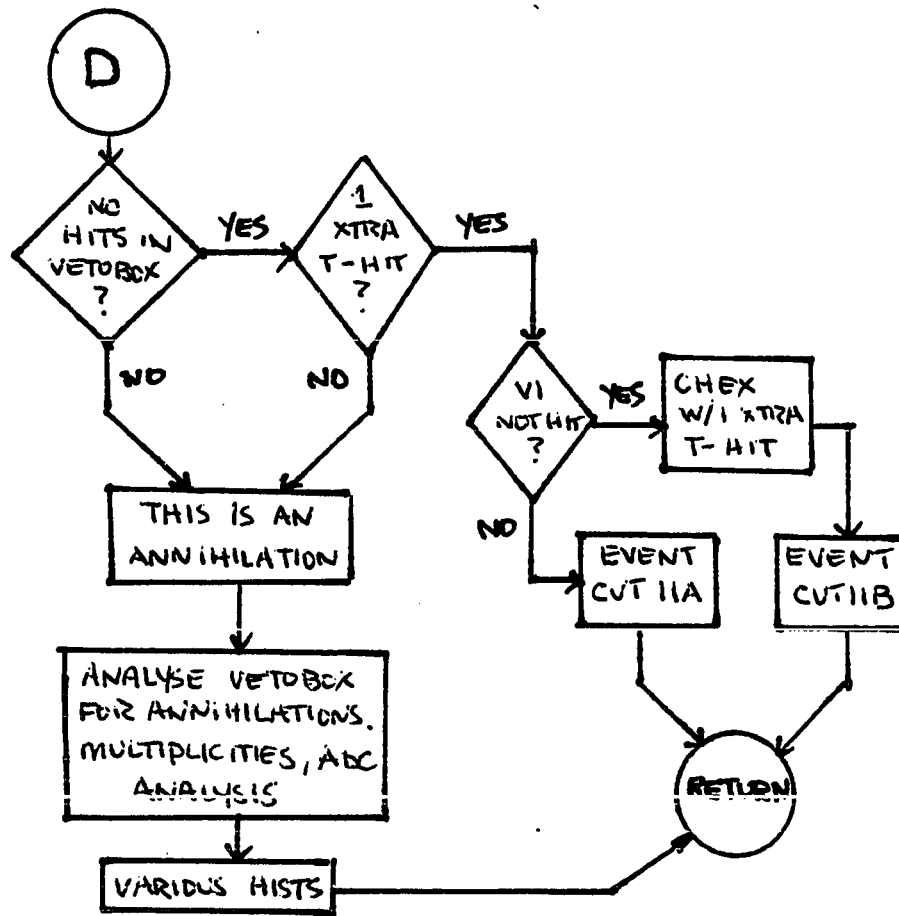


FIGURE 8e



MeV/c were discarded [event cut 5a]. This "weak" condition helps to eliminate a few more events where out-of-time beam pions are confusing the issue. Note that those events which pass cuts 1-5 make up the incident  $\bar{p}$  sample that is used for further analysis [Figure 8b].

Once a "good"  $\bar{p}$  is selected, classification of the event can begin. First, a flag is set if the anticoincidence counter V1 was hit. Then, the T-counters are examined to determine the interaction point. This is done by examining the ADC of each T-counter in sequence, and requiring that the ADC be greater than some minimum value for a  $\bar{p}$  in that counter. When the first counter that is not hit is detected, the preceding counter is designated the interaction point [TLAST]. The location of any subsequent T-counter hits [after a miss] is also recorded. Events in which the first T-counter [T1] was not hit are discarded [event cut 6] [Figure 8c]. Next, two other event types are discarded. The first type are those events where all 20 T-counters and V1 were hit, with no hits in the vetobox [event cut 7]. These are  $\bar{p}$ 's which penetrate the stack without interacting [except for possible scattering]. The second type are those events which had more than 1 extra [non-sequential] T-counter hit after the interaction point TLAST was chosen [event cut 8]. These "non-sequential T-hits" events are probably the result of one of two things: [1]  $\bar{p}$ 's which leave the source volume and are scattered

back in by the vetobox, or [2] fluctuations in the  $\bar{p}$ 's energy loss such that the ADC for one or more T-counters is below the minimum required to declare a  $\bar{p}$  in that counter. After these cuts, events which have only 1 extra [non-sequential] hit after TLAST are flagged, and then the various charge-exchange signatures are examined. Those events in which there were no hits in the vetobox, no extra T-counter hits, and no hit in V1 are declared "pure" charge-exchange events, which are then recorded and removed from the sample [event cut 9]. Events in which there were no extra T-counters hit, no hit in V1, but there was 1 and only 1 hit in the vetobox are also labeled as charge-exchanges, and removed from the sample [event cut 10a]. These should be charge-exchange interactions where the neutron is observed in the vetobox. In addition, events with no extra T-counter hits, 1 hit in the vetobox, and V1 hit are discarded [event cut 10b]. This represents only a very small percentage of the total number of events, and are probably valid charge-exchanges where the neutron is seen in the vetobox and either the antineutron annihilates in V1 or an out-of-time pion is detected by V1 [Figure 8d]. Finally, events which had no hit in the vetobox and 1 and only 1 extra T-counter hit are selected. Those where V1 was not hit are declared charge-exchanges where the neutron gives a hit in a downstream T-counter [event cut 11b] and are removed from the

sample. Those where V1 was hit are also discarded (event cut 11a). Again, these events represent only a very small percentage of the total number of events, and are probably related to those events that satisfied event cut 10b.

Any events which make it this far without being cut are considered  $\bar{p}$  annihilations. The vetobox is then analyzed for the various multiplicities in the annihilations, as well as various histograms of the ADC's in the vetobox (Figure 8e). The program then returns to the main program.

For reference, the various cuts are listed below in the order that they are applied:

- 1 No  $\bar{p}$  or  $> \bar{p}$  in hodoscope
- 2 No  $\bar{p}$  in S1L
- 3 No  $\bar{p}$  in S1R
- 4 No  $\bar{p}$  in S2
- 5 Did not have 1 and only 1 hit/coord in P1 and P2 or  $\bar{p}$  track projected to leave side of source
- 5a  $\bar{p}$  momentum  $< 450$  MeV/c or  $> 750$  MeV/c
- 6 T1 not hit
- 7  $\bar{p}$  "punches through" source
- 8  $> 1$  non-sequential T-counter hit
- 9 "pure" charge-exchange
- 10a charge-exchange with neutron in vetobox
- 10b 1 hit in vetobox, no extra T hits, V1 hit
- 11a No hits in vetobox, 1 extra T hit, V1 hit
- 11b charge-exchange with neutron in T-counters

While the cuts as shown above were common to all runs analyzed, the values used for the different cuts varied from run to run. The primary reason for this is that the energy loss expected in a particular counter is a function of the incident momentum. This point was taken into consideration when the data were analyzed. Cut 5 had a significant impact on the results of data taken at different momenta, because the number of events which pass this cut is strongly dependent on the efficiencies of the two MWPC's P1 and P2, which decreased slightly with increasing momentum. The result of this, however, is only to lower the total number of  $\bar{p}$ 's in the sample, and so will reflect only a larger statistical error in the final results, not a significant change in those results.

There are two main sources of background as far as the source study is concerned: (1) beam pions entering the stack and (2) accidentals giving hits in the vetobox. The combination of trigger requirements and some of the off-line cuts discussed above serve to reduce the number of beam pions to a low level. However, there is evidence that some contamination by out-of-time pions does occur. The accidentals giving uncorrelated hits in the vetobox probably arise primarily from interactions in the lead collimator that sits between P1 and P2 (Figure 1). Photons, pions, and anti-proton annihilation products can be expected. The effect of these backgrounds on the results will be discussed in

Chapter VI. No attempt has been made at this point to make corrections for such interactions as

$$\pi^{-} + p \rightarrow \pi^{-} + p$$

where the pion is from the beam.

## CHAPTER V

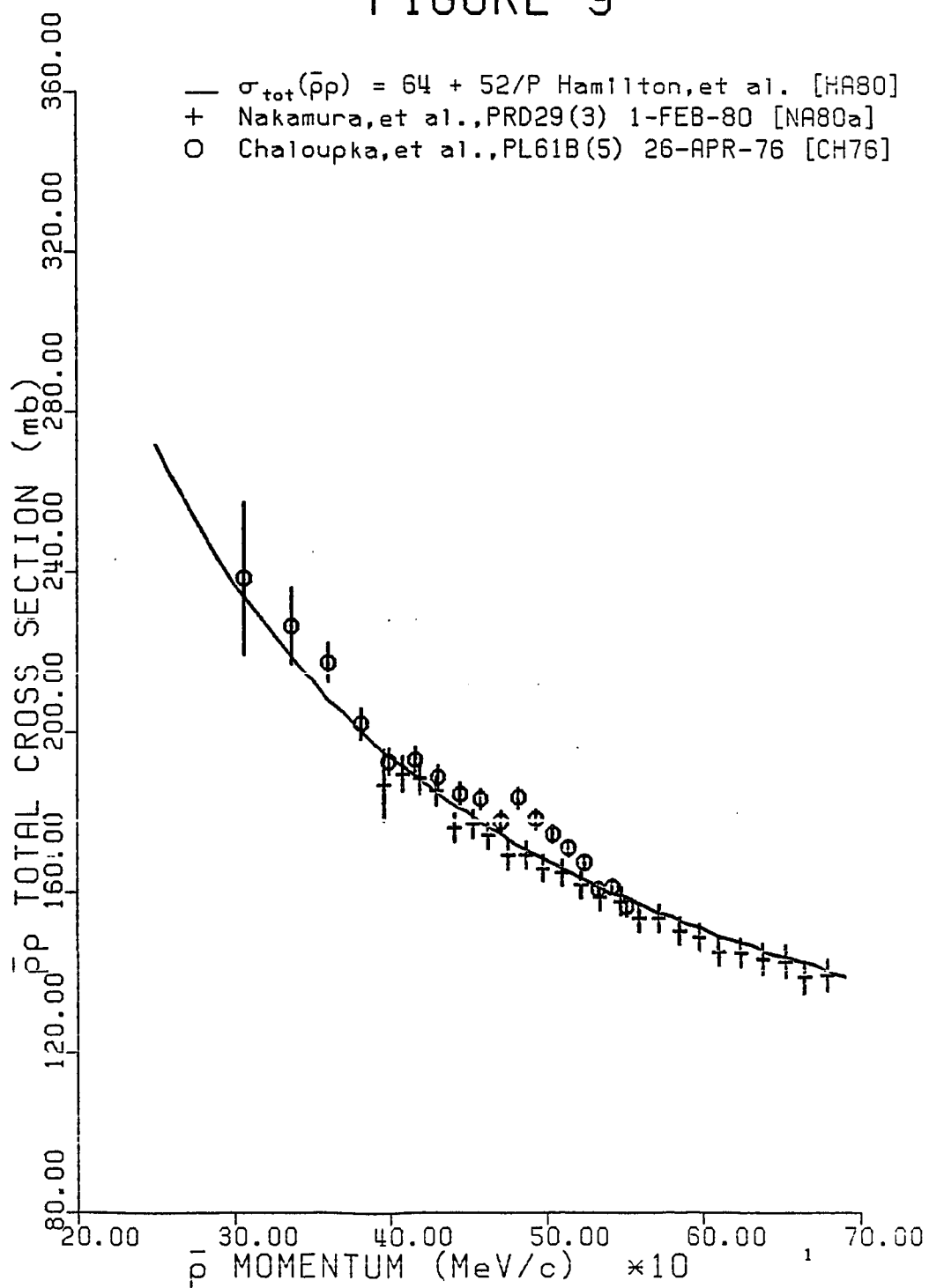
### MONTE-CARLO ANALYSIS

The Monte-Carlo simulation of the antineutron source consists of writing a computer program to simulate the source apparatus. In order to understand the results of the experimental data analysis, the program should include as much of the "known" physics involved as possible. In particular, the following information must be provided in order to simulate the different interactions: (a) total, elastic, annihilation, and charge-exchange cross sections, (b) differential cross sections for elastic and charge-exchange scattering, and (c) multiplicities for annihilations. This information is needed for antiprotons incident on both hydrogen and carbon. The program makes use of parameterized fits to available data wherever possible. In general, much more data is available for hydrogen than carbon.

#### A. Cross Sections

The  $\bar{p}p$  total cross section versus momentum in the region of interest is shown in Figure 9. The circles are the 1976 data of Chaloupka, et al. [CH76], who claimed evidence of the S-meson. The plusses are the 1980 data of

FIGURE 9



Nakamura, et al. [NA80a], which shows no evidence of a significant enhancement of the cross section. The solid curve is the parameterized fit to the high statistics data of Hamilton, et al. [HA80b]. The data of Hamilton (not shown) agrees with that of Nakamura within quoted error limits. The parameterized fit used for the  $\bar{p}p$  total cross section in the Monte-Carlo is

$$\sigma_{TOT}(\bar{p}p) = 64 + 52/P$$

where  $\sigma_{TOT}$  is in millibarns and  $P$  is in GeV/c [GR83]. This parameterization is in good agreement with the most recent measurements from LEAR, where Beard, et al. [BE84] found

$$\sigma_{TOT}(\bar{p}p) = (65.78 \pm 1.71) + (53.759 \pm 0.845)/P$$

in a very high statistics experiment. Very little low energy data is available for the total cross section on carbon, except for some early bubble chamber work [AG60] and the antiproton absorption cross section around 500 MeV/c measured by Aihara, et al. [AI81]. Aihara found that the carbon nucleus is black to antiprotons at these low momenta. A more recent experiment by Nakamura [NA94b] measured the absorption cross section between 470 and 890 MeV/c and the data agrees more or less with that of Aihara within quoted limits. These results indicated that simply scaling the  $\bar{p}p$  cross sections by the carbon nuclear area may be a reasonable

estimate of the interaction cross sections, at least for the total, annihilation, and elastic scattering cross sections. For this reason the Monte-Carlo program used

$$\sigma_{\text{TOT}}(\bar{p}^{12}\text{C}) = A^{2/3} \sigma_{\text{TOT}}(\bar{p}p)$$

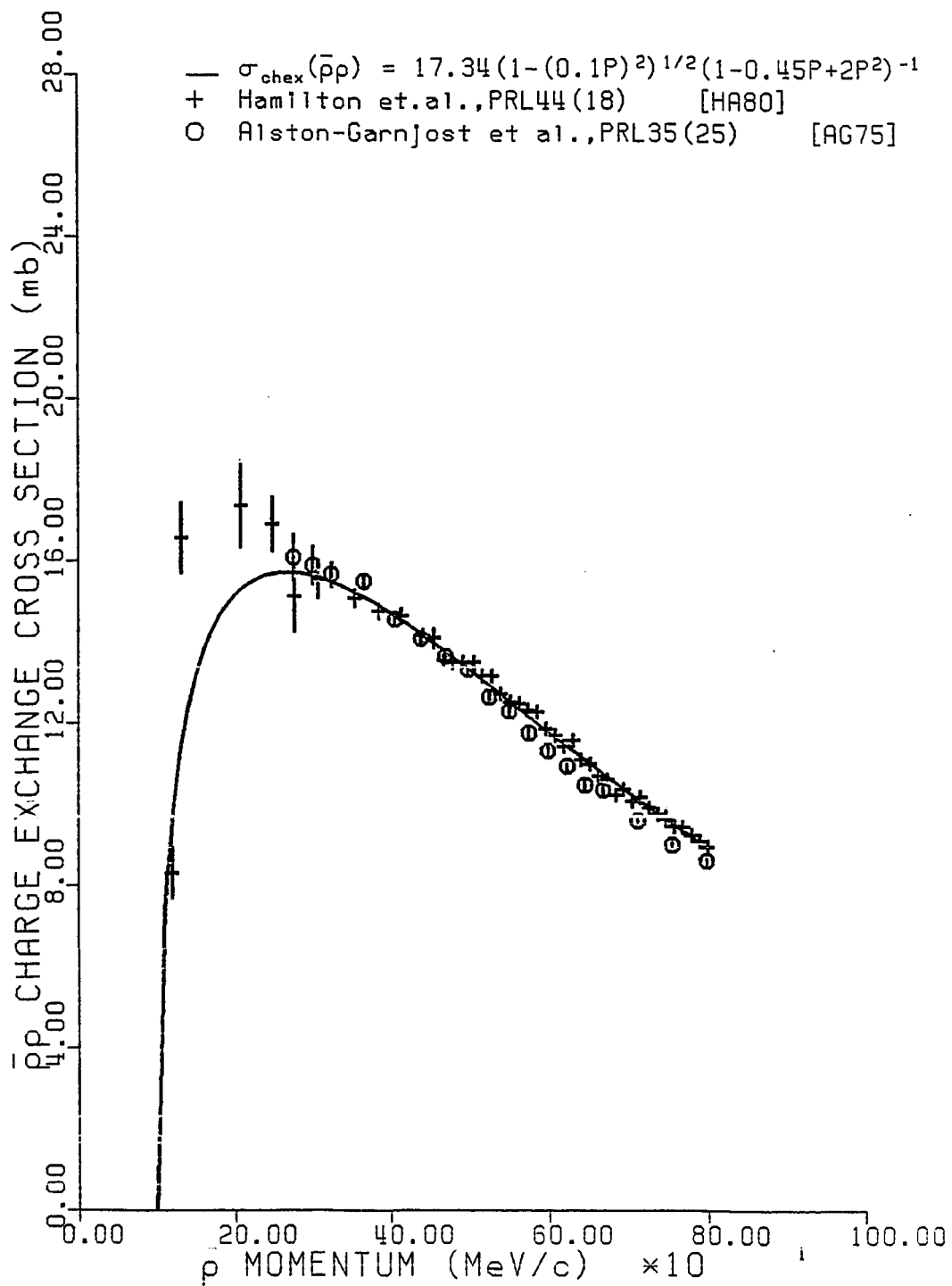
for the total cross section on carbon, where  $A$  is the atomic number of carbon.

The  $\bar{p}p$  charge-exchange cross section at low energy is shown in Figure 10. The data shown are those of Alston-Garnjost et al., [AG75] and Hamilton, et al., [HA80a], which are seen to be in close agreement. The parameterization used by the Monte-Carlo is that of Hamilton, given by

$$\sigma_{\text{CHEX}}(\bar{p}p) = \frac{17.34(1 - (0.1P)^2)^{1/2}}{(1 - 0.45P + 2.0P^2)}$$

where  $\sigma_{\text{CHEX}}$  is in millibarns and  $P$  is in GeV/c. A more recent measurement by Nakamura [NA80c] agrees with the result of Hamilton within quoted limits. Nakamura also measured the differential cross section for charge-exchange [NA80c]. The first observation of  $\bar{n}$  production from anti-protons incident on carbon was reported by Nakamura in 1984 [NA84a]. It was found that the shape of the angular distribution at 590 MeV/c was very similar to the  $\bar{p}p$  charge exchange reaction. Nakamura found the ratio of the  $\bar{n}$  production cross sections on hydrogen and carbon to be

FIGURE 10



$$\frac{\sigma(\bar{p}^{12}\text{C} \rightarrow \bar{n}X)}{\sigma(\bar{p}p \rightarrow \bar{n}n)} = 0.86 \pm 0.05 .$$

This result indicates that the production of antineutrons on carbon is suppressed from that on hydrogen. This can be understood by considering the fact that the mean free path of the antineutron in nuclear matter is very short, so that antineutrons that are produced have a high probability of subsequently annihilating within the residual carbon nucleus. The Monte-Carlo incorporated Nakamura's result and used

$$\sigma_{\text{CHEX}}(\bar{p}^{12}\text{C}) = 0.86 \sigma_{\text{CHEX}}(\bar{p}p)$$

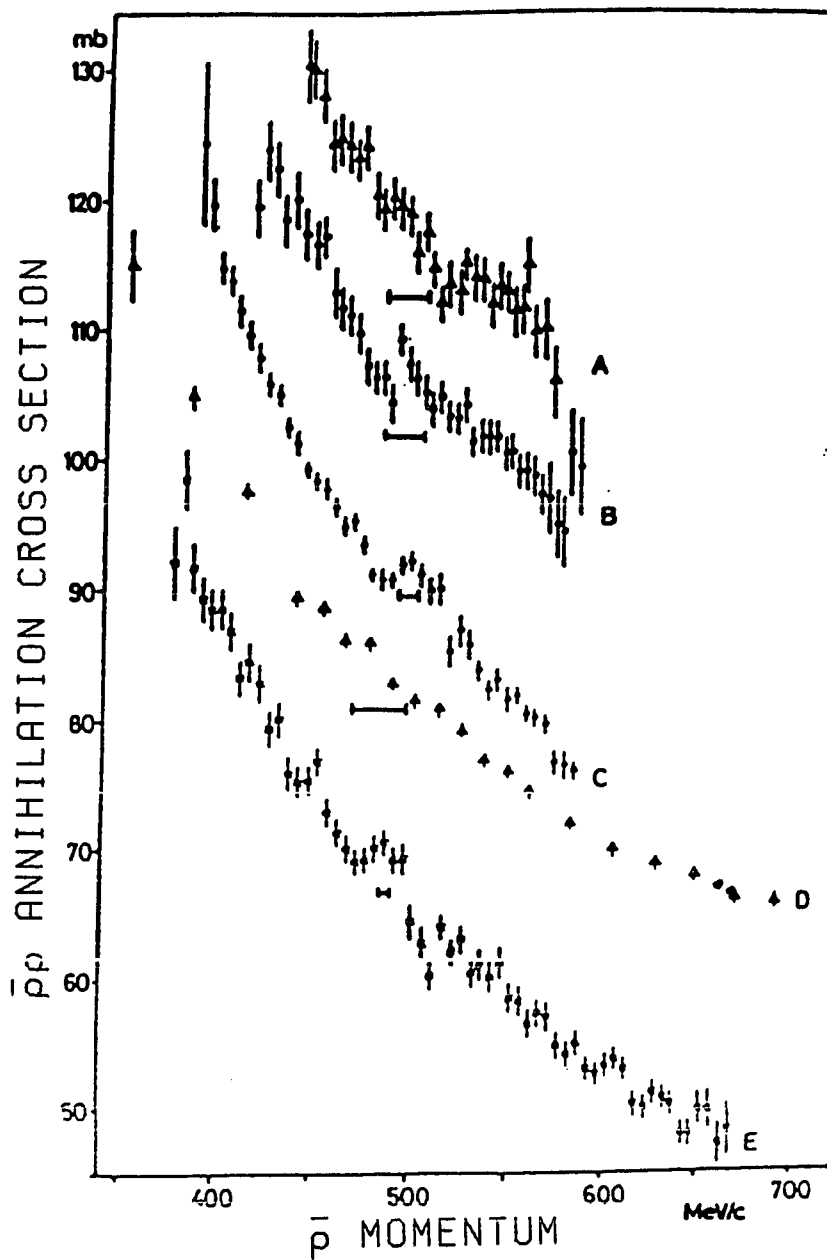
for the charge-exchange cross section on carbon.

Some of the most recent data for the  $\bar{p}p$  annihilation cross section is shown in Figure 11. The different sets of data have been shifted for clarity in the following manner: Lowenstein [LO81], +20 mb; Jastrzembski [EJ81], + 10 mb; Bruckner [BR77], 0 mb; Hamilton [HA80b], -10 mb; Amsler [AM82], -20 mb. The horizontal bars indicate the experimental resolution in the "S meson" region. It should be noted that there seems to be differences in the absolute normalization from experiment to experiment of a few percent. These data can be conveniently parameterized as

$$\sigma_{\text{ANN}}(\bar{p}p) = 38 + 35/P$$

where  $\sigma_{\text{ANN}}$  is in millibarns and  $P$  is in GeV/c (see [XU85]). This is the parameterization used by the Monte-

FIGURE 11



- |   |                     |         |
|---|---------------------|---------|
| A | Lowenstein, et al.  | [LGG1]  |
| B | Jastrzebski, et al. | [JJS1]  |
| C | Bruckner, et al.    | [BR77]  |
| D | Hamilton, et al.    | [HA80b] |
| E | Ameler, et al.      | [AMB2]  |

Carlo program. The cross section was assumed to be featureless. The annihilation cross section for antiprotons on carbon is essentially not known at low energy, except for some early bubble chamber work by Agnew [AG60] with poor statistics. For this reason, the Monte-Carlo assumed that the annihilation cross section scales as the nuclear area, as discussed earlier. Therefore, for annihilations in carbon it is assumed that

$$\sigma_{\text{ANN}}(\bar{p}^{12}\text{C}) = A^{2/3} \sigma_{\text{ANN}}(\bar{p}p)$$

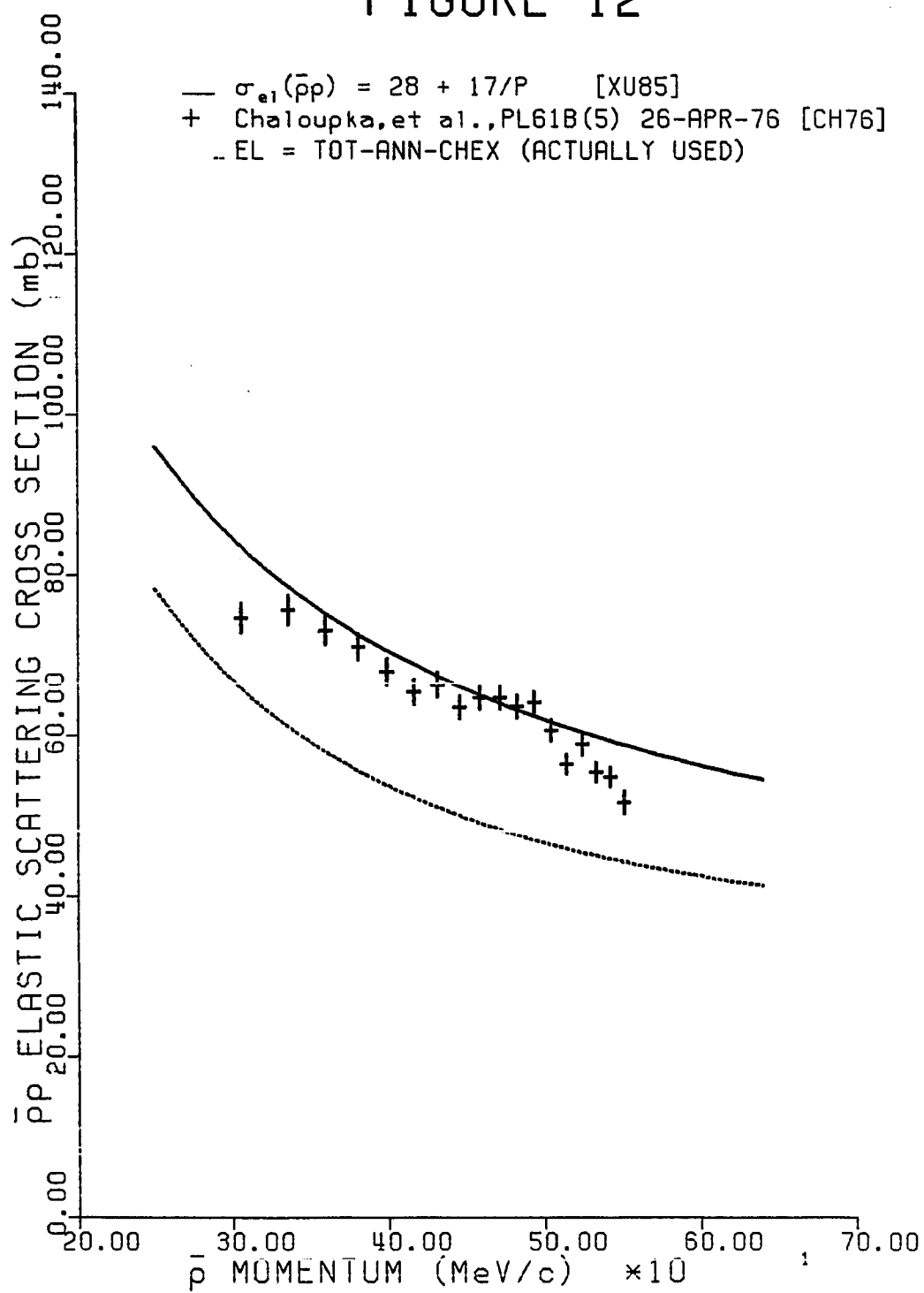
where  $\sigma_{\text{ANN}}$  is in millibarns and  $A$  is the atomic number of carbon.

Figure 12 shows the integrated elastic scattering data of Chaloupka [CH76], along with a convenient parameterization (solid line)

$$\sigma_{\text{el}}(\bar{p}p) = 28 + 17/P$$

where, again,  $\sigma_{\text{el}}$  is in millibarns and  $P$  is in GeV/c [GR83]. The only high statistics differential elastic scattering cross sections at low energy were measured by Nakamura [NA84c]. The differential cross section used by the Monte-Carlo was that measured by Nakamura at 490 MeV/c (see [NA84c]). The Monte-Carlo assumed that the differential elastic scattering cross section for antiprotons on carbon was approximately the same as that for  $\bar{p}p$  scattering.

FIGURE 12



The results of Nakamura [NA84b] and Garreta [GA84] show that this assumption is incorrect. The carbon data is actually much more sharply forward peaked than the  $\bar{p}p$  data because of Coulomb and Coulomb-nuclear-interference effects. At larger angles, the spectra show the characteristic pattern of diffraction scattering [NA84b]. This deficiency in the Monte-Carlo and its effects on the results will be discussed as it arises in Chapters VI and VII. The integrated elastic scattering cross section for carbon is, again, that for  $\bar{p}p$  scaled by the nuclear area:

$$\sigma_{el}(\bar{p}^{12}\text{C}) = A^{2/3} \sigma_{el}(\bar{p}p)$$

To summarize, the parameterizations for  $\bar{p}p$  interactions are as follows:

$$\sigma_{TOT}(\bar{p}p) = 64 + 52/P \quad [\pm 1\%]$$

$$\sigma_{ANN}(\bar{p}p) = 38 + 35/P \quad [\pm 5\%]$$

$$\sigma_{el}(\bar{p}p) = 28 + 17/P \quad [\pm 5\%]$$

$$\sigma_{CHEX}(\bar{p}p) = \frac{17.34(1 - (0.1P)^2)^{1/2}}{(1 - 0.45P + 2.0P^2)} \quad [\pm 2\%]$$

The values in brackets are estimated residual systematic errors (see [GR83]). It is clear from inspection of the above values that some renormalization is required, since the sum of the annihilation, elastic, and charge-exchange cross sections exceeds the value for the total cross section.

Since the elastic scattering cross section is the least well known of the four cross sections, the Monte-Carlo changed its value to be consistent with the other three cross sections, i.e. the program actually used

$$\sigma_{el}(\bar{p}p) = \sigma_{TOT}(\bar{p}p) - \sigma_{ANN}(\bar{p}p) - \sigma_{CHEX}(\bar{p}p).$$

This value for the elastic cross section is displayed as the dotted curve in Figure 12. Note that it is approximately 20% lower than the parameterized value given earlier. The cross sections for carbon use the  $\bar{p}p$  parameterizations given above scaled by the nuclear area  $A^{2/3}$ , except for charge-exchange, which uses the results of Nakamura [NA84a]:

$$\sigma_{CHEX}(\bar{p}^{12}C) = 0.86 \sigma_{CHEX}(\bar{p}p)$$

## B. Annihilation Multiplicities

Even though there have been several microscopic calculations recently attempting to describe the multiplicities of antinucleon-nucleon annihilation (see Chapter I), these theories involve fitting certain branching ratios to the available experimental data. This method may not be as enlightening as a somewhat less complicated approach using a statistical theory. For this reason, the Monte-Carlo described here used a statistical approach to determine the annihilation multiplicities. Most of the detailed information on  $\bar{p}p$  annihilation products comes from early bubble

chamber work, in particular that of Baltay [BA66] and Agnew [AG60]. The average pion multiplicity per annihilation is about 5, with about 4% of the annihilations resulting in a pair of K mesons. The Monte-Carlo program used the statistical theory of Fermi [SE60], [AE60] to determine the average pion multiplicity. This theory has some weak points, namely (a) it does not account for the percentage of kaons produced, and (b) it requires an unusually large interaction volume in order to give the correct average pion multiplicity. Specifically, Fermi's theory requires that the interaction volume be ten times that expected from the Compton wavelength of the pion. Nevertheless, it has been shown by calculation of phase space integrals that this solution is sufficiently accurate [AE60]. A table showing the number of pions expected as a percentage of the number of annihilations is shown in Appendix I. The charge correlations of the final state, i.e. the relative probabilities of the channels corresponding to the various alternatives of charged and neutral pions, are determined in the Monte-Carlo by the "correlation number" theory of Pais [PA60]. In this theory, Pais shows that the properties of a system of  $N$  pions are to a considerable extent determined by three quantum numbers  $(N_1, N_2, N_3)$ , the "correlation numbers" whose sum is  $N$ . The branching ratios for an  $N\pi$ -cloud into the various possible charge distributions compatible with the given  $N$  and the total charge are not

uniquely determined if only the isospin of a specific state is known [PA60]. However, Pais shows that unique results are obtained given the correlation numbers. The correlation numbers relate to the number of triples:  $3\pi$ -subsystems with  $I = 0$ ; the number of pairs:  $2\pi$ -subsystems with  $I = 1$ ; and the remaining singles from which a specific state can be composed. The results of Pais' calculations for  $\bar{p}p$  and  $\bar{p}n$  annihilations are given in Appendix I. Given the ratios calculated by Pais, and the average multiplicity as calculated by Fermi's method, the branching ratios for the various possible annihilation channels are determined. The value for the branching ratios used by the Monte-Carlo are given and compared to some results by Baltay in Appendix I. For annihilations on carbon, the Monte-Carlo assumed that the annihilation products at the instant of annihilation are the same as that for  $\bar{p}p$  or  $\bar{p}n$ , with the observed annihilation products resulting from subsequent pion interactions within the residual nucleus. For annihilations which have no protons or neutrons in the final state, the multiplicities are just those for  $\bar{p}p$  or  $\bar{p}n$  annihilation, depending upon which nucleon in the carbon nucleus annihilated. For annihilations which have one or more protons in the final state, the  $\bar{p}p$  or  $\bar{p}n$  multiplicities are modified by assuming that one of the outgoing pions is absorbed and ejects a proton (or neutron) from the residual nucleus. It is assumed that it is equally probable for any particular

pion to cause this, irrespective of its charge. The results of this scheme gives the branching ratios for  $\bar{p}$ -carbon annihilations given in Appendix I. Experimentally, Agnew [AG60] shows that the average number of pions emitted in a  $\bar{p}$ -carbon annihilation is about 4, with approximately one "heavy prong" per star. In one of the only high statistics experiments on  $\bar{p}$ -carbon annihilations, Wade [WA76] gives two crucial bits of information required to make this Monte-Carlo scheme work: (1) the ratio of  $\bar{p}p$  to  $\bar{p}n$ -like annihilations on carbon is 0.632, and (2) the percentage of annihilations on carbon which result in "heavy prongs" (protons) being emitted are: no protons, 46.5%; one proton, 28.7%; two protons, 14.7%. The Monte-Carlo allowed total multiplicities up to seven, with as many as two protons in the final state.

### C. Monte-Carlo Flow Chart

The flow chart for the Monte-Carlo program is given in Figures 13a-j. First arrays for the energy loss of various particles in different media are calculated. These arrays are calculated using the Bethe-Bloch equation, without the density and shell correlation terms. Later the energy loss for a given pathlength is calculated using a fast parabolic interpolation technique. Next, the arrays for the differential elastic cross-sections used are read in, and the

FIGURE 13a

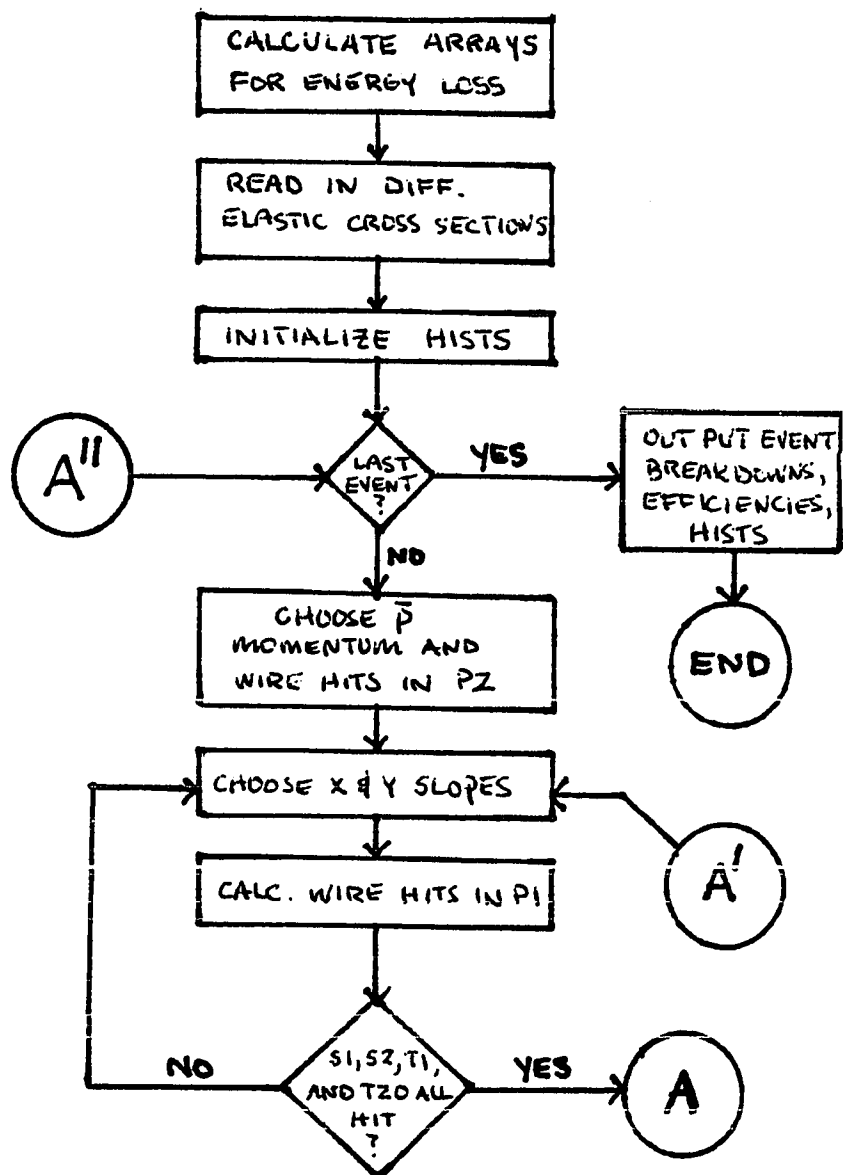


# FIGURE 13b

62

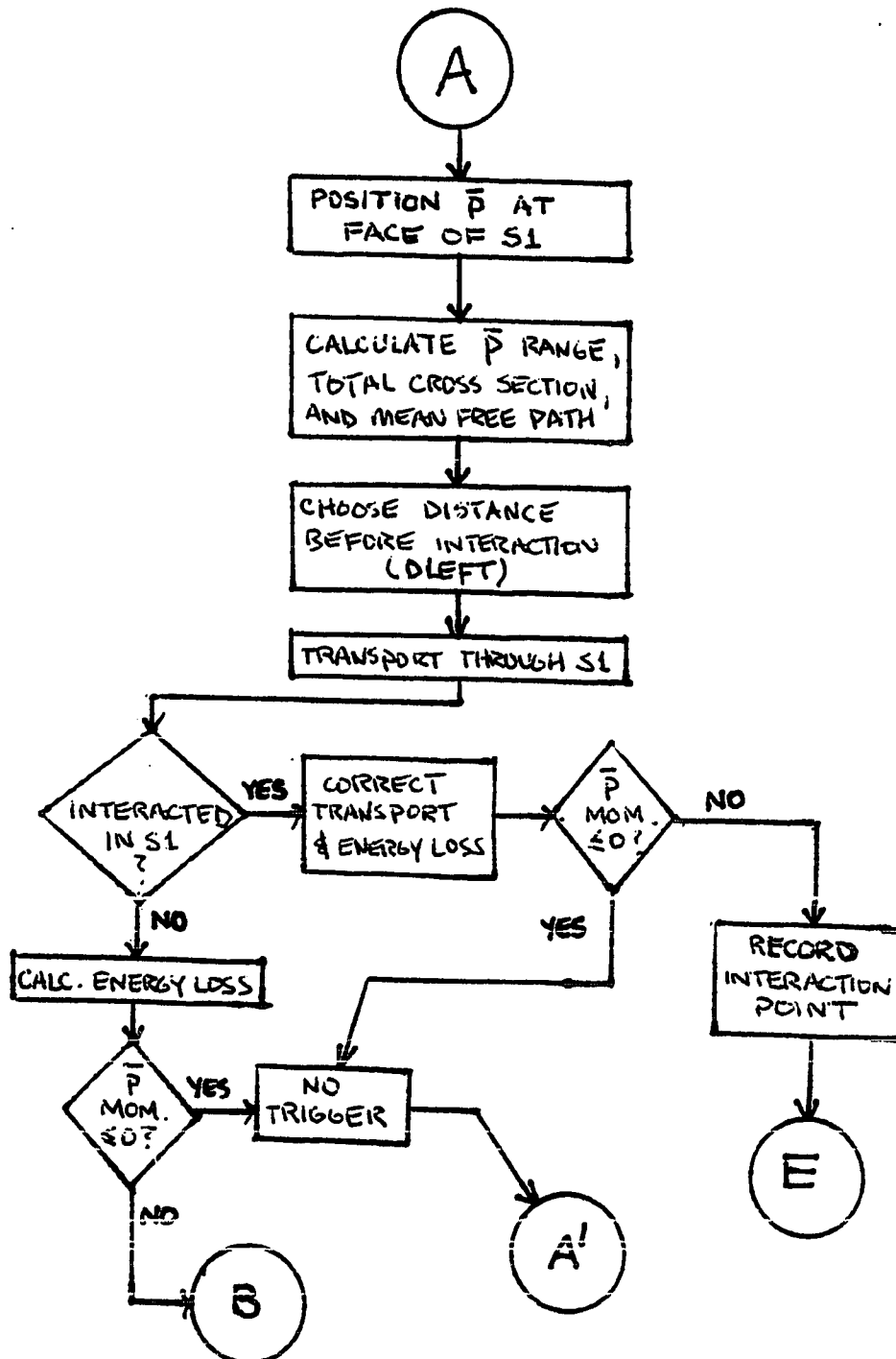


FIGURE 13c

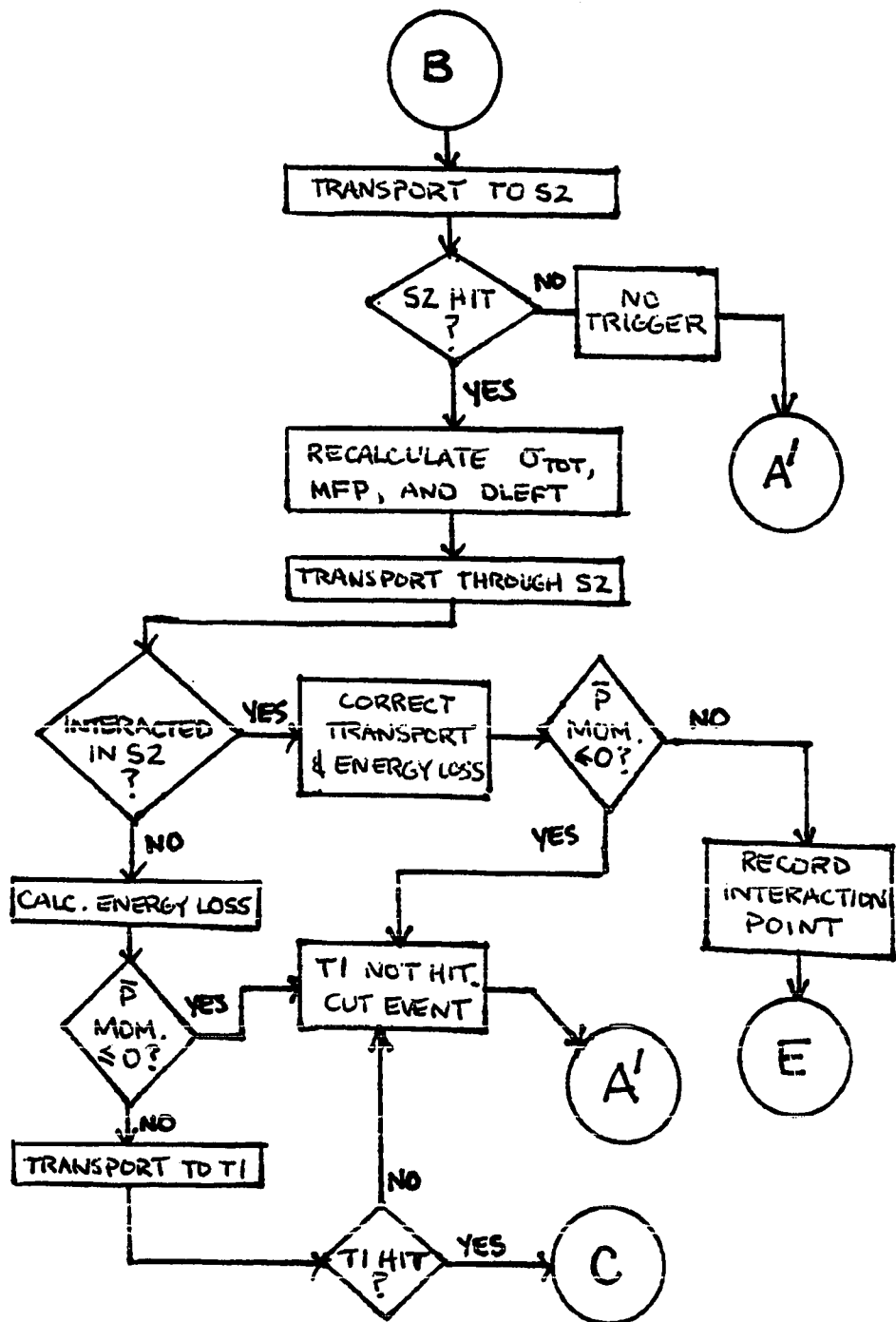


FIGURE 13d

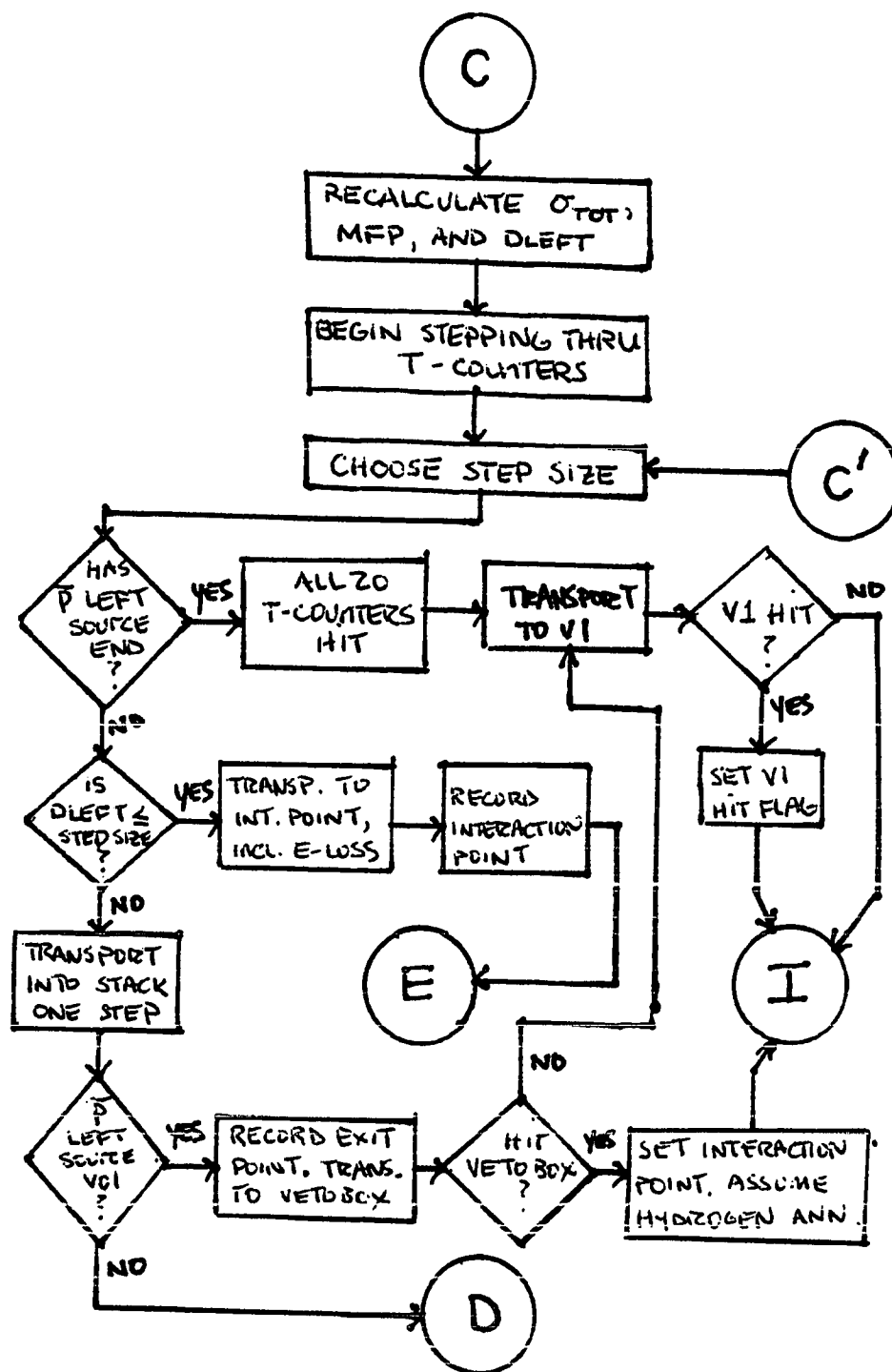


FIGURE 13e

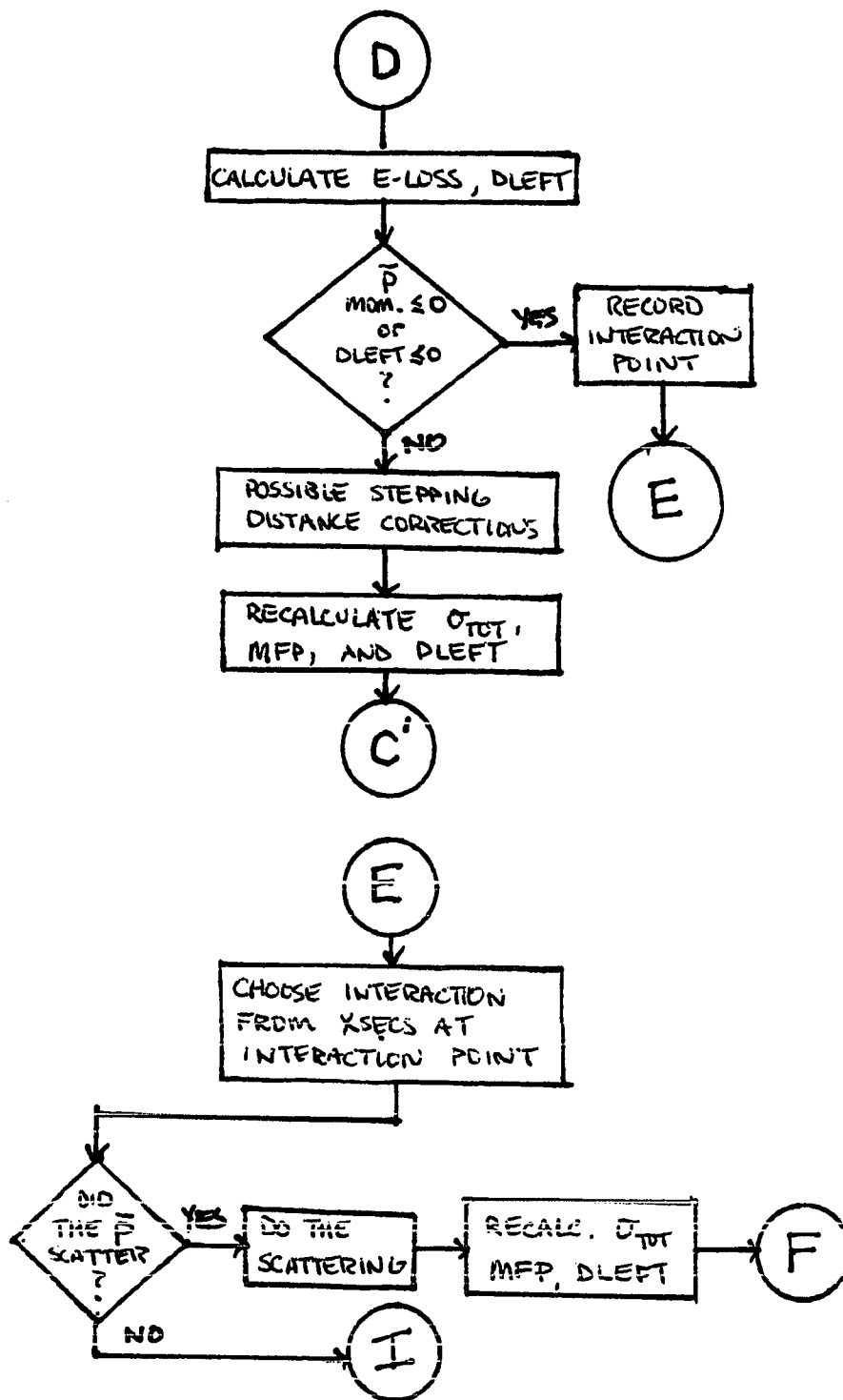


FIGURE 13f

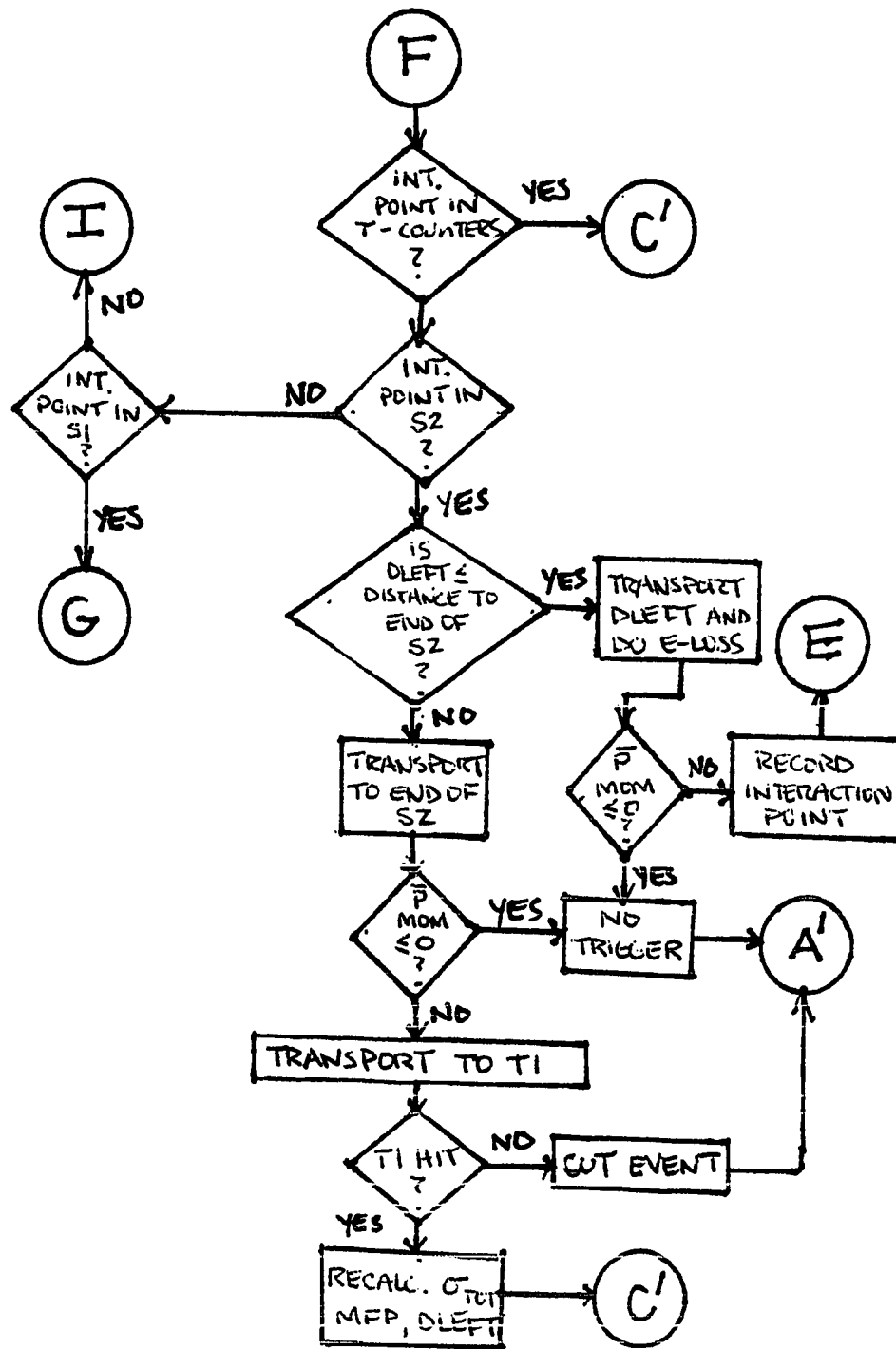


FIGURE 13g

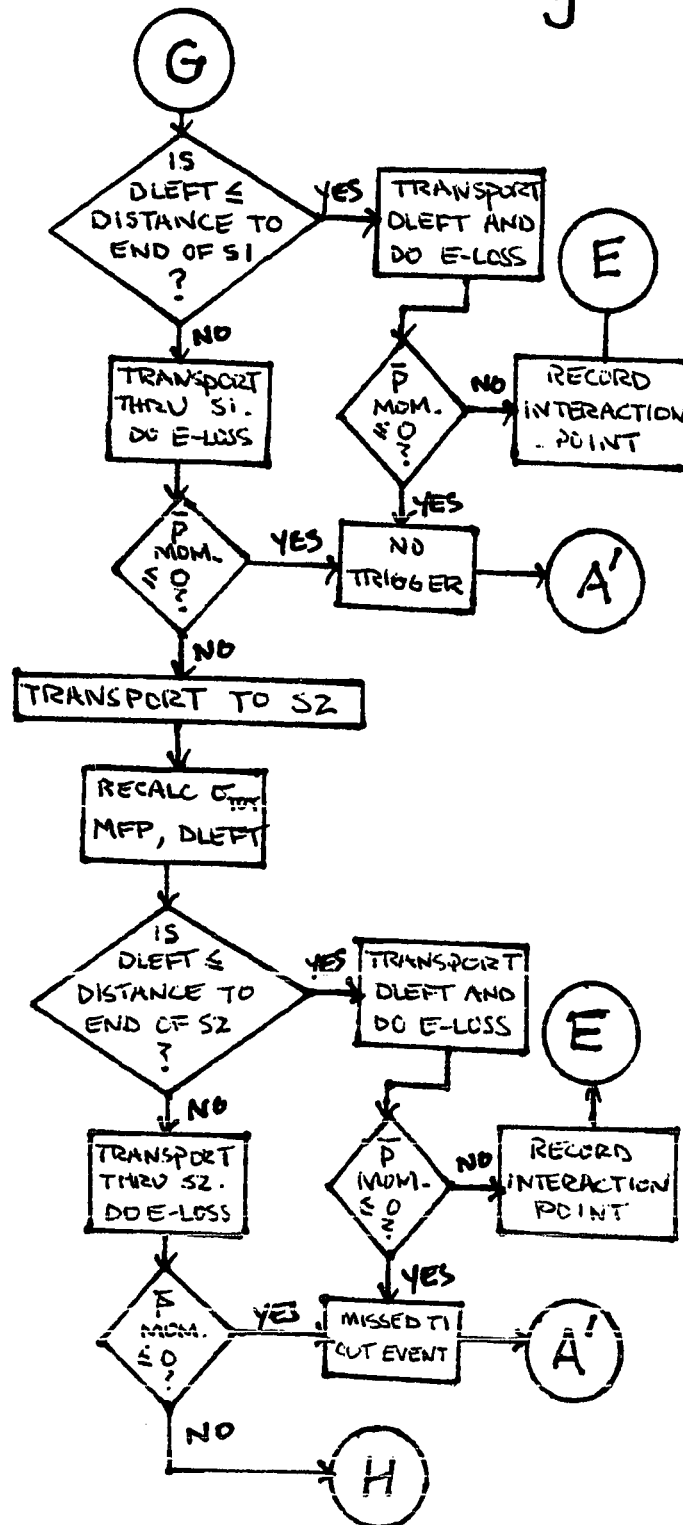


FIGURE 13h

68

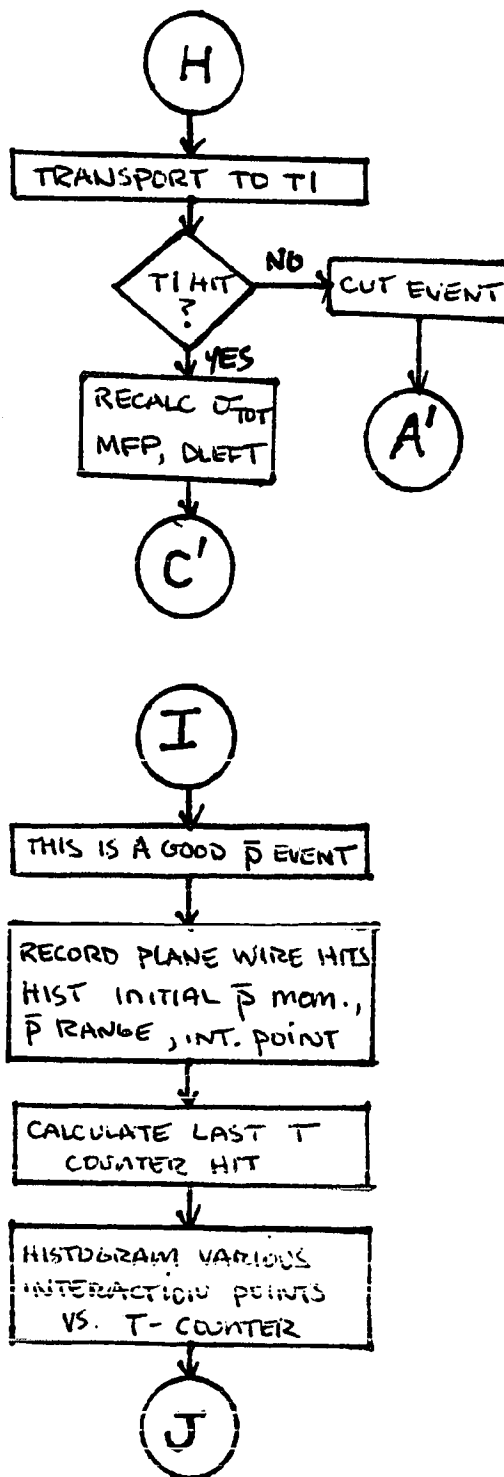


FIGURE 13i

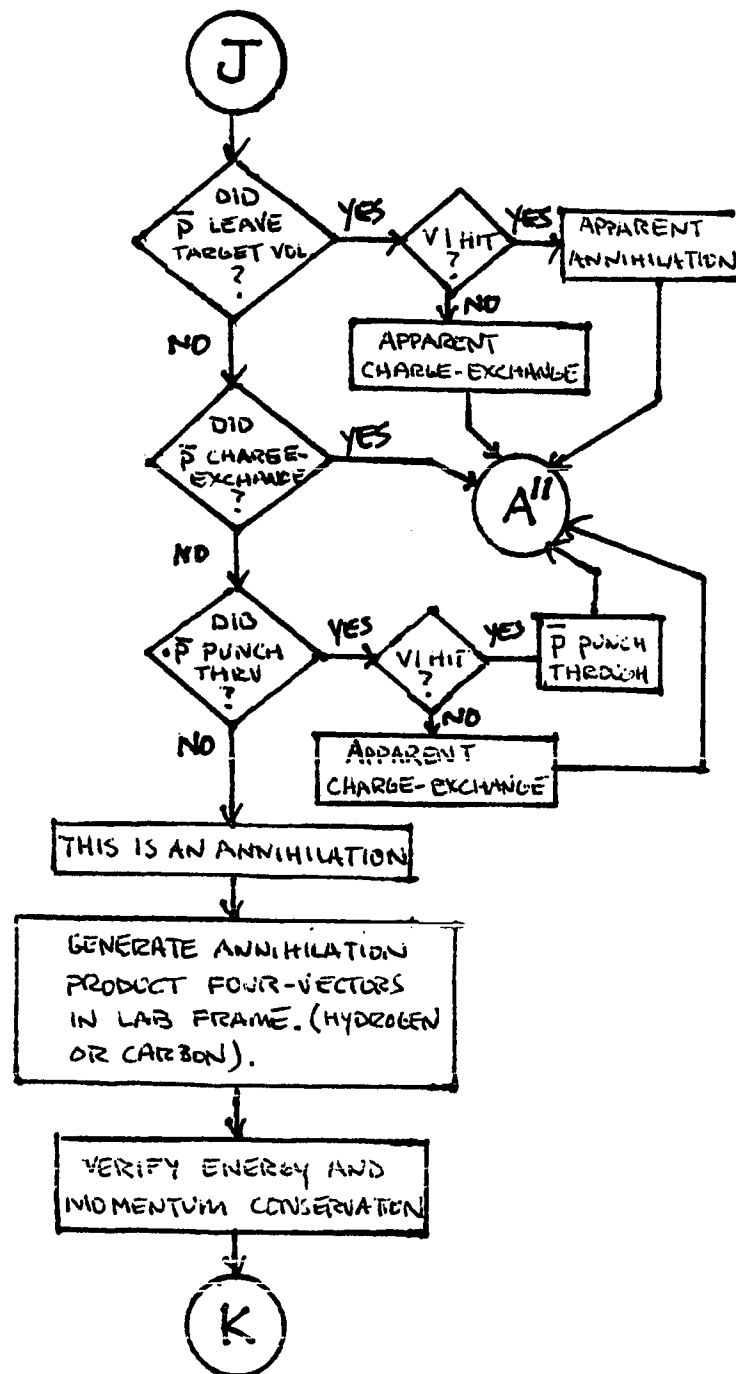
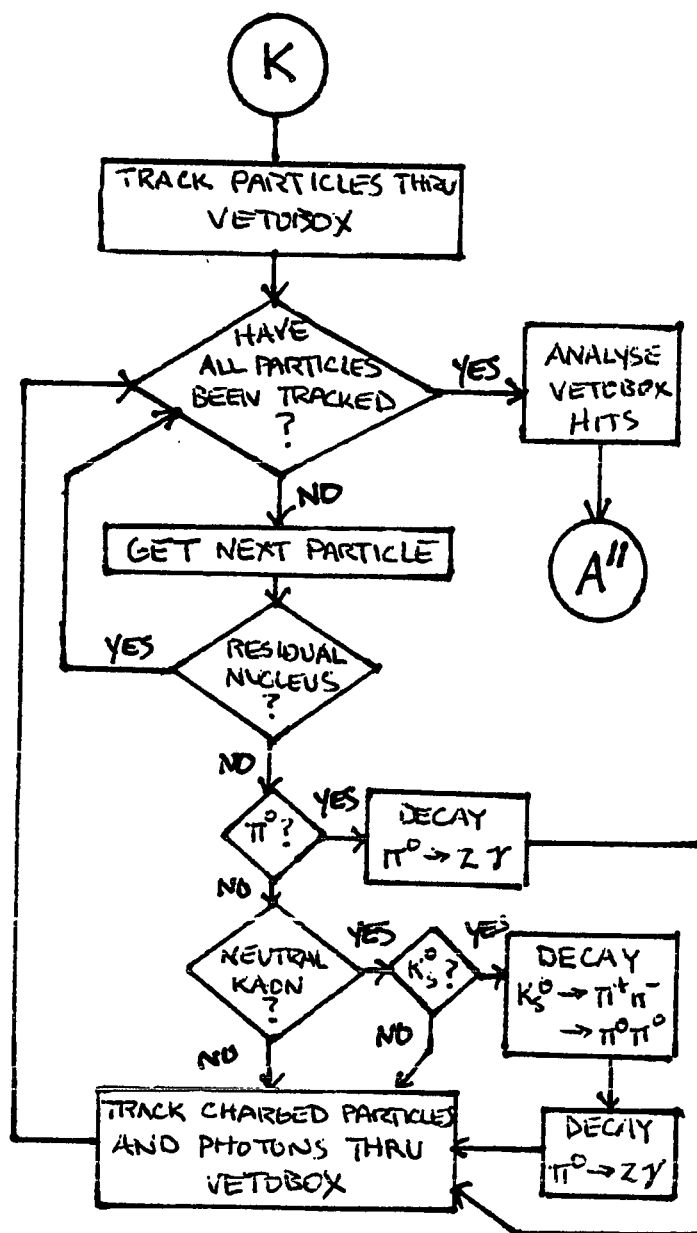


FIGURE 13j



histograms are initialized. With these preliminaries out of the way, event generation is begun. First the antiproton's initial momentum is chosen from a gaussian distribution centered on the beam momentum, with  $\Delta p/p \sim 7\%$ . In addition, wire hits on the X and Y coordinates of plane 2 are chosen based on triggered (measured) beam profiles. Next, the X and Y slopes of the particles trajectory are chosen. The measured X slope was the least well behaved and the most difficult to parameterize because of its assymmetry. Most of the error in the beam's phase space probably lies in this step. Once the slopes are chosen, the  $\bar{p}$ 's track is projected through the first plane, as well as counters S1, S2, T1, and T20. Hits in both S1 and S2 are required by the actual trigger logic. In addition, the analysis program required both that the particle's projected track lie completely within the source volume, and that there was a single hit in all four MWPC coordinates. Particles which do not meet these criteria are rejected, and new X and Y slopes are chosen. The  $\bar{p}$ 's momentum and hits in plane 2 are not rechosen (Figure 13a).

Antiprotons that make it this far are positioned at the face of S1 (Figure 13b). Here the  $\bar{p}$ 's range, apparent total cross section, and mean free path are calculated. Then a random "distance left before the next interaction" (DLEFT) is chosen based on an exponential decay of the beam and the calculated MFP. The  $\bar{p}$  is now transported stepwise through

the counters S1, S2, and T1-T20 until it reaches its interaction point. The  $\bar{p}$  has reached its interaction point when it comes to rest or when it has traveled the distance DLEFT. Stopping antiprotons are assumed to annihilate with a 1-1 ratio on hydrogen or carbon. The data analysis program required that the  $\bar{p}$  hit T1, so that any interactions in S1 or S2 other than scattering are rejected (Figures 13b,c). When a scattering does take place (Figure 13e) the kinematics are performed and the cross section, MFP, and new DLEFT are calculated. Transport resumes from the scattering point (Figure 13f). Multiple elastic scattering is allowed (Figures 13e-h).

The antiprotons are transported through the source (T1-T20) in small steps which become smaller as the  $\bar{p}$  gets farther into the stack (Figures 13d-e). This is done because of the rapid rise of the cross section at low momenta. The  $\bar{p}$  continues to step through the source until (a) it leaves the downstream end of the source stack after hitting all twenty T-counters, (b) it interacts, or (c) it leaves the source volume through the sides. Antiprotons which hit all twenty T-counters are transported downstream to determine if they hit the beam veto paddle V1. Those which miss V1 are "fake" charge-exchange events, while those that hit V1 are  $\bar{p}$ 's "punching through" (Figure 13i). Antiprotons which leave the source sides are first transported to the first layer in the vetobox. If the  $\bar{p}$  hits the vetobox it is

assumed to have the same multiplicities as annihilation on hydrogen. If the  $\bar{p}$  misses the vetobox and V1 it is assumed to be a "fake" charge-exchange (Figure 13i).

Once the  $\bar{p}$  reaches its interaction point, the interaction that takes place is chosen based on the ratios of the cross sections at the point of interaction. Events where the  $\bar{p}$  scatters are handled as described above (Figure 13e). Events where the  $\bar{p}$  leaves the target volume are classified appropriately and the next event is begun (Figure 13i). For events where a charge-exchange occurs, the interaction point is recorded appropriately and the next event is begun. Note that the two-body kinematics of the charge-exchange reactions are not performed, and the resulting neutron and antineutron are not tracked through the apparatus (Figure 13i). The effects of the deficiency on the results will be discussed in Chapters VI and VII.

The only events which have not ended by this point are annihilations, both at rest and in flight. The four-vectors of the annihilation products are generated uniformly in Lorentz-invariant phase space by a simplified version of the program SAGE, written by Jerome Friedman [JF71]. The annihilation products themselves are chosen randomly from the different possible modes, based on the distributions discussed earlier (see Appendix I). After the annihilation four-vectors are chosen, the resulting mesons are tracked

through the vetobox, and the resulting hits in counters B1-B12 and V1 are recorded in an array. Residual nuclei from carbon events are not tracked because of their short range. All neutral pions are decayed into two photons before tracking. The neutral  $K_S^0$  mesons are also allowed to decay before tracking. This program does not simulate the showering of photons in the lead of the vetobox. The vetobox counters are assumed to be 98% efficient for photon detection. Once all of the annihilation products have been tracked, the array of vetobox hits for the event is analyzed to determine the various multiplicities in the same fashion as in the data analysis program (Figure 13j). After the vetobox analysis, the next event is begun. Finally, after all of the requested events have been generated, the output of event breakdowns, multiplicities, and histograms occurs and the program is terminated (Figure 13a).

#### D. Energy Loss

It should be noted that as the antiproton traverses the source, the apparent total cross section, mean free path, and random distance left before interaction (DLEFT) are recalculated every time the particle loses energy. In addition, an attempt has been made to approximate the fluctuations in the  $\bar{p}$ 's energy loss. The equation describing the energy loss of heavy charged particles in thin targets was

first solved by Landau [LA44], and later solved rigorously by Vavilov [VA57], whose distribution is a generalization of the Landau distribution. Vavilov's significant parameter is designated  $\kappa$ , which is the ratio of the mean energy loss for a given path length to the maximum possible energy loss per collision. Vavilov showed that for  $\kappa \leq 0.01$  the Vavilov distribution may be replaced by the Landau distribution. In addition, Seltzer and Berger [SB64] showed that for  $\kappa \geq 10.0$ , the Vavilov distribution goes over to a gaussian distribution with mean value

$$\mu = \gamma - 1 - \beta^2 - \ln \kappa$$

and variance

$$\sigma^2 = (2 - \beta^2) / 2\kappa.$$

Here  $\gamma$  is Euler's constant. Programs for the generation of random numbers from the Landau and Vavilov distributions are available in the CERN program library [SC74]. However, inclusion of the exact Vavilov solution into this Monte-Carlo proved excessively time consuming, increasing the CPU time required for a given event by over an order of magnitude. Study of the energy loss of the antiprotons in scintillator at the momenta typical of this experiment showed that even though  $\kappa$  was typically around 0.2-0.4 for the path lengths chosen, the gaussian distribution was a sufficient approximation to the exact solution, especially for

the in-flight region. For this reason the gaussian approximation for the energy loss fluctuations was used exclusively, except for those instances where the Landau distribution was clearly applicable.

## CHAPTER VI

### COMPARISON OF DATA AND MONTE-CARLO RESULTS

The data for the  $\bar{n}$  source study was taken at incident antiproton momenta of 475, 515, 550, and 578 MeV/c. Three runs ( $\sim 30,000$  events each) were taken at each point in March, 1984. The trigger used for this study was

$$\text{PBAR} \cdot 50\% \text{ NBARSAMPLE}$$

as discussed in Chapter III (see Figure 6).

#### A. Antiproton Momenta

The measurement of the antiproton momentum by time-of-flight between the beam hodoscope and S1 had two main problems: (1) poor time resolution at the hodoscope (typically no better than  $2 \sim 3$  ns), and (2) insufficient knowledge of the length of the actual flight path. These two points made calibration with beam pions very difficult. The first problem caused the momentum distribution of the  $\bar{p}$ 's (as measured by TOF) to have  $\Delta p/p$  of 11.5-13.5%. The distribution was approximately gaussian, with a high momentum tail. The second problem caused the measured central beam momentum to be 2-3% lower than expected from the  $\bar{p}$ 's range in the T-counters. It was determined by Monte-Carlo calculations that the antiproton beam momentum could be determined to

better than 1% by matching the shape and location of the peak at the end of the  $\bar{p}$ 's range in the T-counters (see section B of this chapter). For 475 and 515 MeV/c data, this peak fell well within the source and the determination was more accurate than for 550 and 578 MeV/c data, where a large fraction of the  $\bar{p}$ 's punch through all twenty counters. The Monte-Carlo reproduced the shape of the peak quite well for the 475 and 515 MeV/c data using a centered gaussian distribution and a  $\Delta p/p$  of 6.7%. A calculation of beam optics based on the magnet settings was performed by J. Kruk [JK85] which indicated that the two higher momenta should be approximately 550 and 578 MeV/c. The width of these distributions was taken to be the same as before. Since few of the  $\bar{p}$ 's stop in the T-counters at these momenta, there is a large error in the absolute value of the momentum when calculated from the  $\bar{p}$ 's range, possibly as much as 2 to 3%. Therefore, it was decided that the values calculated from the magnet settings were more accurate than using the time of flight or the antiproton's range.

#### B. Annihilation Point

The annihilation point as a function of T-counter number for the four different incident  $\bar{p}$  momenta is shown in Figures 14-17. The Monte-Carlo values shown are for all annihilations with the exception of those which registered

FIGURE 14 475 MeV/c

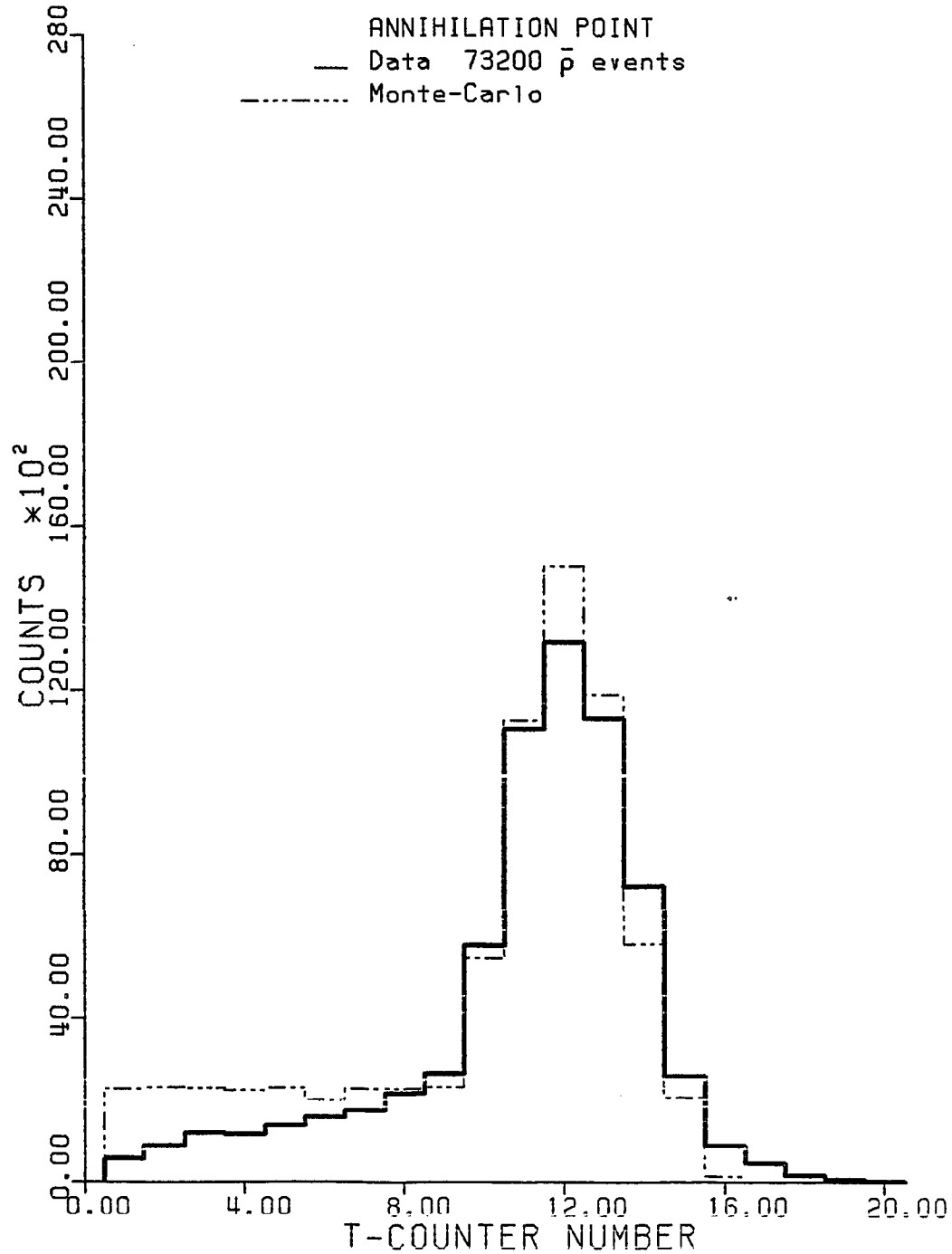


FIGURE 15 515 MeV/c

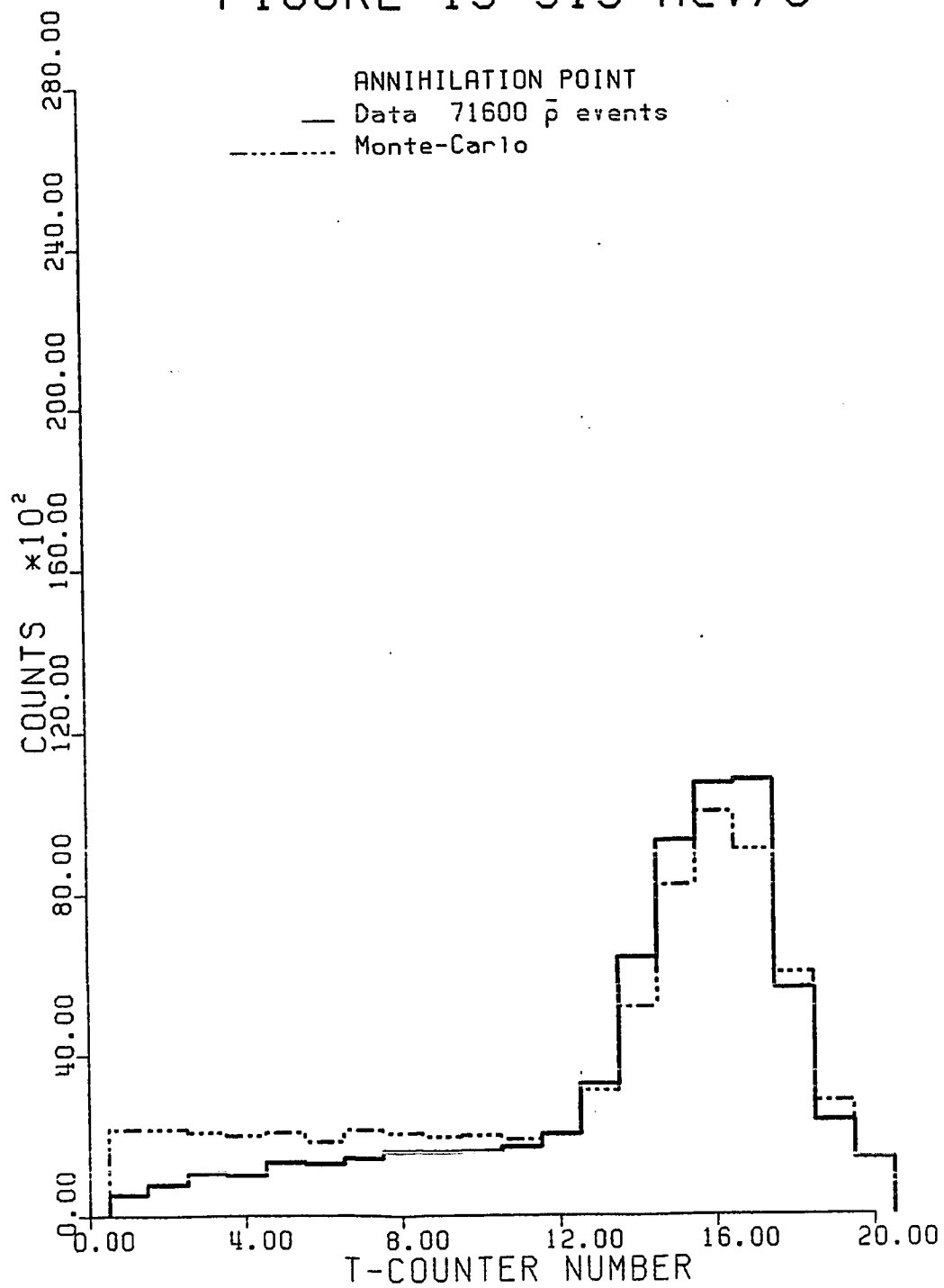


FIGURE 16 550 MeV/c

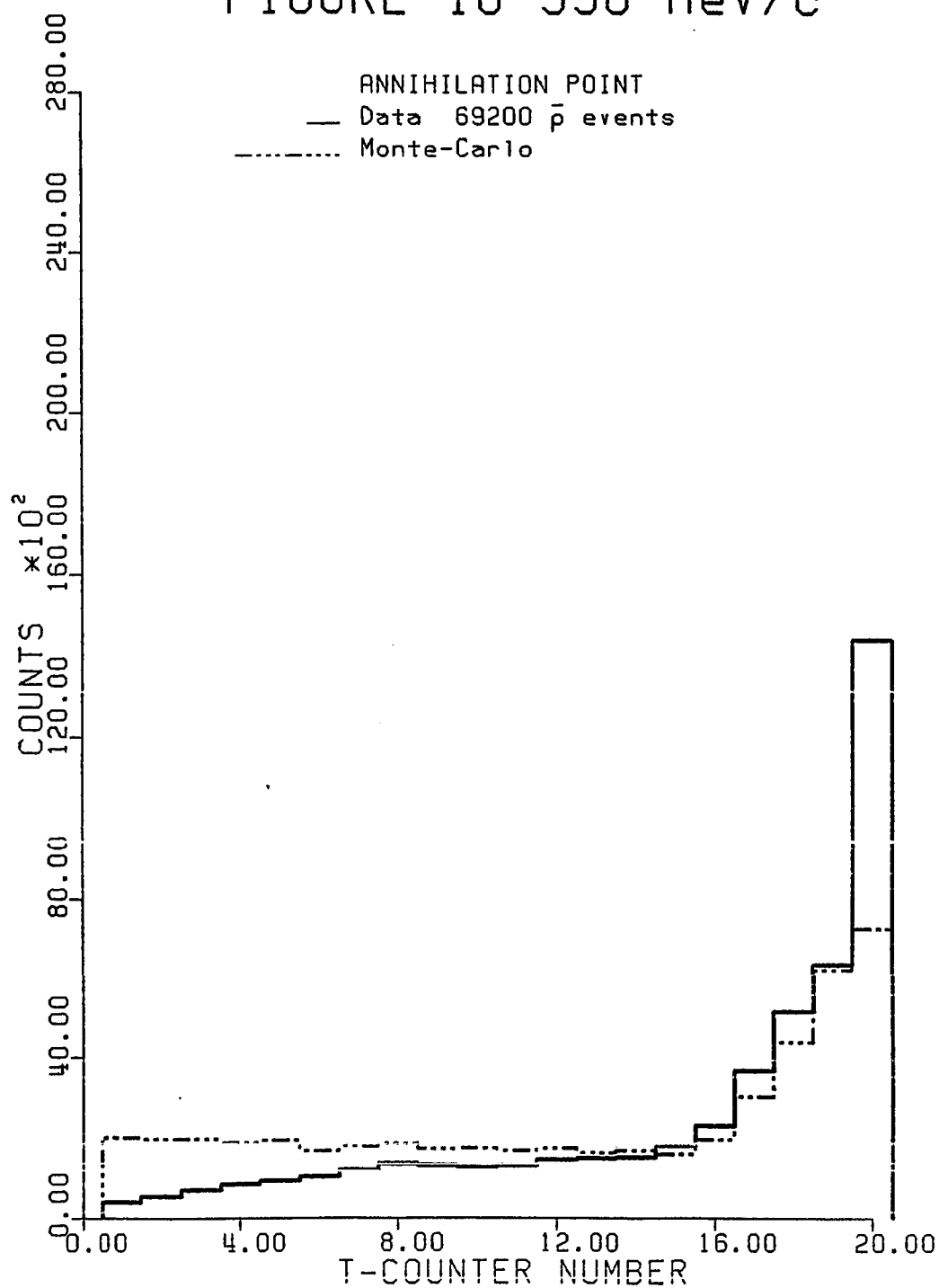
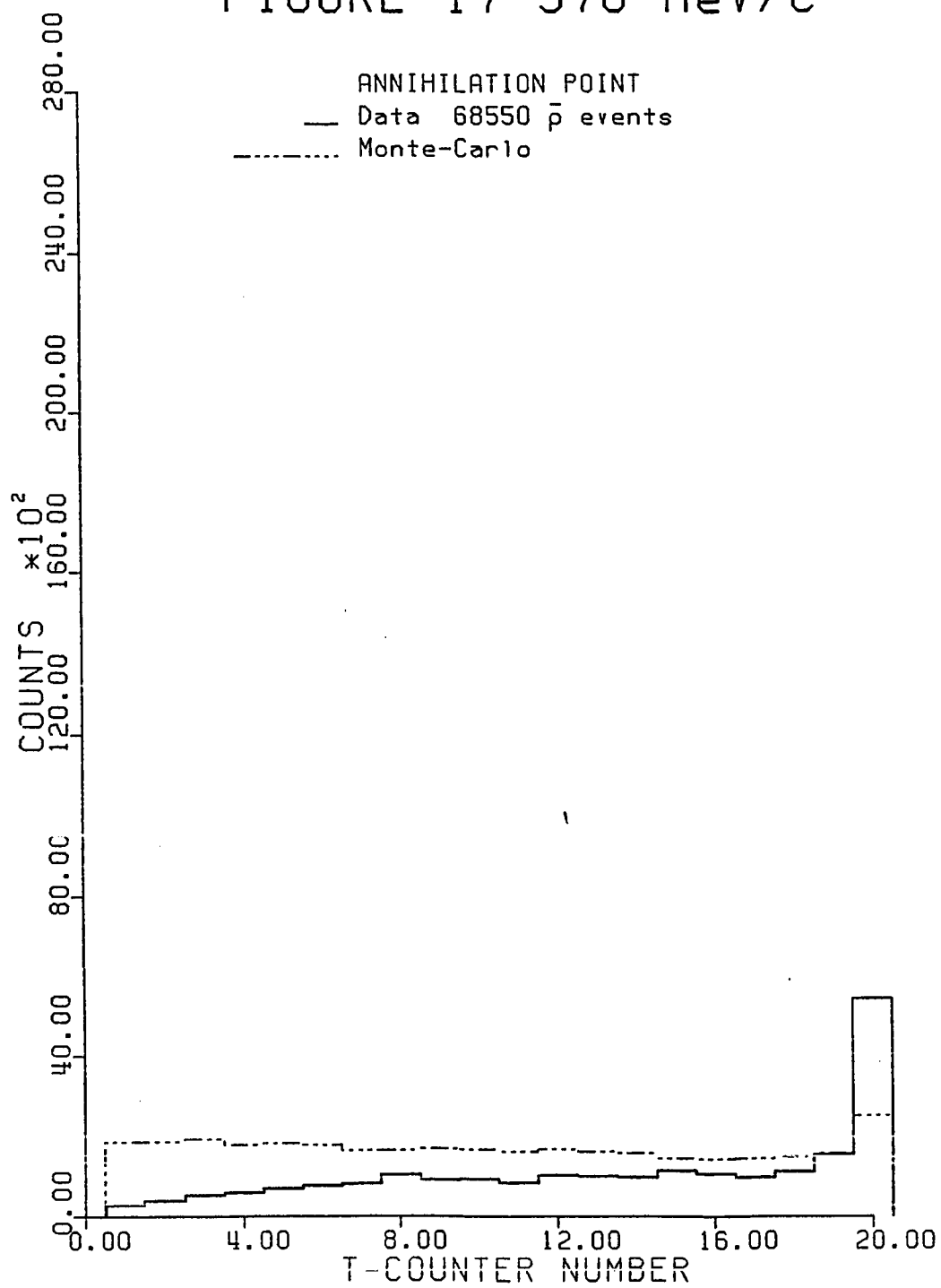


FIGURE 17 578 MeV/c



either (a) no hits in any of the veto counters, or (b) a single hit in the vetobox and no hit in V1. The unobserved annihilations of (a) were included in the charge-exchange sample. The annihilations of (b) were also included in the charge-exchange sample to mimic the hardware veto which allowed such events as possible charge-exchanges. (See Chapter II, section C.) The large peak seen in the 475 and 515 MeV/c data (Figures 14 and 15, respectively) corresponds to annihilations which occur as the  $\bar{p}$  comes to the end of its range. These are the peaks used to determine the  $\bar{p}$ 's momentum distribution as mentioned in section A of this chapter. At 550 MeV/c (Figure 16), about 24% of the antiprotons have a range that would stop them in the source. Thus, the rise at the end of the source is also due primarily to annihilations at rest. At 578 MeV/c (Figure 17), virtually none of the antiprotons should have a range that is less than or equal to T20. Thus, essentially all of the events at this momentum are annihilations in flight. This makes determining the momentum for these runs quite difficult and subject to greater uncertainty. At the two higher momenta, the data shows about a factor of two more counts in T20 than the Monte-Carlo. This excess of hits in T20 is probably due to the V1 TDC being out of time, so that when a  $\bar{p}$  punches through it does not register a hit in V1. A very early accidental pion could also strobe the V1 TDC in such a manner.

In general, the fit between the Monte-Carlo results and the data for the annihilation point is good. Examination of the figures shows that there are several features that appear not to be functions of momentum. Note that while the Monte-Carlo results are consistently higher than the data for the in-flight regions of the source, in general the peak at the end of the range is somewhat higher in the data than the Monte-Carlo. It is also important to note that the rise in the data in the first eight T-counters is also not a function of momentum. It was thought that this apparent lack of events in T1-T8 in the data may be due to the events that were cut which had greater than one non-sequential T-counter hit. A histogram was created from the data which showed the last sequential hit on those events which had  $>1$  non-sequential hit. This histogram showed tall peaks in counters T2 and T8, on a relatively flat background. These peaks must be due to either a malfunction in the discriminator or a weak tube in counters T3 and T9. This is seen irrespective of momentum. Clearly then, some of the missing events in T1-T8 are in fact annihilations which were cut because the event had  $>1$  non-sequential hit in the T-counters. However, this serves only to lower the apparent number of annihilation in the data, and does not explain the rise in T1-T8.

Another possibility for the difference in T1-T8 is a difference in the Monte-Carlo phase space, i.e. the angular

spread of the beam. If, in fact, the particles in the beam have a greater divergence than that used in the Monte-Carlo, they would tend to leave the source sooner, near the front of the source.

One more possibility was that the events cut for no hit in T1 and  $> 1$  non-sequential T hit were mostly valid annihilations where fluctuations in the  $\bar{p}$ 's energy loss caused the ADC for a given counter to fall below the threshold value required in the data analysis program for a  $\bar{p}$  in that counter. However, an attempt to verify this by lowering the ADC thresholds in the program by 10 and 25% proved unsuccessful. This was not surprising, since a reasonable approximation for the energy loss fluctuation was included in the Monte-Carlo program (see Chapter V, section D).

Another point to mention is that in the in-flight region, the annihilation pions tend to go forward in the lab, and this could fool the analysis program if multiple pions in a single counter gave a large enough pulse height to mimic a  $\bar{p}$ . It is worth noting that, because of the nature of the source analysis, when the data analysis program makes an error in determining the last sequential counter hit, it almost always will place the event further downstream than it actually occurred. On the other hand, the Monte-Carlo analysis tends to place the annihilation point further upstream than the actual data, especially in the in-flight region. This is because the Monte-Carlo does

not take into account such possibilities as multiple annihilation products mimicing a  $\bar{p}$  after the annihilation. This is the most likely reason for the rise seen in T1-T8 in the data.

### C. Charge-Exchange Point

The possible charge-exchange events from the data consisted of two types: (1) events which had no vetobox counters fire, and (2) events which had one vetobox counter fire. Events of the second type were included because the trigger logic for E-767 allowed such events to go to tape. This was done so that charge-exchange events where the neutron or antineutron gave a hit in one of the vetobox counters or where there was a spurious single hit in the vetobox would not be vetoed.

These two types of charge-exchange events should be compared with events from the Monte-Carlo which would be triggered in the same way. For events which had no vetobox counters fire, the Monte-Carlo includes actual charge-exchanges as well as undetected annihilations. For events which had a single vetobox counter fire, the Monte-Carlo includes only those annihilations where only one counter was hit. The effect of charge-exchange neutrons or antineutrons giving single hits in the vetobox was not included.

As mentioned in Chapter V, the Monte-Carlo program does not actually generate the antineutron and neutron four-vectors when the charge-exchange takes place. This means that any subsequent interactions of the neutron or antineutron in the surrounding veto counters are ignored. The effect of this will be to include more events with no hits in the vetobox (specifically, actual charge-exchanges) in the Monte-Carlo sample than will appear in the actual data. This is because the data will classify an event where the  $\bar{n}$  annihilates in or near the vetobox as either an annihilation or as an event with non-sequential T hits.

In order to estimate the magnitude of this effect, the  $\bar{n}$  annihilation cross section must be known at low energy. By considering the result for  $\bar{p}p$  annihilation shown in Figure 11, a reasonable number for the annihilation cross section is at least 100 mb. This value can be scaled by the nuclear area  $A^{2/3}$  for the various materials in the vetobox in order to determine a mean free path in each of the different layers of lead, aluminum, and scintillator. For the value of 100 mb, the various mean free paths are: lead, 8.6 cm (3.4"); NE102A, 33 cm (13"); aluminum, 18.4 cm (7.25"). Now, given the amount of material in the vetobox layers (see Figure 3), and assuming (a) 45° incidence, (b) a constant cross section, and (c) all layers were hit, these mean free paths indicate that 23-25% of the incident  $\bar{n}$ 's will annihilate in the sides of the vetobox.

There are several contributing factors which make this value an underestimate. First, the initial value of 100 mb for the annihilation cross sections is probably a reasonable guess for the peak of the  $\bar{n}$  momentum spectrum (  $\sim 450$  MeV/c ), but clearly antineutrons with a lower momentum initially will start out with a higher cross section and thus a greater chance of annihilating in the vetobox. Second, the antineutron will occasionally scatter and lose energy, and the annihilation cross section is probably a rapidly increasing function of the decreasing momentum, rising at least as fast as  $1/p$ . Third, there is a substantial amount of material in the immediate vicinity of the source and vetobox that was not included in this calculation that, nevertheless, will provide material for  $\bar{n}$  annihilations. This material includes the plexiglass light guides of the T-counters (see Figure 2), the vetobox light guides, phototubes, and the source stand. Any material that is close enough to allow annihilation pions to hit the vetobox counters in time will contribute to the number of  $\bar{n}$ 's removed from the sample. Fourth, and finally, the differential charge-exchange cross section of Nakamura [NA80c], is forward peaked, allowing a substantial number of  $\bar{n}$ 's to go through the vetobox at shallower angles so as to produce longer flight paths in the various media.

Taking all of these factors into account, it seems possible that the initial estimate of 23-24% could be low

by as much as a factor of 2 or 3. Therefore, it seems reasonable to consider that anywhere from 25-75% of the anti-neutrons produced in the source may be lost due to subsequent annihilation in the vetobox and surrounding material. The effects of this on the results can be anticipated. Specifically, the number of events in the data with no hits in the vetobox will be lower than that predicted by the Monte-Carlo by a substantial fraction. Assuming that the angular distribution does not change substantially with momentum, this will give the T-counter distribution in the data essentially the same shape as the Monte-Carlo, but with fewer counts. In addition, if the Monte-Carlo is correctly estimating the number of events with one hit in the vetobox that are due to  $\bar{p}$  annihilations, the number of events with one hit in the vetobox in the data will be slightly higher than in the Monte-Carlo because the Monte-Carlo does not include the possibility of the neutron or antineutron scattering and giving a single hit in the vetobox. This means that the number of events with one hit in the vetobox will be a larger percentage of the possible charge exchange events in the data than in the Monte-Carlo. These conclusions are valid at all momenta, keeping in mind that the number of annihilations included as possible charge-exchanges is a function of momentum, since most of them occur at rest.

Figure 18 shows the Monte-Carlo results for charge-exchange events at 475 MeV/c. The dotted curve shows

FIGURE 18 475 MeV/c

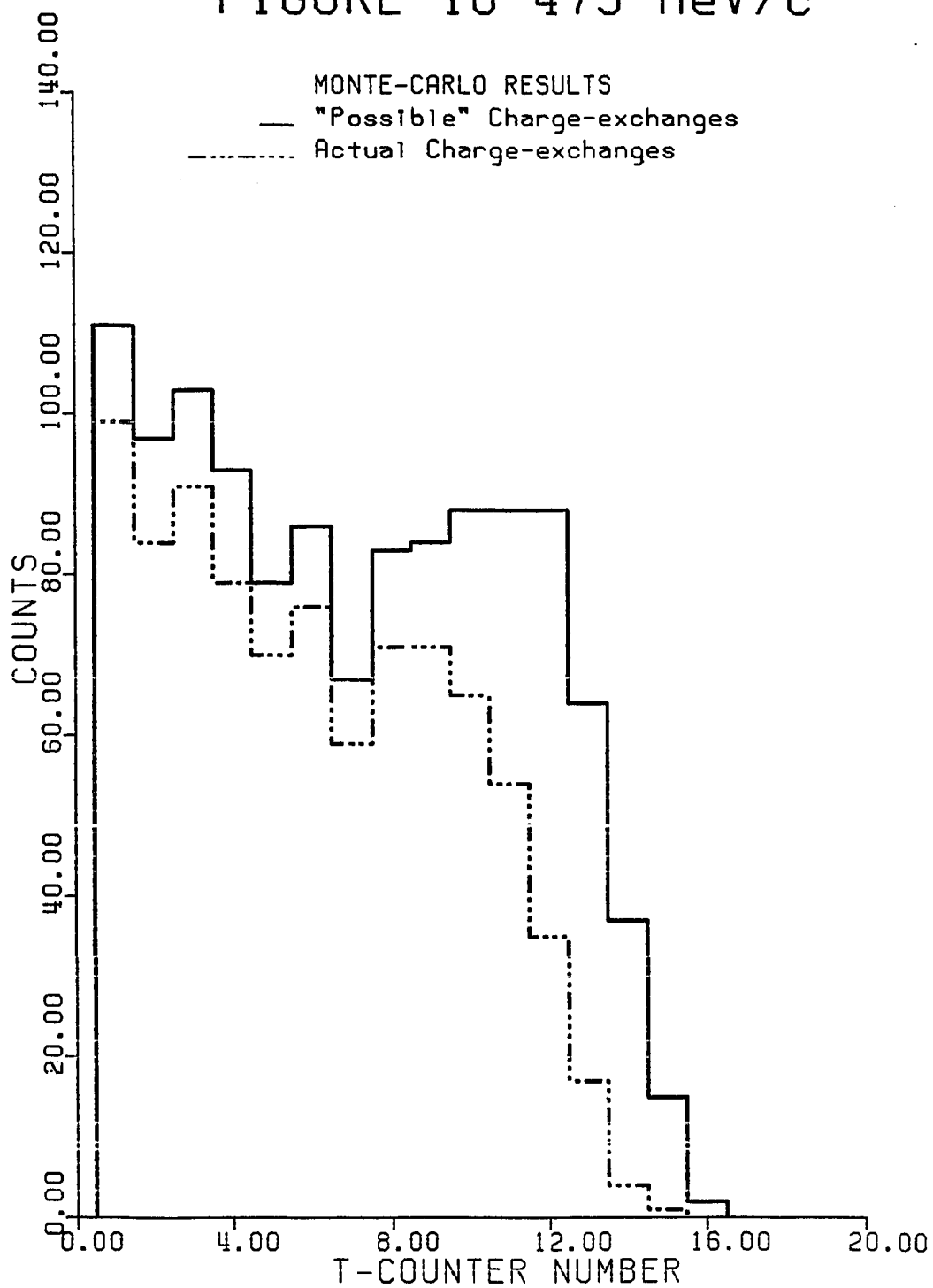


FIGURE 19 475 MeV/c

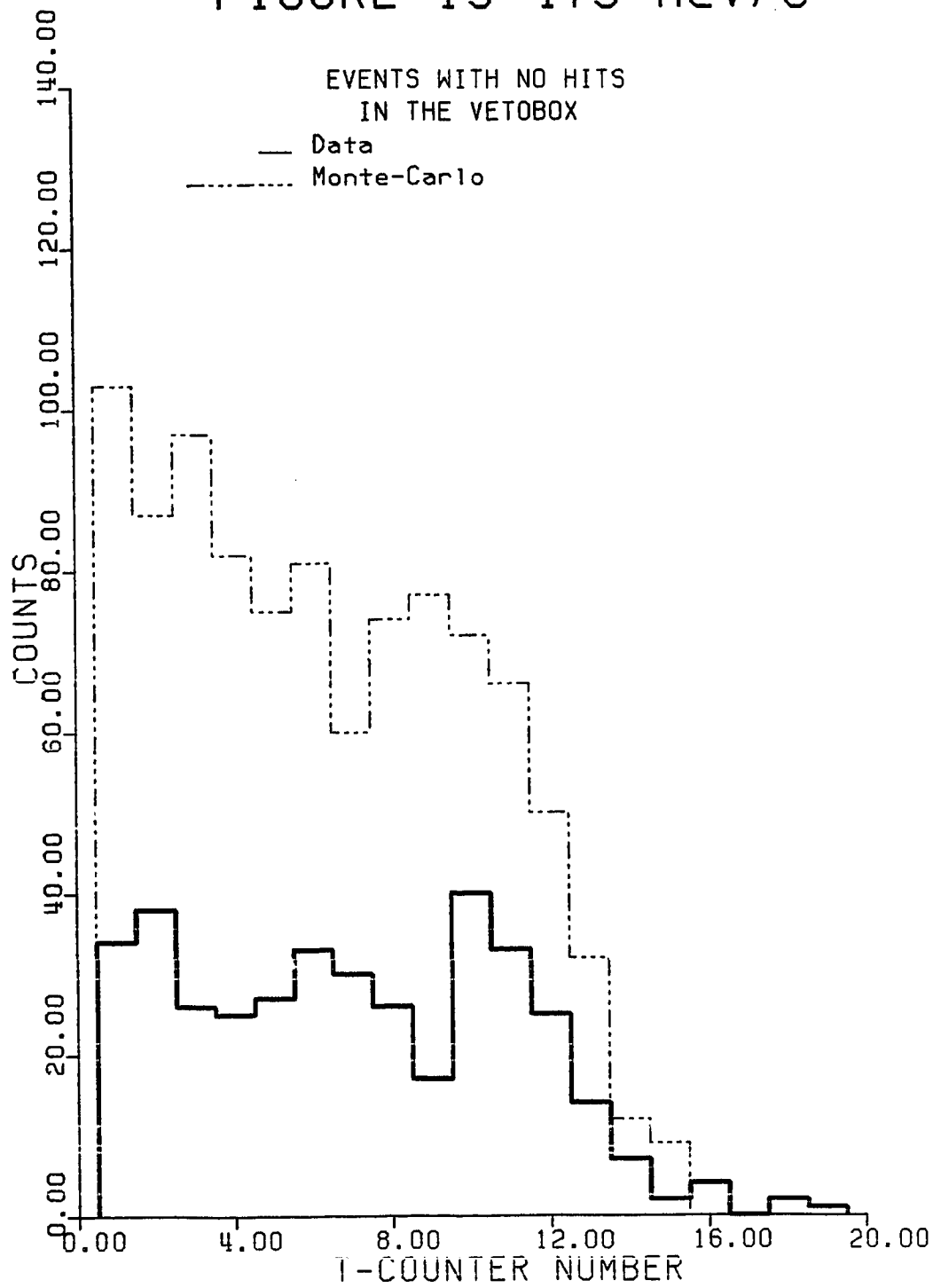
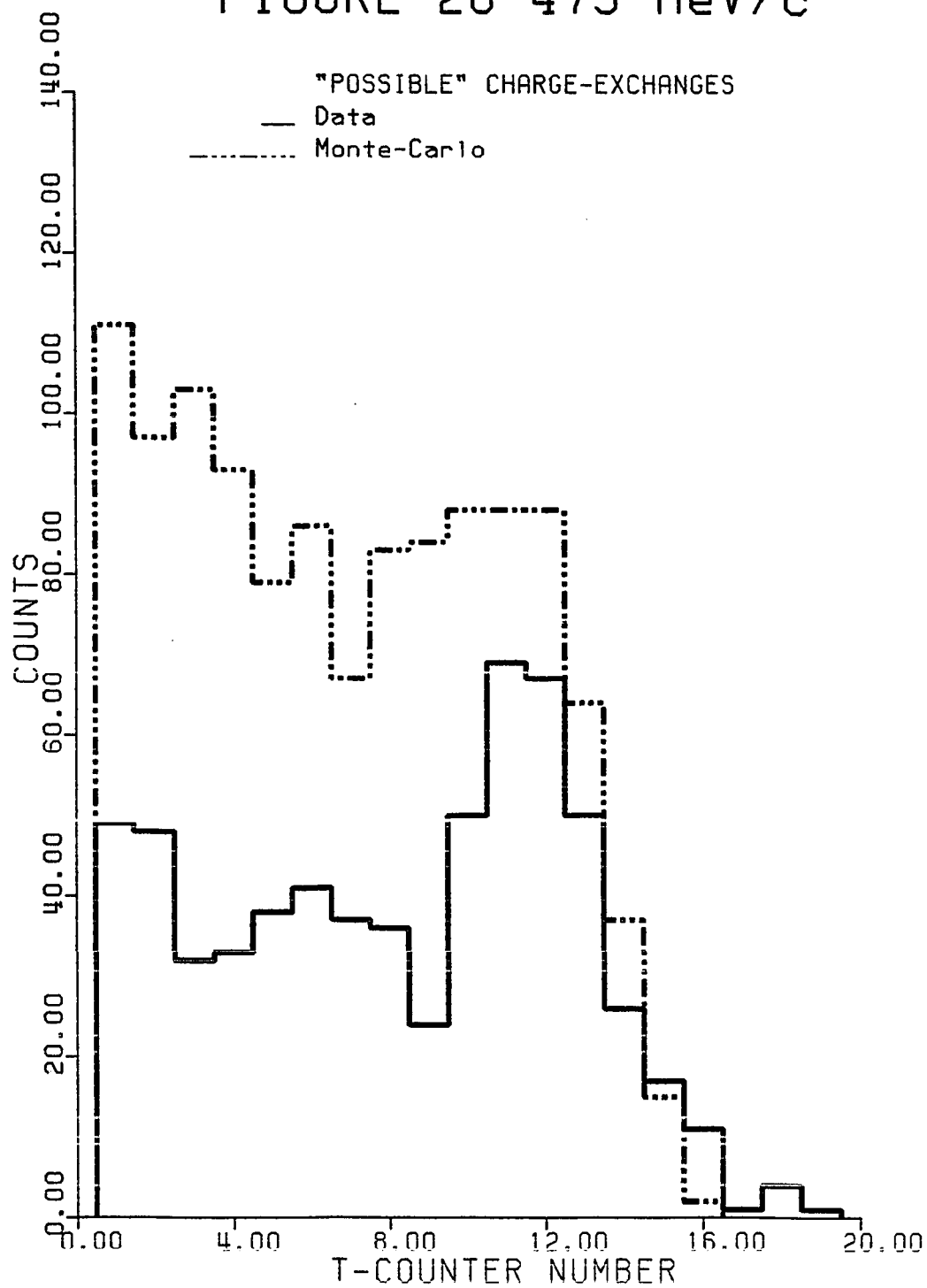


FIGURE 20 475 MeV/c



actual charge-exchanges from both hydrogen and carbon. The solid curve shows the total "possible" charge-exchange events that are used for comparison to the data. This includes both the actual charge-exchange events and annihilations where either (1) none of the annihilation products were observed in the vetobox or V1, or (2) a single counter in the vetobox was hit, but not V1. These annihilation events make up about 26% of the "possible" charge-exchanges at this momentum, with two-thirds of them occurring from annihilations at the end of the  $\bar{p}$ 's range.

The conclusions drawn above are seen to be confirmed by considering Figure 19. In this figure the events with no hits in the vetobox at 475 MeV/c are compared for the data and the Monte-Carlo results. The distributions show approximately the same cut-off point in the T-counters, which is typical of the 100 MeV/c threshold for the charge-exchange reaction. The experimental data has less than one-half of the events predicted by the Monte-Carlo, which is the anticipated result.

Figure 20 shows the total "possible" charge-exchanges for 475 MeV/c. Both the data and the Monte-Carlo curves include the events with no hits in the vetobox shown in Figure 19, as well as the events which had a single vetobox counter fire. The data has most of its events with one hit in the vetobox occurring at the end of the  $\bar{p}$ 's range, which indicates that they are primarily due to

annihilations at rest. These events account for about 0.34% of the total number of events in the data, as compared to 0.28% expected from the Monte-Carlo. These results are in good agreement, considering the earlier discussions.

The Monte-Carlo results for charge-exchange events at 515 MeV/c are shown in Figure 21. These results are quite similar to those at 475 MeV/c, except that more of the source can now produce antineutrons. About 24% of the "possible" charge-exchange events are annihilations, most of which occur at rest. The events with no hits in the vetobox from the data and the Monte-Carlo are compared in Figure 22. We again see the anticipated factor of 2 more Monte-Carlo events. Figure 23 compares the "possible" charge-exchanges at 515 MeV/c. The events in the data with one hit in the vetobox are seen to fall at the end of the  $\bar{p}$ 's range, and so are probably due to annihilations at rest. They account for about 0.32% of the total number of events, as compared to 0.28% expected from the Monte-Carlo.

The charge-exchange points for the Monte-Carlo events at 550 MeV/c are displayed in Figure 24. At this momentum, the Monte-Carlo predicts that about 26% of the  $\bar{p}$ 's should punch through the T-counters. This means that the momentum is now high enough to allow  $\bar{n}$  production in every T-counter. However, note that the Monte-Carlo also predicts a large number of annihilation events in T20. Figure 25 compares

FIGURE 21 515 MeV/c

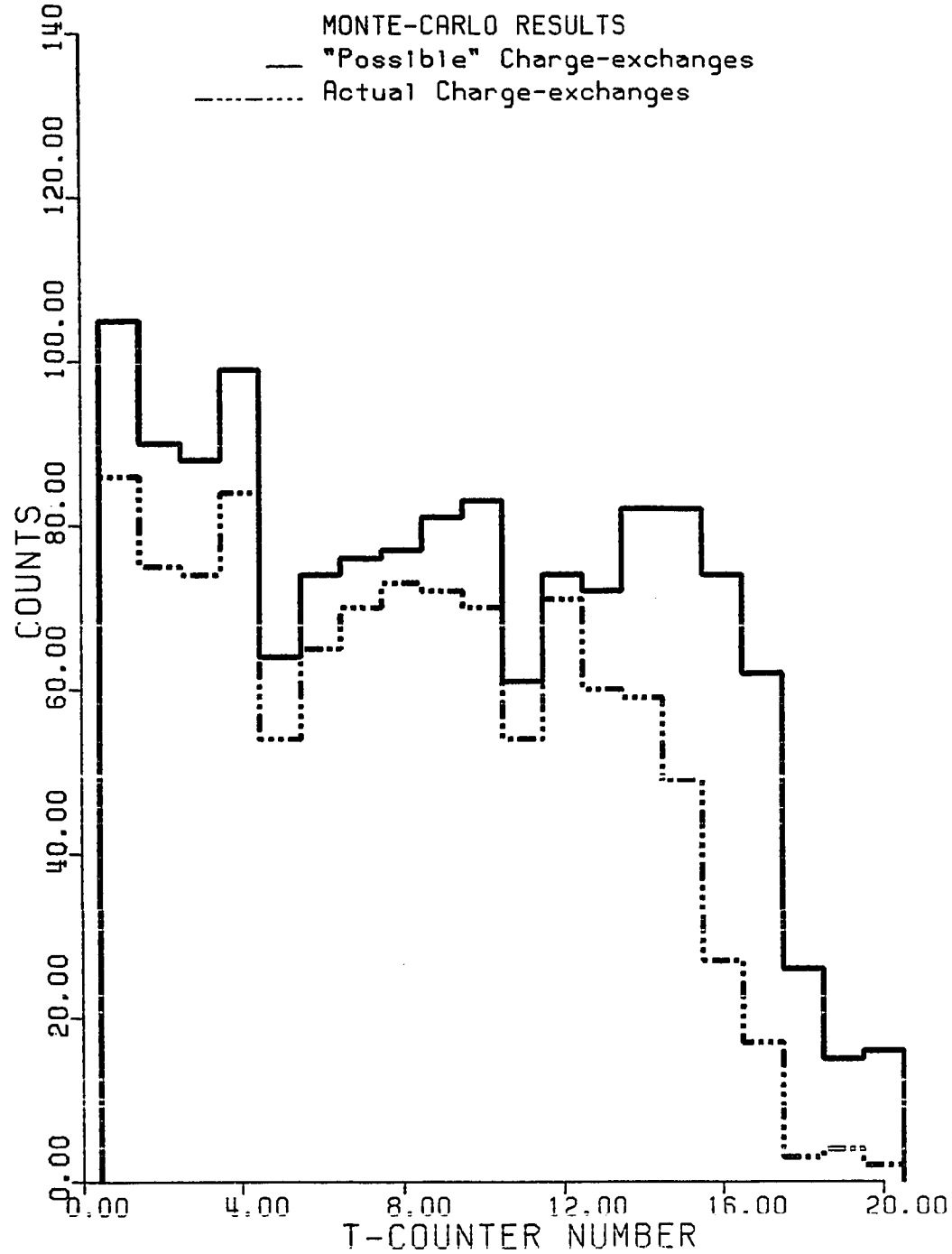


FIGURE 22 515 MeV/c

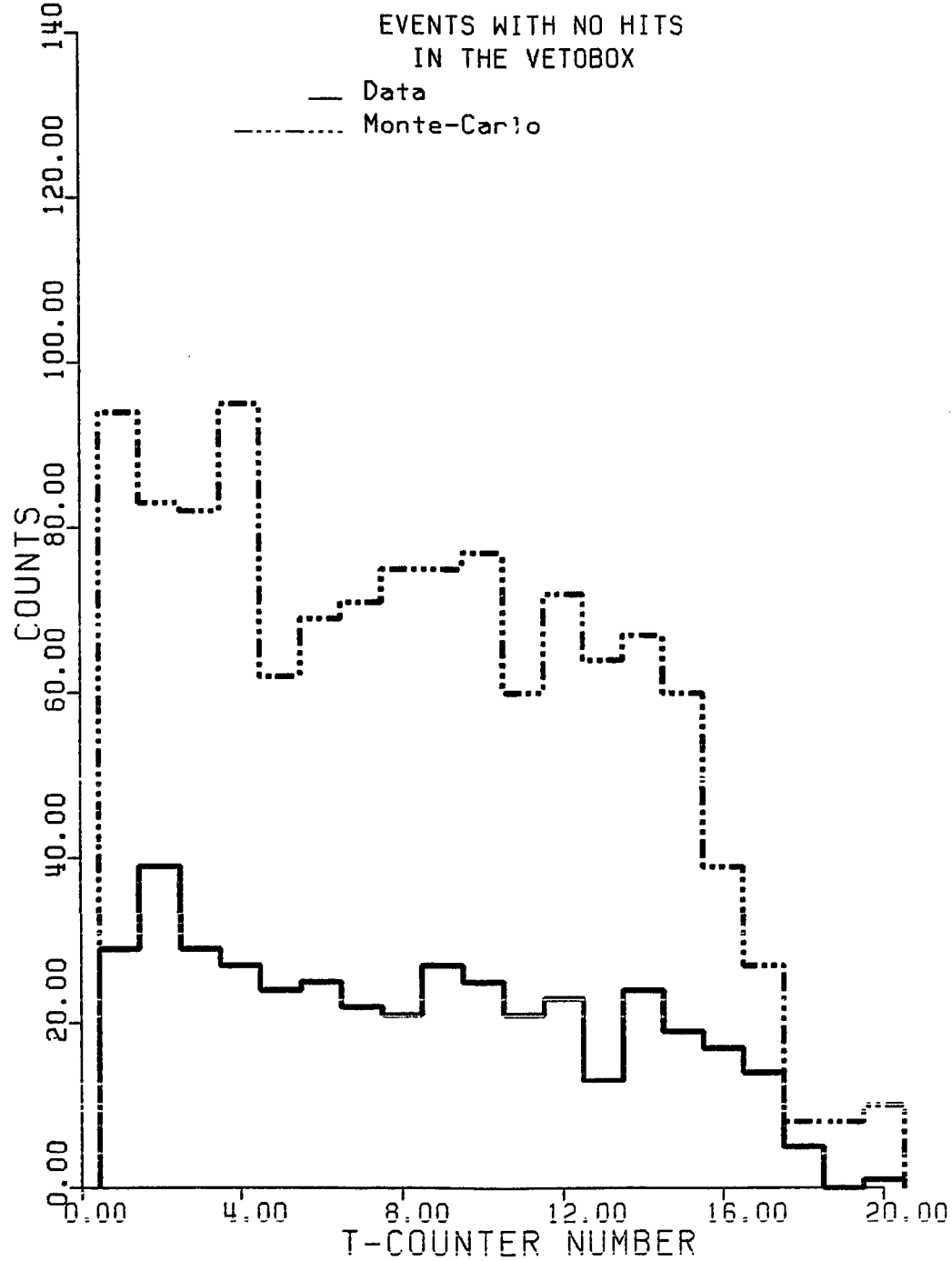


FIGURE 23 515 MeV/c

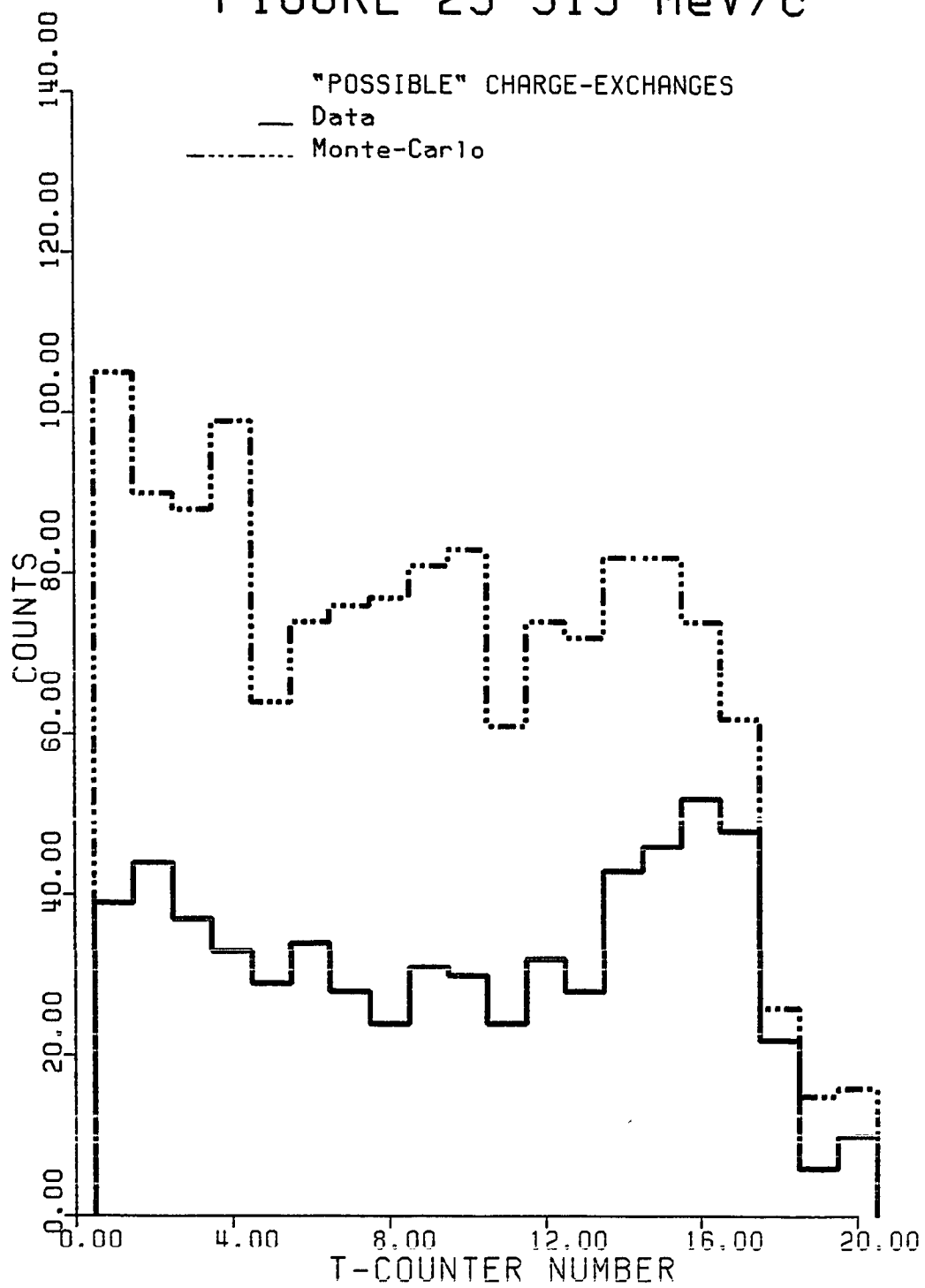


FIGURE 24 550 MeV/c

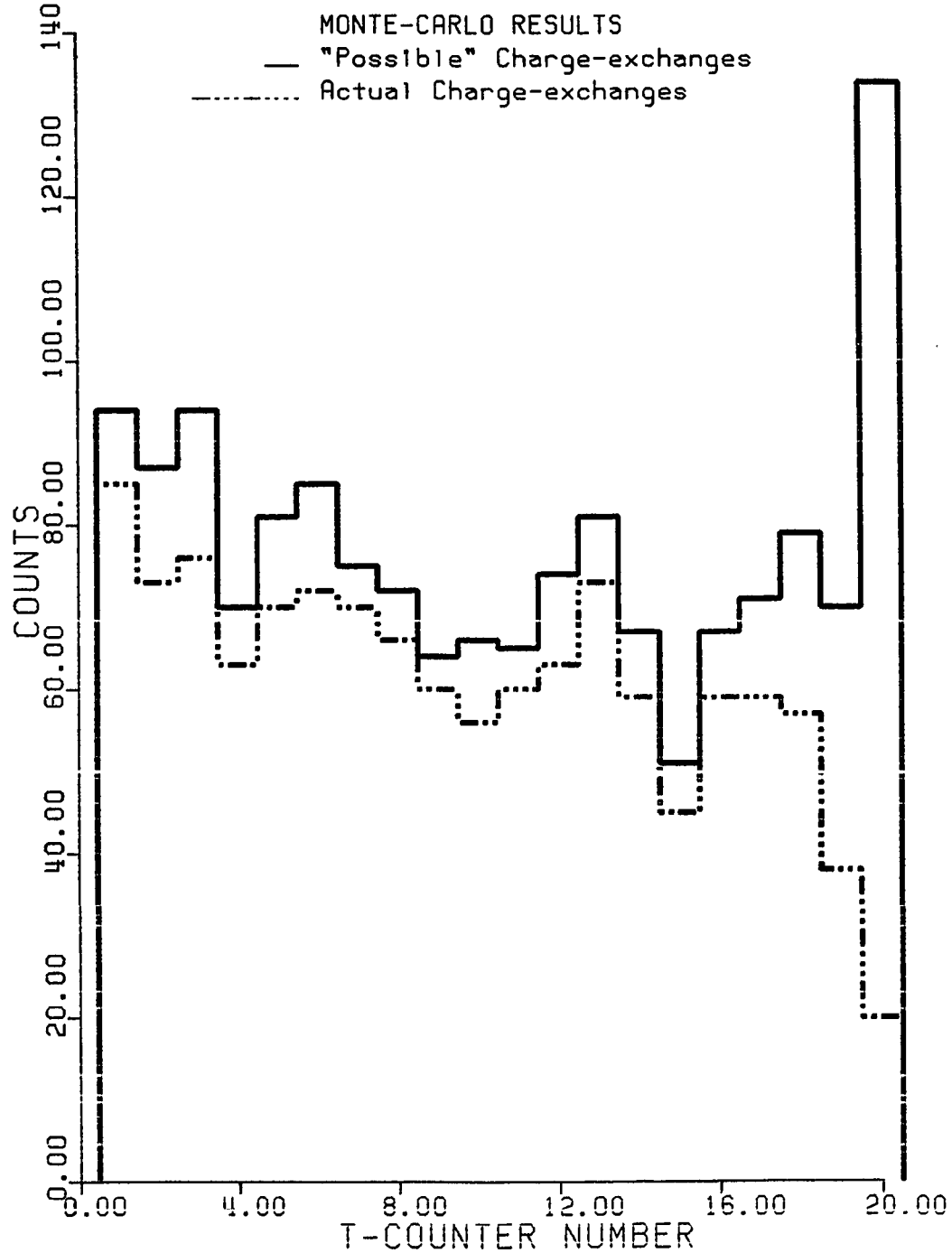


FIGURE 25 550 MeV/c

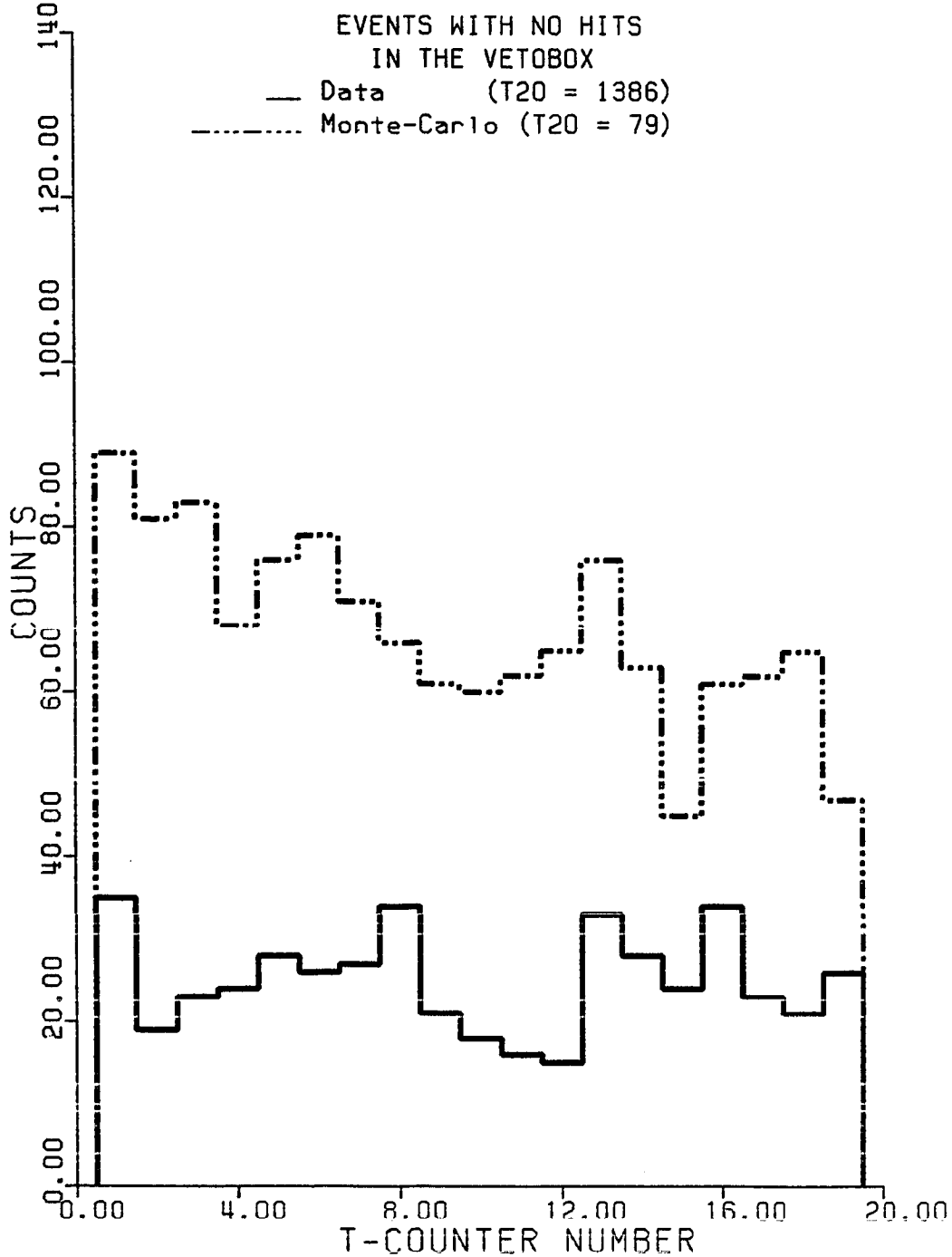
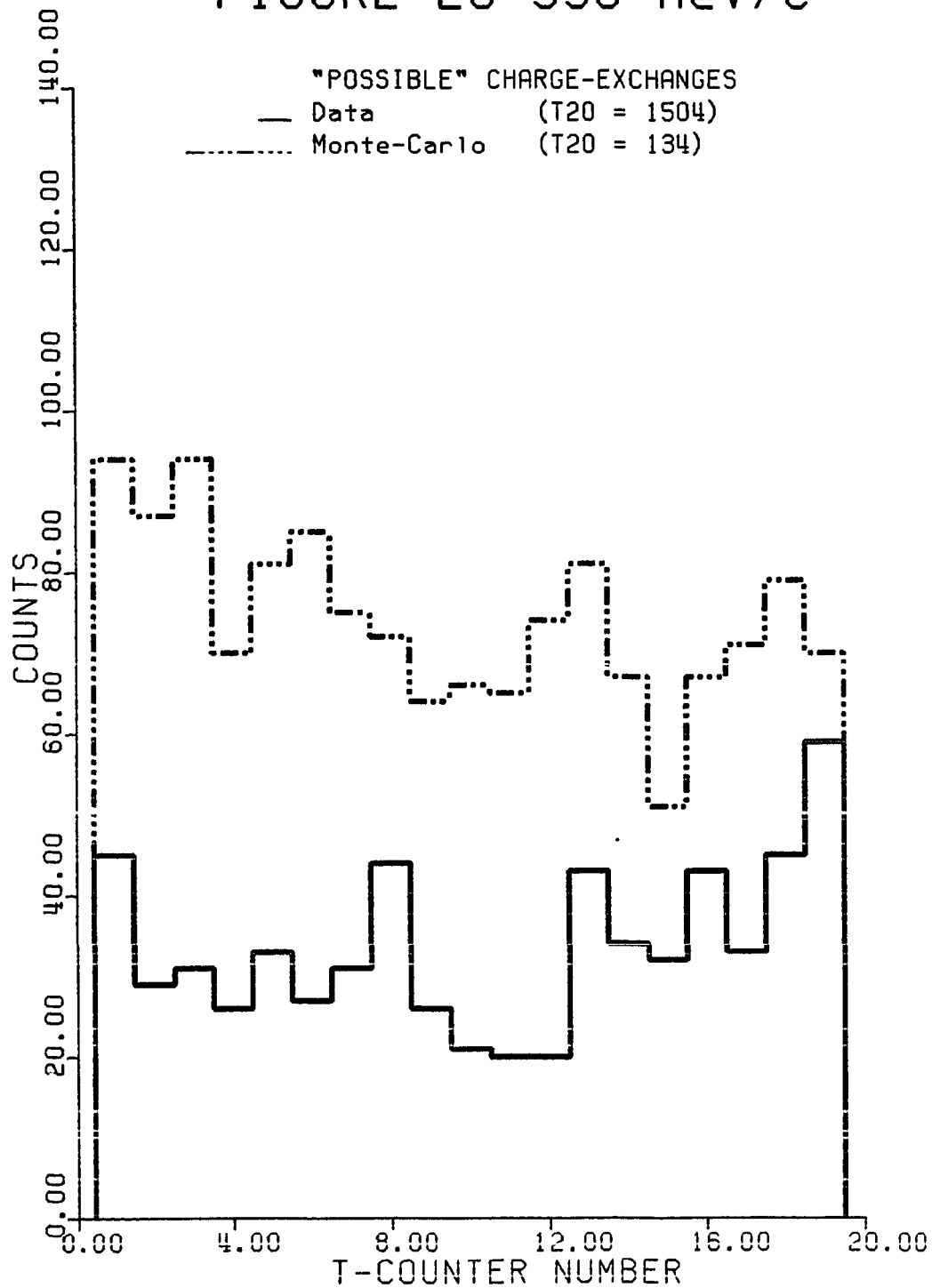


FIGURE 26 550 MeV/c



the data and Monte-Carlo results for the events with no hits in the vetobox. The number of counts in T20 is given at the top of the figure, but is not plotted for clarity. It is seen that the data has almost three times as many counts in T20 (1386) as in the other nineteen counters combined (475). Clearly, at this momentum a large number of events (almost 2% of the total number of  $\bar{p}$  events) are being classified as charge-exchanges in T20 when they are actually antiprotons punching through and failing to give a hit in V1. Figure 26 shows the "possible" charge-exchanges at this momentum. Again, T20 is not plotted for clarity. It is seen that the number of events in the data with one hit in the vetobox amounts to about 0.41% of the total number of events, and in the Monte-Carlo about 0.27%. This agrees with the statements made earlier that the Monte-Carlo estimates the number of events with one hit in the vetobox reasonably well, since most of them are apparently annihilations.

The Monte-Carlo results at 578 MeV/c are shown in Figure 27. At this momentum the antiprotons do not range out in the T-counters, so that the peak at the end of the range is not visible. The Monte-Carlo does predict an excess number of annihilation events in T20, however. At this momentum about 0.14% of the total number of events are predicted to be annihilations with one hit in the vetobox. The events with no hits in the vetobox are compared in Figure 28. The data has a large excess of counts in T20 (not

FIGURE 27 578 MeV/c

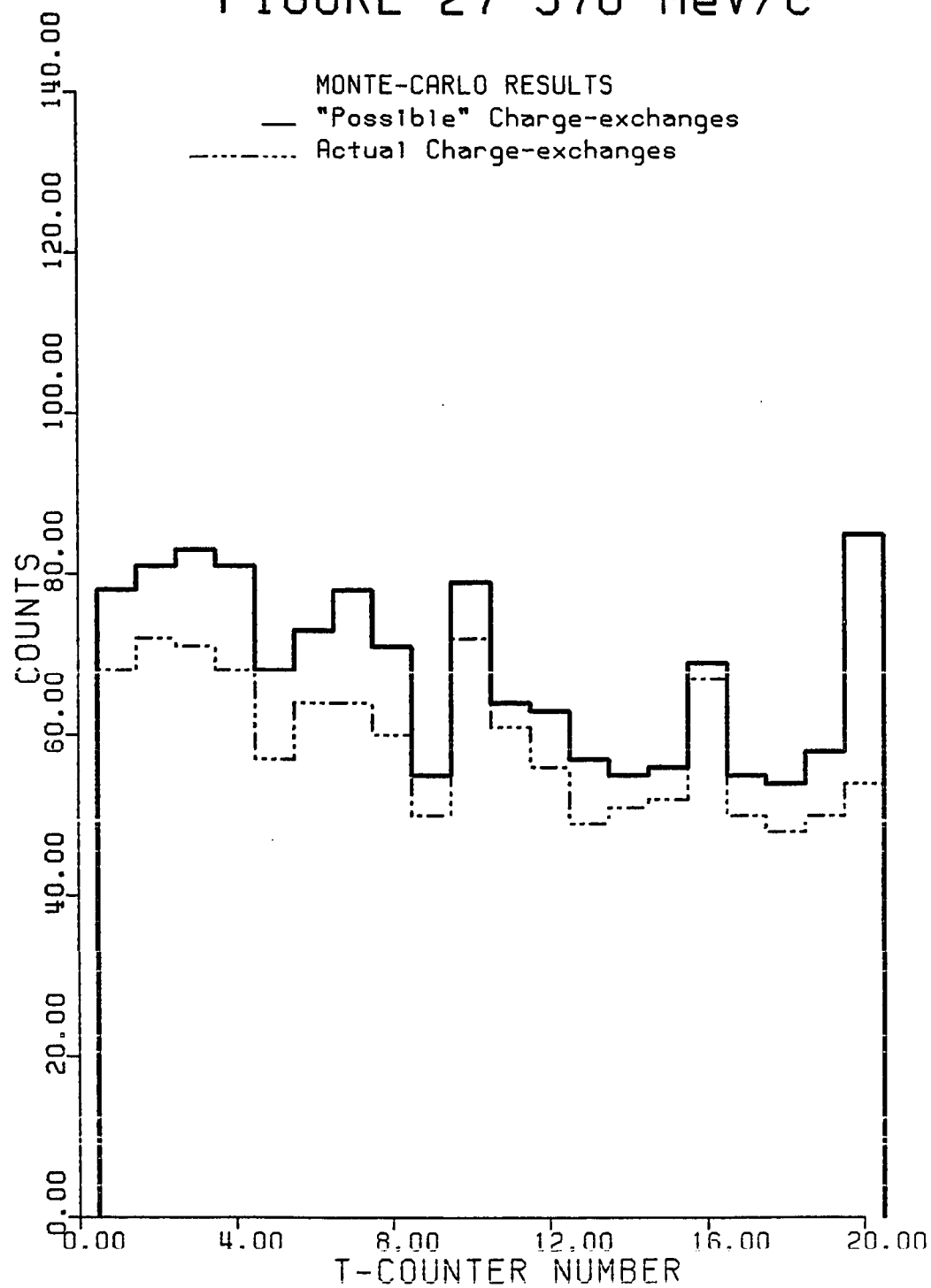


FIGURE 28 578 MeV/c

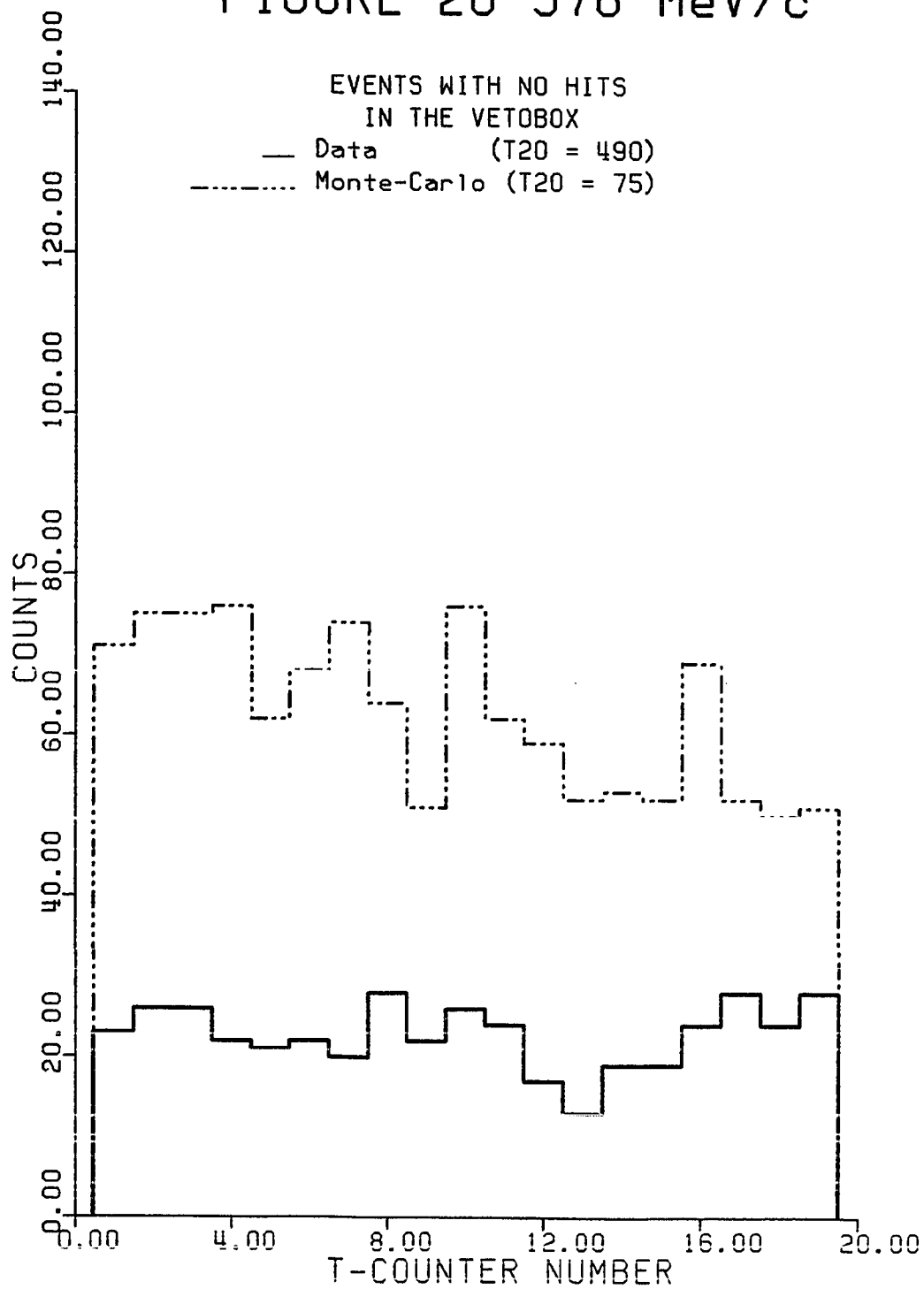
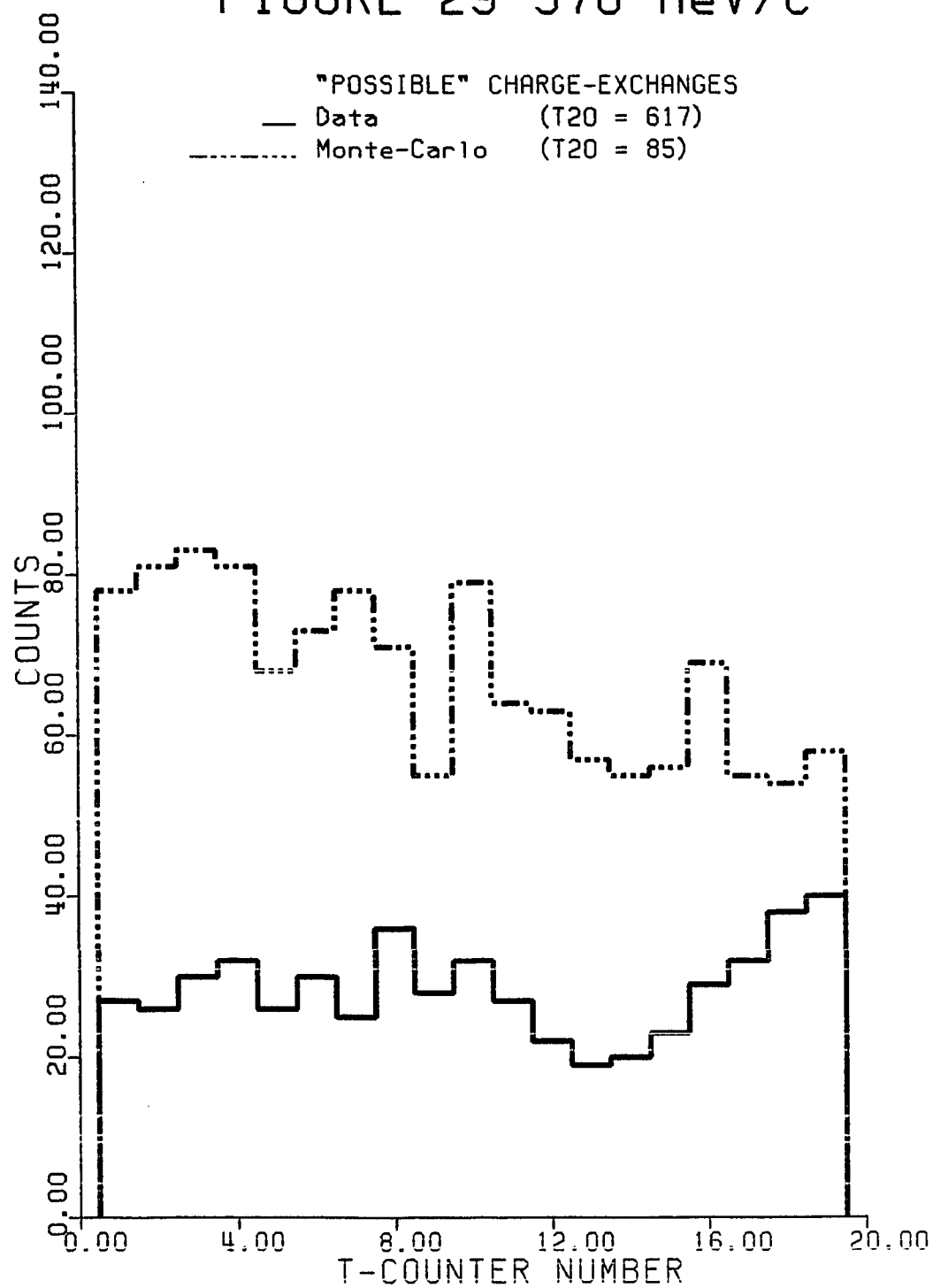


FIGURE 29 578 MeV/c



shown), similar to the 550 MeV/c data. The total "possible" charge-exchanges of Figure 29 show a rise at the end of the source due to events in the data with one hit in the vetobox. T20 is not shown for clarity. At this momentum the data had 0.35% of the events with one hit in the vetobox as compared to 0.14% predicted by the Monte-Carlo.

#### D. Event Classification

A breakdown of all of the data analyzed to give the final  $\bar{p}$  sample is given in Table 2. The top of the table begins with the total number of events on tape for each momentum point. The number of  $\bar{p}$  events is the number of events which passed cuts 1-4 (see Chapter IV). The next entry shows the number of events which had one and only one hit in all four MWPC coordinates. Clearly, inefficiencies in the MWPC's were the single largest factor in reducing the size of the data sample. The entries for "missed" T1 and "missed" T20 give the number of events where the  $\bar{p}$  was projected to miss T1 or T20 based on the MWPC information. Events which pass cuts 1-5 (see Chapter IV) are given in the row labeled 'good beam profile'. After imposing a weak requirement on the  $\bar{p}$ 's momentum (cut 5a), the data sample is reduced to the so-called "good"  $\bar{p}$  events, which represent the sample of antiproton events which undergo further analysis. This is the sample of events which is

TABLE 2  
BREAKDOWN OF PBAR EVENTS

PBAR MOMENTUM (MeV/c)	475	515	550	578
EVENTS ANALYSED	106085	109859	108837	107224
PBAR EVENTS	100786	102356	102028	98247
1 & ONLY 1 IN P1,P2	79262	78561	76459	71723
'MISSED' T1	3811	3989	3354	1460
'MISSED' T20	2181	2836	3265	1416
GOOD BEAM PROFILE	73270	71736	69840	68847
"GOOD" PBAR EVENTS	73204	71607	69202	68552

compared to the Monte-Carlo calculation.

Table 3 gives the detailed classification of the data which underwent further analysis. The percentages shown are percentages of the total number of "good"  $\bar{p}$  events, i.e. those which pass cuts 1-5a. The classification of Monte-Carlo events is given in Table 4. These values are to be compared to the values listed in Table 3. These two tables give a summary of the results of sections B and C of this chapter.

At 475 and 515 MeV/c, essentially none of the antiprotons punch through the source. While the number of annihilations predicted by the Monte-Carlo is higher than observed in the data, the inclusion of events which were cut that failed the cut on T1 or which had  $>1$  non-sequential T hit as "possible" annihilations brings these numbers into much closer agreement. This is supported by the evidence presented in section B that at least some of the events with non-sequential hits are in fact annihilations. For the charge-exchange events at these momenta, the data has about a factor of 2 fewer events with no hits in the veto-box than predicted by the Monte-Carlo. This effect is discussed in detail in section C of this chapter. Note that the entries for events with one hit in the vetobox are in fairly good agreement, indicating that the Monte-Carlo is giving a reasonable approximation for these events. This implies that the primary source of events which give

TABLE 3  
CLASSIFICATION OF DATA

PBAR MOMENTUM (MeV/c)	475	515	550	578
"GOOD" PBAR EVENTS	73204	71607	69202	68552
T1-T20-V1 ONLY HIT	0 -	1 -	11226 16.22%	39877 58.17%
ANNIHILATIONS	66064 90.25%	65443 91.39%	48695 70.37%	21759 31.74%
NO HIT IN T1	2727 3.73%	845 1.18%	2299 3.32%	504 0.74%
>1 NON-SEQ. T HIT	3696 5.05%	4588 6.41%	4676 6.76%	4920 7.18%
"POSSIBLE" ANNIHILATIONS	72487 99.02%	70876 98.98%	55670 80.45%	27183 39.65%
1 HIT IN BOX & V1	81 0.11%	85 0.12%	131 0.19%	214 0.31%
1 NON-SEQ. T HIT & V1	2 -	5 -	29 0.04%	119 0.17%
CHARGE-EXCHANGES:				
NO HITS IN VETOBOX	384 0.52%	405 0.57%	1861 2.69%	922 1.34%
ONE HIT IN VETOBOX	250 0.34%	235 0.32%	285 0.41%	237 0.35%
TOTAL "POSSIBLE"	634 0.87%	640 0.89%	2146 3.10%	1159 1.69%
CHARGE-EXCHANGES, WITHOUT T20				
NO HITS IN VETOBOX	384 0.52%	404 0.56%	475 0.69%	432 0.63%
ONE HIT IN VETOBOX	250 0.34%	226 0.32%	167 0.24%	110 0.16%
TOTAL "POSSIBLE"	634 0.87%	630 0.88%	642 0.93%	542 0.79%

TABLE 4  
CLASSIFICATION OF MONTE-CARLO EVENTS

PEAR MOMENTUM (MeV/c)	475	515	550	578
"GOOD" PEAR EVENTS	73200	71600	69200	68550
T1-T20-V1 ONLY HIT	0 -	165 0.23%	18146 26.22%	33262 48.52%
ANNIHILATIONS	72015 98.38%	70034 97.81%	49507 71.54%	33925 49.95%
CHARGE-EXCHANGES:				
ACTUAL CHEX	876 1.20%	1069 1.49%	1224 1.77%	1184 1.73%
UNDETECTED ANNIHILATIONS	101 0.14%	129 0.18%	135 0.20%	83 0.12%
NO HITS IN VETOBOX	977 1.33%	1198 1.67%	1359 1.96%	1267 1.85%
ONE HIT IN VETOBOX	208 0.28%	203 0.28%	188 0.27%	96 0.14%
TOTAL "POSSIBLE"	1185 1.62%	1401 1.96%	1547 2.24%	1363 1.99%

only one hit in the vetobox are annihilations. This is apparently primarily a geometric effect.

The data at 550 and 578 MeV/c are different from the two lower momenta primarily in that now a large number of antiprotons are predicted to punch through the source. At 550 MeV/c the data analysis showed many fewer punch through events than predicted by the Monte-Carlo. Considering the quality of agreement between the Monte-Carlo and the data at the two lower momenta, it seems apparent from examining the annihilation point (Figure 16) and the charge-exchange point for events with no hits in the vetobox (Figure 25) that a large number of events that were actually  $\bar{p}$ 's punching through were incorrectly placed in T20. Two possible causes for this effect in the data are poor timing of V1 or accidental pions confusing the trigger. It is probably a combination of these effects in the data and deficiencies in the Monte-Carlo. Further evidence in favor of this interpretation is shown in the charge-exchange entries for the data where T20 has been removed from the sample. Comparison of these values with those of the Monte-Carlo show a level of agreement comparable to the lower momenta. The number of events in T20 in the Monte-Carlo was small compared to the number in the data, and did not affect the percentage shown in Table 4 significantly.

The comparison of the data at 578 MeV/c in Tables 3 and 4 indicate that the momentum used in the Monte-Carlo is actually lower than that of this data sample, considering the number of punch through events and the number of annihilations. Even though the problem with extra hits in T20 due to mislabeled punch throughs still exists, it is not as large an effect and cannot account for the differences here as it did for 550 MeV/c. Raising the Monte-Carlo value of the  $\bar{p}$  momentum about 4% (to 600 MeV/c) did not improve matters much. Apparently the Monte-Carlo value for the momentum is as much as 10% too low, with probably a greater FWHM than was used here (see Figures 17 and 29). It should be pointed out that the pion flux was highest at this momentum, which caused both greater inefficiencies in the MWPC's and increased possibility of accidental pions fooling the program into thinking a  $\bar{p}$  had punched through.

#### E. Annihilation Multiplicities

The apparent multiplicities for annihilations at 475, 515, 550 and 578 MeV/c are shown in Tables 5-8, respectively. The top part of each table shows the percentage of annihilations which had annihilation products detected in the number of quadrants of the vetobox shown. The bottom part of each table shows the percentage of annihilations which had the number of "sides" hit by annihilation

TABLE 5  
ANNIHILATION MULTIPLICITIES 475 MeV/c

ANNIHILATIONS	DATA (REQUIRES ONLY 1 HIT PER QUAD)		DATA (REQUIRES 2 HITS PER QUAD)		MONTE-CARLO (CORRECTED FOR FAKE CH-EX)	
	66064		66064		72015	
NO QUADS, NO V1	-	-	266	0.40 %	-	-
V1 ONLY	43	0.07 %	125	0.19 %	106	1.47 %
1 QUAD ONLY	2037	3.08 %	7585	11.48 %	3359	4.66 %
1 QUAD & V1	462	0.70 %	1581	2.39 %	1205	1.67 %
2 QUADS ONLY	20617	31.21 %	30569	46.27 %	27158	37.71 %
2 QUADS & V1	3335	5.05 %	4523	6.85 %	6055	8.41 %
3 QUADS ONLY	26118	39.53 %	16749	25.35 %	22980	31.91 %
3 QUADS & V1	3527	5.34 %	1904	2.88 %	4018	5.58 %
4 QUADS ONLY	8928	13.51 %	2531	3.83 %	6235	8.66 %
4 QUADS & V1	997	1.51 %	231	0.35 %	899	1.25 %
ZERO 'SIDES'	-	-	266	0.40±0.02 %	-	-
ONE 'SIDE'	2080	3.15±0.07 %	7710	11.67±0.13 %	3465	4.81±0.08 %
TWO 'SIDES'	21079	31.91±0.22 %	32150	48.66±0.27 %	28363	39.38±0.23 %
THREE 'SIDES'	29453	44.58±0.26 %	21272	32.20±0.22 %	29035	40.32±0.24 %
FOUR 'SIDES'	12455	18.85±0.17 %	4435	6.71±0.10 %	10253	14.24±0.14 %
FIVE 'SIDES'	997	1.51±0.05 %	231	0.35±0.02 %	899	1.25±0.04 %

TABLE 6  
ANNIHILATION MULTIPLICITIES 515 MeV/c

ANNIHILATIONS	DATA (REQUIRES ONLY 1 HIT PER QUAD)		DATA (REQUIRES 2 HITS PER QUAD)		MONTE-CARLO (CORRECTED FOR FAKE CH-EX)	
	65443		65443		70034	
NO QUADS, NO V1	-	-	275	0.42 %	-	-
V1 ONLY	60	0.09 %	163	0.25 %	138	0.20 %
1 QUAD ONLY	2049	3.13 %	7614	11.63 %	3450	4.93 %
1 QUAD & V1	586	0.90 %	1956	2.99 %	1369	1.95 %
2 QUADS ONLY	19923	30.44 %	29121	44.50 %	26334	37.60 %
2 QUADS & V1	4186	6.40 %	5504	8.41 %	6687	9.55 %
3 QUADS ONLY	24927	38.09 %	15825	24.18 %	20959	29.93 %
3 QUADS & V1	4238	6.48 %	2344	3.58 %	4377	6.25 %
4 QUADS ONLY	8306	12.69 %	2372	3.62 %	5699	8.14 %
4 QUADS & V1	1168	1.78 %	272	0.42 %	1021	1.46 %
ZERO 'SIDES'	-	-	275	0.42±0.03 %	-	-
ONE 'SIDE'	2109	3.22±0.07 %	7777	11.88±0.13 %	3588	5.12±0.09 %
TWO 'SIDES'	20509	31.34±0.22 %	31077	47.48±0.27 %	27703	39.56±0.24 %
THREE 'SIDES'	29113	44.49±0.26 %	21329	32.59±0.22 %	27646	39.48±0.24 %
FOUR 'SIDES'	12544	19.17±0.17 %	4716	7.21±0.10 %	10076	14.39±0.14 %
FIVE 'SIDES'	1168	1.78±0.05 %	272	0.42±0.03 %	1021	1.46±0.05 %

TABLE 7  
ANNIHILATION MULTIPLICITIES 550 MeV/c

ANNIHILATIONS	DATA (REQUIRES ONLY 1 HIT PER QUAD)		DATA (REQUIRES 2 HITS PER QUAD)		MONTE-CARLO (CORRECTED FOR FAKE CH-EX)	
	48695		48695		49507	
NO QUADS, NO V1	-	-	256	0.53 %	-	-
V1 ONLY	67	0.14 %	146	0.30 %	89	0.18 %
1 QUAD ONLY	1793	3.68 %	6160	12.65 %	2601	5.25 %
1 QUAD & V1	496	1.02 %	1635	3.36 %	1041	2.10 %
2 QUADS ONLY	15195	31.20 %	21808	44.78 %	18394	37.15 %
2 QUADS & V1	3198	6.57 %	4127	8.47 %	4855	9.81 %
3 QUADS ONLY	18110	37.19 %	11220	23.04 %	14802	29.90 %
3 QUADS & V1	3075	6.31 %	1620	3.33 %	3292	6.65 %
4 QUADS ONLY	5885	12.09 %	1539	3.16 %	3714	7.50 %
4 QUADS & V1	876	1.80 %	184	0.38 %	719	1.45 %
ZERO 'SIDES'	-	-	256	0.53±0.03 %	-	-
ONE 'SIDE'	1860	3.82±0.09 %	6306	12.95±0.16 %	2690	5.43±0.10 %
TWO 'SIDES'	15691	32.22±0.26 %	23443	48.14±0.31 %	19435	39.26±0.28 %
THREE 'SIDES'	21308	43.76±0.30 %	15347	31.52±0.25 %	19657	39.71±0.28 %
FOUR 'SIDES'	8960	18.40±0.19 %	3159	6.49±0.11 %	7006	14.15±0.17 %
FIVE 'SIDES'	876	1.80±0.06 %	184	0.38±0.03 %	719	1.45±0.05 %

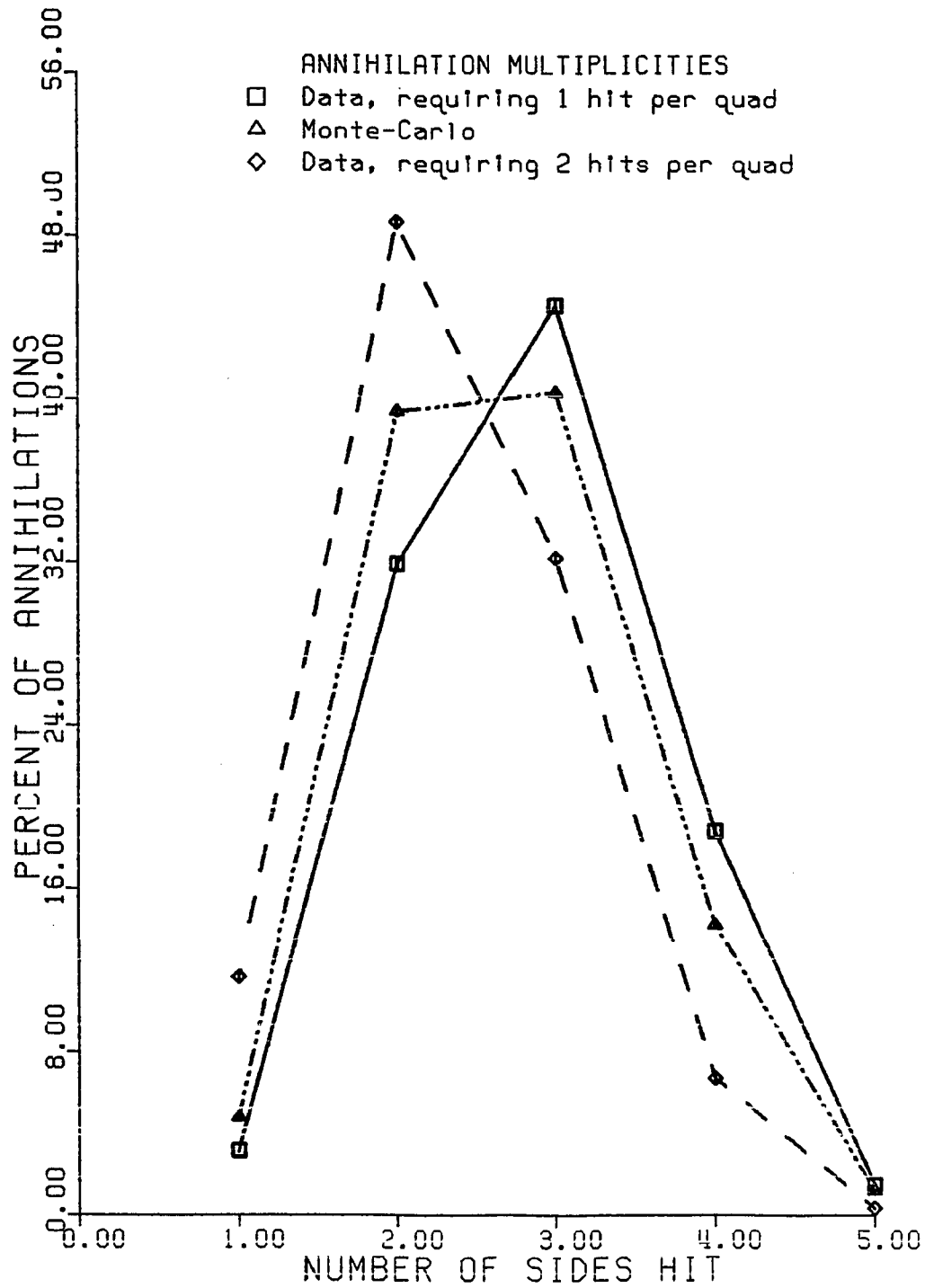
TABLE 8  
ANNIHILATION MULTIPLICITIES 578 MeV/c

ANNIHILATIONS	DATA (REQUIRES ONLY 1 HIT PER QUAD)		DATA (REQUIRES 2 HITS PER QUAD)		MONTE-CARLO (CORRECTED FOR FAKE CH-EX)	
	21759		21759		33925	
NO QUADS, NO V1	-	-	156	0.72 %	-	-
V1 ONLY	331	1.52 %	396	1.82 %	43	0.13 %
1 QUAD ONLY	1059	4.87 %	3353	15.41 %	1822	5.37 %
1 QUAD & V1	362	1.66 %	1029	4.73 %	688	2.03 %
2 QUADS ONLY	6622	30.43 %	9453	43.44 %	12736	37.54 %
2 QUADS & V1	1716	7.89 %	1513	6.95 %	3244	9.56 %
3 QUADS ONLY	7448	34.23 %	4378	20.12 %	10216	30.11 %
3 QUADS & V1	1600	7.35 %	800	3.68 %	2128	6.27 %
4 QUADS ONLY	2223	10.22 %	618	2.84 %	2605	7.68 %
4 QUADS & V1	398	1.83 %	63	0.29 %	443	1.31 %
ZERO 'SIDES'	-	-	156	0.72±0.06 %	-	-
ONE 'SIDE'	1390	6.39±0.17 %	3749	17.23±0.28 %	1865	5.50±0.13 %
TWO 'SIDES'	6984	32.10±0.38 %	10482	48.17±0.47 %	13424	39.57±0.34 %
THREE 'SIDES'	9164	42.12±0.44 %	5891	27.07±0.35 %	13460	39.68±0.34 %
FOUR 'SIDES'	3823	17.57±0.28 %	1418	6.52±0.17 %	14733	13.95±0.20 %
FIVE 'SIDES'	398	1.83±0.09 %	63	0.29±0.04 %	443	1.31±0.06 %

products (four vetobox quadrants and V1). It is assumed that the geometrical effects are the same for the data and the Monte-Carlo results. The effects of the beam tune are considered unimportant in the comparison of these results since the Monte-Carlo used approximations for measured beam profiles for the incident antiprotons. In addition to the Monte-Carlo results, each table has two entries for the data. The first column requires only one counter to fire to declare a vetobox quadrant hit. The second column is a reanalysis of the same data but requiring at least two of the three counters in a quadrant to fire to declare that quadrant hit.

Comparison for the four tables shows that the apparent multiplicities decrease slightly with increasing momentum. The Monte-Carlo shows the same trend. This is expected since most of the annihilations occur at rest, and as the antiproton's range moves from near the center of the T-counters at 475 MeV/c to the end of the source and beyond at 578 MeV/c, the solid angle subtended by the vetobox decreases. Aside from the slight momentum dependence, the multiplicities were very similar at the four different incident momenta. The typical behavior can be considered by taking as an example the data of Table 5 at 475 MeV/c, which is plotted in Figure 30. Comparison of the Monte-Carlo results with the data shows that the apparent multiplicity of the data is somewhat higher than that expected

FIGURE 30 475 MeV/c



from the Monte-Carlo. However, earlier discussions have indicated that there is probably a non-negligible number of single hits in the vetobox, either from accidental pions, or photons. With this in mind, the data was reanalyzed requiring at least two hits in a quadrant to declare that quadrant hit. Now it is seen that the apparent multiplicity is indeed shifted to a lower value, but now it is overcompensated and is actually lower than predicted by the Monte-Carlo. It would appear from this result that singles in the vetobox are contributing to the higher apparent multiplicity, but that clearly some of these single hits are valid (probably photons). Without extensive Monte-Carlo work on the showering of photons in the vetobox, more detailed information is difficult to extract from the data.

#### F. Efficiency of Antineutron Source

The efficiency for production of antineutrons can only be calculated with the help of the Monte-Carlo. The number of actual charge-exchange events expected is given in Table 4. Based on the parameterizations of the cross sections, these percentages should be good to within 2% of the value given. The Monte-Carlo clearly shows that the number of  $\bar{n}$ 's produced increases until 550 MeV/c, where all of the T counters are in use and the charge-exchange cross section is highest (see Figure 24). The number of  $\bar{n}$ 's produced at

578 MeV/c is lower because the charge-exchange cross section decreases with increasing momentum. This same trend is seen in the actual data (Table 3).

Table 9 gives the percentage of possible charge-exchanges that have only one hit in the vetobox as a function of momentum. The Monte-Carlo entries show that the percentage of possible charge-exchanges that have one hit in the vetobox decreases as the  $\bar{p}$ 's range moves out of the source volume. This is because most of those events are annihilations at rest. If we assume that essentially all of the events with one hit in the vetobox are in fact annihilations, then the entries in Table 9 indicate the percentage of triggered events (using the E-767 trigger) that are not useful as charge-exchanges. This gives an estimate of the efficiency of the trigger for E-767. The entries for the data indicate a minimum at 550 MeV/c. However, this is due to the mislabeled events in T20 which were actually punch throughs. If we assume that almost all of the excess events in T20 in the data are in fact these punch throughs, then the efficiency for data collection is much poorer at the two higher momenta. This is shown in the entries for the data labeled "corrected for T20." This entry indicates that even though more actual charge-exchanges occurred at 550 MeV/c (see Table 4), it is much more efficient to collect data at 515 MeV/c, since fewer events on tape will

TABLE 9  
 PERCENTAGE OF POSSIBLE CHARGE EXCHANGES THAT  
 HAVE ONLY ONE HIT IN THE VETOBOX

PBAR MOMENTUM (MeV/c)	475	515	550	578
MONTE-CARLO	17.6 %	14.5 %	12.2 %	7.0 %
DATA	39.4 %	36.7 %	13.2 %	20.4 %
DATA,CORRECTED FOR T20 PINCH THROUGHs	39.4 %	36.7 %	77.8 %	62.7 %
DATA,WITHOUT T20	39.4 %	36.7 %	26.0 %	20.2 %

be useless events. It was for reasons such as these that the data for experiment 767 were taken at 505 MeV/c. If we simply remove T20 from consideration in the data, thereby removing the spurious punch through events, we see in Table 9 that the data exhibits the same trend as the Monte-Carlo. Clearly there is a larger percentage of these events in the data because of omissions in the Monte-Carlo discussed earlier. It is worth noting that the data taking for experiment 767 would have been more efficient had T20 been included in the veto and the momentum raised to 550 MeV/c, assuming that the extra events in T20 at this momentum are in fact mislabeled punch throughs. The veto efficiency for annihilations at 475 and 515 MeV/c was better than 99%, as is seen from Tables 3 and 4. The efficiency decreased two or three percent at 550 and 578 MeV/c because of the extra hits in T20. By ignoring T20, the veto efficiency for annihilations is better than 99% for all momenta studied.

## CHAPTER VII

### CONCLUSIONS

From the detailed study of the data and Monte-Carlo analysis presented in Chapter VI, it is seen that the data is reasonably well explained by the assumptions of the Monte-Carlo. The agreement between the data and the Monte-Carlo on the annihilation point indicates that the cross section used is accurate and that the energy loss of the  $\bar{p}$  is well known. The comparison also pointed out an apparent problem with counters T3 and T9, whereby a large number of events with non-sequential T hits are produced. The agreement is also good for the charge-exchange events, once all the factors not included in the Monte-Carlo are considered.

Even though the Monte-Carlo does not include the effects of photons showering in the vetobox and the effects of showering on the observed multiplicity for annihilations, it is in semiquantitative agreement with the data on the observed multiplicities and the expected number of "possible" charge-exchange events due to annihilations. Because this apparatus was not specifically designed to measure annihilation multiplicities, it is not sensitive to the details of the branching ratios given in Appendix I. The agreement is mainly the result of the geometry of the apparatus and

the high multiplicity for the annihilation products. Nevertheless, the Monte-Carlo scheme for the annihilation branching ratios appears to be sufficient for the purpose of understanding the source operation and output.

The Monte-Carlo was useful in determining the efficiency for  $\bar{n}$  production by pointing out that the number of actual charge-exchanges produced was a maximum at 550 MeV/c. Comparison with the data showed that even though more charge-exchanges were produced at 550 MeV/c, inefficiencies in the ability to tag  $\bar{p}$ 's that punched through caused the most efficient data taking to occur around 515 MeV/c for the trigger used during E-767 data taking. It seems clear that including T20 in the veto and raising the  $\bar{p}$  momentum to 550 MeV/c would maximize the number of  $\bar{n}$ 's produced as well as lower the number of useless events. Allowing only no hits in the vetobox would also increase data taking efficiency, if we assume that the events with one hit in the vetobox are annihilations, as indicated by the Monte-Carlo. Specifically, at 515 MeV/c 0.57% of the events were charge-exchanges with no hits in the vetobox and 36.7% of the possible charge-exchange events had one hit in the vetobox. By including T20 in the veto and raising the momentum to 550 MeV/c, these values could have been improved to 0.69% of the events being charge-exchanges with no hits in the vetobox, with only 26% of the possible charge-exchanges

having one hit in the vetobox. Note that in both cases the veto efficiency for annihilations is better than 99%, indicating the success of the vetobox design.

The veto efficiency is already very high, so the goal for future work is to increase the number of  $\bar{n}$ 's produced. Since the results of Nakamura are confirmed, namely that antineutron production via charge-exchange on carbon is suppressed from the corresponding process on hydrogen, it seems clear that the number of antineutrons can be increased by increasing the amount of hydrogen in the source target. The most obvious way to do this would be to replace the T-counters with a liquid hydrogen target.

In a calibration run for the E-767 calorimeter made in May, 1985, a 60.96 cm (24") long 7.62 cm (3") diameter liquid hydrogen target was used as an antineutron source. A vetobox was built by the Rice collaborators with a design similar to that of E-767. A 475 MeV/c  $\bar{p}$  will come to a stop in a hydrogen target this long. A Monte-Carlo calculation for this new source showed that 2.4% of the events were actual charge-exchanges, while 37.8% of the possible charge-exchanges had a single hit in the vetobox. These values agreed reasonably well with the online analysis of the data. Comparison of these results with the results analyzed here shows a clear increase in the number of events with no hits in the vetobox. It should be pointed out that the vetobox used for this calibration run

subtended a smaller percentage of the solid angle and had fewer layers of lead and scintillator. This means that there is a larger percentage of undetected annihilations than for the E-767 source apparatus. Nevertheless, these preliminary results indicate that liquid hydrogen is indeed a better source of antineutrons than plastic scintillator. This is primarily because of longer flight lengths in the liquid hydrogen and the lack of carbon, on which charge-exchange is suppressed.

One of the most important aspects of the antineutron source used for E-767 was that it was active. This allowed measurement of the antineutrons energy more precisely. One interesting design would be a segmented, active hydrogen target as an antineutron source. Such a source might have cells of liquid hydrogen separated by thin scintillators. The distance between the scintillators could vary along the length to improve energy resolution. There are many technical details which must be worked out before such an apparatus might be constructed. For example, the problem of having phototubes in close proximity to the liquid hydrogen, which is at low temperature and surrounded by vacuum, requires careful consideration. Just such an apparatus is under serious consideration for a proposed experiment to be done in 1986. This experiment would extend the data for E-767 even closer to the threshold by

requiring a coincidence between the neutron and the anti-neutron in a two-arm arrangement.

Since we want more hydrogen in the source volume in order to produce more antineutrons, one method that could be used would be to simply use polyethylene ( $-\text{CH}_2-$ ) as part of the source material. This would improve the hydrogen to carbon ratio by a factor of two over plastic scintillators, and it does not have many of the problems associated with the construction of a liquid hydrogen target. Perhaps a combination of these two ideas will prove to be most practical.

This study of the antineutron source for experiment 767 has shown that physics with low energy antineutrons is possible and in fact practical. The development of better  $\bar{n}$  sources will undoubtedly go a long way to improving the low energy  $\bar{N}N$  data currently available, and will be an important part of future  $\bar{N}N$  physics.

## APPENDIX I

### MONTE-CARLO ANNIHILATION BRANCHING RATIOS

Fermi statistical theory is used for the correct average annihilation multiplicities. See [SE60] and [AE60].

<u>No. of pions</u>	<u>% of annihilations</u>
2	0.1
3	5.6
4	21.7
5	44.0
6	23.7
7	5.1
Avg	5.0

Charge correlations for the different possible final states are taken from the "correlation number" theory of Pais [PA60]. For  $\bar{p}p$  annihilation we have the following correlations:

$$\pi^+ \pi^- / \pi^0 \pi^0 = 5/1$$

$$\pi^+ \pi^- \pi^0 / 3\pi^0 = 17/3$$

$$2\pi^+ 2\pi^- / \pi^+ \pi^- 2\pi^0 / 4\pi^0 = 18/26/1$$

$$2\pi^+ 2\pi^- \pi^0 / \pi^+ \pi^- 3\pi^0 / 5\pi^0 = 94/50/3$$

$$3\pi^+ 3\pi^- / 2\pi^+ 2\pi^- 2\pi^0 / \pi^+ \pi^- 4\pi^0 / 6\pi^0 = 65/228/63/1$$

$$3\pi^+ 3\pi^- \pi^0 / 2\pi^+ 2\pi^- 3\pi^0 / \pi^+ \pi^- 5\pi^0 / 7\pi^0 = 155/192/33/1$$

For  $\bar{p}n$  annihilation we have the following correlations:

$$\pi^-\pi^0 = 1$$

$$\pi^-2\pi^0/\pi^+2\pi^- = 6/9$$

$$\pi^-3\pi^0/\pi^+2\pi^-\pi^0 = 6/24$$

$$\pi^-4\pi^0/\pi^+2\pi^-2\pi^0/2\pi^+3\pi^- = 9/66/30$$

$$\pi^-5\pi^0/\pi^+2\pi^-3\pi^0/2\pi^+3\pi^-\pi^0 = 9/108/135$$

$$\pi^-6\pi^0/\pi^+2\pi^-4\pi^0/2\pi^+3\pi^-2\pi^0/3\pi^+4\pi^- = 4/69/165/35$$

The combination of these results gives the branching ratios for  $\bar{p}p$  and  $\bar{p}n$  annihilation used in the Monte-Carlo. For comparison the experimental data of Baltay [BA66] is also shown. The values given are percentages of the total number of annihilations.

	Monte-Carlo	Baltay
$\bar{p}p \rightarrow \pi^+\pi^-$	0.08	$0.37 \pm 0.03$
$2\pi^0$	0.02	
$3\pi^0$	0.84	
$\pi^+\pi^-\pi^0$	4.76	$7.8 \pm 0.9$
$2\pi^+2\pi^-$	8.68	$5.8 \pm 0.3$
$\pi^+\pi^-2\pi^0$	12.54	
$4\pi^0$	0.48	
$2\pi^+2\pi^-\pi^0$	28.12	$18.7 \pm 0.9$
$\pi^+\pi^-3\pi^0$	14.97	
$5\pi^0$	0.90	
$3\pi^+3\pi^-$	4.32	$1.9 \pm 0.2$
$2\pi^+2\pi^-2\pi^0$	15.14	

	Monte-Carlo	Baltay
$\pi^+ \pi^- 4\pi^0$	4.18	
$6\pi^0$	0.07	
$3\pi^+ 3\pi^- \pi^0$	2.07	$1.6 \pm 0.3$
$2\pi^+ 2\pi^- 3\pi^0$	2.57	
$\pi^+ \pi^- 5\pi^0$	0.44	
$7\pi^0$	0.01	
all neutral	2.32	$3.2 \pm 0.5$
$\pi^+ \pi^- x^0$	32.13	$34.5 \pm 1.2$
$2\pi^+ 2\pi^- x^0$	17.71	$21.3 \pm 1.1$
$\bar{p}n \rightarrow \pi^- \pi^0$	0.1	
$\pi^- 2\pi^0$	2.24	
$\pi^+ 2\pi^-$	3.36	
$\pi^- 3\pi^0$	4.34	
$\pi^+ 2\pi^- \pi^0$	17.36	
$\pi^- 4\pi^0$	3.77	
$2\pi^+ 3\pi^-$	12.57	
$\pi^+ 2\pi^- 2\pi^0$	27.66	
$\pi^- 5\pi^0$	0.85	
$\pi^+ 2\pi^- 3\pi^0$	10.16	
$2\pi^+ 3\pi^- \pi^0$	12.70	
$\pi^- 6\pi^0$	0.70	
$\pi^+ 2\pi^- 4\pi^0$	1.29	
$2\pi^+ 3\pi^- 2\pi^0$	3.08	
$3\pi^+ 4\pi^-$	0.65	

For annihilations on carbon it is assumed that at the instant of annihilation the annihilation products are the same as that for  $\bar{p}p$  or  $\bar{p}n$ , with the observed annihilation products resulting from subsequent pion interactions within the residual nucleus. For annihilations which have no protons among the final products, the multiplicities are just those for  $\bar{p}p$  or  $\bar{p}n$ , depending upon which nucleon in the carbon nucleus annihilated. For annihilations which have one or more protons in the final products, the  $\bar{p}p$  or  $\bar{p}n$  multiplicities are modified by assuming that one of the outgoing pions is absorbed and ejects a proton from the residual nucleus. It is assumed that it is equally probable for any particular pion to cause this, irrespective of its charge. Using this scheme, the following lists give the branching ratios (in percent of the number of annihilations) for  $\bar{p}$ -carbon annihilations when the indicated type of final state results.

$\bar{p}p$ -Like Annihilations with 1 Proton in the Final State

$\pi^+ p^+$	0.04	$2\pi^- 2\pi^0 \pi^+ p^+$	5.13
$\pi^- p^+$	0.04	$\pi^+ \pi^- 3\pi^0 p^+$	2.79
$\pi^0 p^+$	0.02	$\pi^+ 4\pi^0 p^+$	0.70
$2\pi^0 p^+$	0.84	$\pi^- 4\pi^0 p^+$	0.70
$\pi^+ \pi^- p^+$	1.58	$5\pi^0 p^+$	0.07
$\pi^- \pi^0 p^+$	1.58	$3\pi^+ 3\pi^- p^+$	0.30
$\pi^+ \pi^0 p^+$	1.58	$3\pi^+ 2\pi^- \pi^0 p^+$	0.89
$2\pi^+ \pi^- p^+$	4.34	$3\pi^- 2\pi^+ \pi^0 p^+$	0.89
$2\pi^- \pi^+ p^+$	4.34	$2\pi^+ 2\pi^- 2\pi^0 p^+$	1.10
$\pi^+ \pi^- \pi^0 p^+$	6.28	$2\pi^+ 3\pi^0 \pi^- p^+$	0.73
$\pi^- 2\pi^0 p^+$	3.14	$2\pi^- 3\pi^0 \pi^+ p^+$	0.73
$\pi^+ 2\pi^0 p^+$	3.14	$\pi^+ \pi^- 4\pi^0 p^+$	0.31
$3\pi^0 p^+$	0.48	$\pi^+ 5\pi^0 p^+$	0.06
$2\pi^+ 2\pi^- p^+$	5.62	$\pi^- 5\pi^0 p^+$	0.06
$2\pi^+ \pi^- \pi^0 p^+$	11.25	$6\pi^0 p^+$	0.01
$2\pi^- \pi^+ \pi^0 p^+$	11.25		
$\pi^+ \pi^- 2\pi^0 p^+$	8.98		
$\pi^+ 3\pi^0 p^+$	2.99		
$\pi^- 3\pi^0 p^+$	2.99		
$4\pi^0 p^+$	0.90		
$3\pi^+ 2\pi^- p^+$	2.16		
$3\pi^- 2\pi^+ p^+$	2.16		
$2\pi^+ 2\pi^- p^+$	5.13		
$2\pi^+ 2\pi^0 \pi^- p^+$	5.13		

$\bar{p}n$ -Like Annihilations with 1 Proton in the Final State

$\pi^- p^+$	0.05	$2\pi^+ 2\pi^- \pi^0 p^+$	6.25
$\pi^0 p^+$	0.05	$\pi^+ 3\pi^- \pi^0 p^+$	4.23
$\pi^- \pi^0 p^+$	1.50	$\pi^- 5\pi^0 p^+$	0.06
$2\pi^0 p^+$	0.75	$6\pi^0 p^+$	0.01
$\pi^+ \pi^- p^+$	2.24	$\pi^+ 2\pi^- 3\pi^0 p^+$	0.74
$2\pi^- p^+$	1.12	$\pi^+ \pi^- 4\pi^0 p^+$	0.39
$\pi^- 2\pi^0 p^+$	3.26	$2\pi^- 4\pi^0 p^+$	0.18
$3\pi^0 p^+$	1.09	$2\pi^+ 3\pi^- \pi^0 p^+$	0.88
$\pi^+ 2\pi^- p^+$	4.34	$2\pi^+ 2\pi^- 2\pi^0 p^+$	1.32
$\pi^+ \pi^- \pi^0 p^+$	8.68	$\pi^+ 3\pi^- 2\pi^0 p^+$	0.88
$2\pi^- \pi^0 p^+$	4.34	$3\pi^+ 3\pi^- p^+$	0.37
$\pi^- 3\pi^0 p^+$	3.02	$2\pi^+ 4\pi^- p^+$	0.28
$4\pi^0 p^+$	0.75		
$2\pi^+ 2\pi^- p^+$	7.54		
$\pi^+ 3\pi^- p^+$	5.03		
$\pi^+ 2\pi^- \pi^0 p^+$	11.06		
$\pi^+ \pi^- 2\pi^0 p^+$	11.06		
$2\pi^- 2\pi^0 p^+$	5.53		
$\pi^- 4\pi^0 p^+$	0.71		
$5\pi^0 p^+$	0.14		
$\pi^+ 2\pi^- 2\pi^0 p^+$	5.08		
$\pi^+ \pi^- 3\pi^0 p^+$	3.39		
$2\pi^- 3\pi^0 p^+$	1.69		
$2\pi^+ 3\pi^- p^+$	2.12		

$\bar{p}p$ -Like Annihilations with 2 Protons in the Final State

$2p^+$	0.08	$2\pi^+2\pi^-2p^+$	1.38
	0.02	$2\pi^+2\pi^02p^+$	1.38
$\pi^02p^+$	0.84	$2\pi^-2\pi^02p^+$	1.38
$\pi^+2p^+$	1.58	$2\pi^+\pi^-\pi^02p^+$	5.51
$\pi^-2p^+$	1.58	$\pi^+2\pi^-\pi^02p^+$	5.51
$\pi^02p^+$	1.58	$\pi^+\pi^-2\pi^02p^+$	1.05
$2\pi^+2p^+$	2.17	$\pi^+3\pi^02p^+$	1.39
$2\pi^-2p^+$	2.17	$\pi^-3\pi^02p^+$	1.39
$\pi^+\pi^-2p^+$	4.34	$4\pi^02p^+$	0.35
$\pi^+\pi^-2p^+$	2.51	$4\pi^02p^+$	0.07
$\pi^+\pi^02p^+$	5.02	$3\pi^+2\pi^-2p^+$	0.52
$\pi^-\pi^02p^+$	5.02	$3\pi^+\pi^-\pi^02p^+$	0.52
$2\pi^02p^+$	0.48	$2\pi^+3\pi^-2p^+$	0.52
$2\pi^+\pi^-2p^+$	9.37	$\pi^+3\pi^-\pi^02p^+$	0.52
$2\pi^+\pi^02p^+$	4.69	$2\pi^+2\pi^-\pi^02p^+$	0.41
$\pi^+2\pi^-2p^+$	9.37	$2\pi^+3\pi^02p^+$	0.14
$2\pi^-\pi^02p^+$	4.69	$2\pi^-3\pi^02p^+$	0.14
$\pi^+\pi^-\pi^02p^+$	4.50	$\pi^+\pi^-3\pi^02p^+$	0.54
$\pi^+2\pi^02p^+$	4.50	$2\pi^+\pi^-2\pi^02p^+$	0.68
$\pi^-2\pi^02p^+$	4.50	$\pi^+2\pi^-2\pi^02p^+$	0.68
$3\pi^02p^+$	1.50	$\pi^+\pi^-3\pi^02p^+$	0.16
$3\pi^02p^+$	0.90	$\pi^+4\pi^02p^+$	0.13
$3\pi^+\pi^-2p^+$	1.44	$\pi^-4\pi^02p^+$	0.13
$\pi^+3\pi^-2p^+$	1.44	$5\pi^02p^+$	0.30
$2\pi^+2\pi^-2p^+$	1.44	$5\pi^02p^+$	0.01

$\bar{p}n$ -Like Annihilations with 2 Protons in the Final State

$2p^+$	0.1	$\pi^+ 3\pi^0 2p^+$	0.68
$\pi^- 2p^+$	0.75	$\pi^+ \pi^- 2\pi^0 2p^+$	4.06
$\pi^0 2p^+$	1.49	$2\pi^- 2\pi^0 2p^+$	2.03
$\pi^+ 2p^+$	1.12	$\pi^- 3\pi^0 2p^+$	1.35
$\pi^- 2p^+$	2.24	$3\pi^- \pi^0 2p^+$	0.85
$\pi^- \pi^0 2p^+$	2.17	$2\pi^+ \pi^- \pi^0 2p^+$	2.54
$2\pi^0 2p^+$	2.17	$\pi^+ 3\pi^- 2p^+$	1.69
$\pi^+ \pi^0 2p^+$	2.89	$2\pi^+ 2\pi^- 2p^+$	2.54
$\pi^+ \pi^- 2p^+$	5.79	$\pi^+ 2\pi^- \pi^0 2p^+$	5.08
$2\pi^- 2p^+$	2.89	$\pi^- 4\pi^0 2p^+$	0.05
$\pi^- \pi^0 2p^+$	5.79	$5\pi^0 2p^+$	0.02
$\pi^- 2\pi^0 2p^+$	1.89	$\pi^+ 4\pi^0 2p^+$	0.06
$3\pi^0 2p^+$	1.89	$\pi^+ 2\pi^- 2\pi^0 2p^+$	0.36
$3\pi^- 2p^+$	1.26	$\pi^- 4\pi^0 2p^+$	0.12
$2\pi^+ \pi^- 2p^+$	3.77	$2\pi^- 3\pi^0 2p^+$	0.25
$\pi^+ 2\pi^- 2p^+$	7.54	$\pi^+ \pi^- 3\pi^0 2p^+$	0.49
$\pi^+ 2\pi^- 2p^+$	2.77	$2\pi^+ 3\pi^- 2p^+$	0.15
$\pi^+ 2\pi^0 2p^+$	2.77	$2\pi^+ 2\pi^0 \pi^- 2p^+$	0.44
$\pi^- 2\pi^0 2p^+$	5.53	$3\pi^- 2\pi^0 2p^+$	0.15
$\pi^0 2\pi^- 2p^+$	5.53	$\pi^+ 2\pi^- 2\pi^0 2p^+$	0.88
$\pi^+ \pi^- \pi^0 2p^+$	11.06	$\pi^+ 3\pi^- \pi^0 2p^+$	0.59
$\pi^- 3\pi^0 2p^+$	0.57	$2\pi^+ 2\pi^- \pi^0 2p^+$	0.88
$4\pi^0 2p^+$	0.28	$3\pi^+ 2\pi^- 2p^+$	0.19
$\pi^+ 2\pi^- \pi^0 2p^+$	2.03	$\pi^+ 4\pi^- 2p^+$	0.09
		$2\pi^+ 3\pi^- 2p^+$	0.37

## BIBLIOGRAPHY

- [AE60] A. Ekspong, et al., Nucl. Phys. 22, 353 (1961).
- [AG60] L. Agnew, et al., Phys. Rev. 118 (5), 1371 (1960).
- [AG75] M. Alston-Garnjost, et al., Phys. Rev. Lett. 35 (25), 1685 (1975).
- [AH84] A. Hicks, Penn. St. Univ. thesis, unpublished.
- [AI81] H. Aihara, et al., J. Nucl. Phys. A360, 291 (1981).
- [AM82] C. Amsler, et al., CERN-EP/82-93 (1982).
- [BA66] C. Baltay, et al., Phys. Rev. 145 (4), 1103 (1966).
- [BE84] C. Beard, et al., Inst. Phys. Conf. Ser. No. 73; Section 3. VII Eur. Symp. Antiproton Interaction; Durham, 147 (1984).
- [BP68] R. Bryan and R. J. N. Phillips, Nucl. Phys. B5, 201 (1968).
- [BR77] W. Brückner, et al., Phys. Lett. 67B (2), 222 (1977).
- [BS69] R. Bryan and B. Scott, Phys. Rev. 177, 1435 (1969).
- [BU57] J. Button, et al., Phys. Rev. 108 (6), 1557 (1957).
- [CA74] A. Carroll, et al., Phys. Rev. Lett. 32 (5), 247 (1974).
- [CE84] C. Elinon, Penn. St. Univ. thesis, unpublished.
- [CH76] V. Chaloupka, et al., Phys. Lett. 61B (5), 487 (1976).

- [CO82] J. Côté, et al., Phys. Rev. Lett. 48 (19), 1319 (1982).
- [CL84] B. Clark, et al., Phys. Rev. Lett. 53 (15), 1423 (1984).
- [DC71] D. Cline, et al., Phys. Rev. Lett. 27 (1), 71 (1971).
- [DE71] S. Devons, et al., Phys. Rev. Lett. 27 (23), 1614 (1971).
- [DO84] C. Dover, Nucl. Phys. A416, 313 (1984).
- [DR79a] W. Buck, et al., Ann. Phys. 121 (1-2), 47 (1979).
- [DR79b] C. Dover and J. Richard, Ann. Phys. 121 (1-2), 70 (1979).
- [DR80] C. Dover and J. Richard, Phys. Rev. C21, 1466 (1980).
- [EJ81] E. Jastrzembski, et al., Phys. Rev. D23, 2784 (1981).
- [FT47] E. Fermi and E. Teller, Phys. Rev. 72 (5), 399 (1947).
- [GA84] D. Garreta, et al., Phys. Lett. 135B (4), 266 (1984).
- [GA85] D. Garreta, et al., Phys. Lett. 150B (1-3), 95 (1985).
- [GR83] A. Green and J. Niskanen, Univ. of Helsinki Preprint Series in Theo. Phys. No: HV-TFT-83-54 (1983).

- [HA80a] R. Hamilton, et al., Phys. Rev. Lett. 44 (18), 1179 (1980).
- [HA80b] R. Hamilton, et al., Phys. Rev. Lett. 44 (18), 1182 (1980).
- [JA78] R. Jaffe, Phys. Rev. D17 (5), 1444 (1978).
- [JF71] J. Friedman, J. Comp. Phys. 7, 201 (1971).
- [JK85] J. Kruk, Rice Univ., private communication.
- [KA75] T. Kalogeropoulos, et al., Phys. Rev. Lett. 34, 1047 (1975).
- [KA80] T. Kamae, et al., Phys. Rev. Lett. 44 (22), 1439 (1980).
- [LA44] L. Landau, J. Phys. VIII (4), 201 (1944).
- [LA80] M. Lacombe, et al., Phys. Rev. C21, 861 (1980).
- [LO81] D. Lowenstein, et al., Phys. Rev. D23 (11), 1439 (1981).
- [MA83] M. Maruyama, Prog. Theor. Phys. 69 (3), 937 (1983).
- [MU81] M. Maruyama and T. Ueda, Nucl. Phys. A364, 297 (1981).
- [MU83] M. Maruyama and T. Ueda, Phys. Lett. 124B (1-2), 121 (1983).
- [MU84] M. Maruyama and T. Ueda, Phys. Lett. 149B (6), 436 (1984).
- [NA84a] K. Nakamura, et al., Inst. Phys. Conf. Ser. No. 73; Section 3. VII Eur. Symp. Antiproton Interactions; Durham, 575 (1984).

- [NA84b] K. Nakamura, et al., Phys. Rev. Lett. 52 (9), 731 (1984).
- [NA84c] K. Nakamura, et al., Inst. Phys. Conf. Ser. No. 73; Section 3. VII Eur. Symp. Antiproton Interactions; Durham, 329 (1984).
- [NA84d] K. Nakamura, et al., Phys. Rev. D29 (3), 349 (1984).
- [OC57] O. Chamberlain, et al., Phys. Rev. 108 (6), 1553 (1957).
- [OD84] O. Dalkarov, et al., Phys. Lett. 147B (1-3), 1 (1984).
- [PA60] A. Pais, Ann. Phys. 9, 548 (1960).
- [PA78] P. Pavlopoulos, et al., Phys. Lett. 72B, 415 (1978).
- [RL83] R. Lewis, Penn. St. Univ., private communication.
- [RPP84] Tables of Particle Properties, Rev. Mod. Phys. 56 (2), Part II (1984).
- [SB64] S. Seltzer and M. Berger, Studies in Penetration of Charged Particles in Matter, NAS-NRC publ. 1133, 187 (1964).
- [SC74] B. Schorr, Comp. Phys. Comm. 7, 215 (1974).
- [SE60] E. Segré, Ann. Rev. Nucl. Sci. 8, 127 (1960).
- [SU82] T. Sumiyoshi, et al., Phys. Rev. Lett. 49 (a), 628 (1982).
- [TW84] T. Walcher, Proc. Conf. on Intersections between Part. and Nucl. Phys., Steamboat Springs, 48 (1984).

- [UE79] T. Ueda, Prog. Theor. Phys. 62 (6), 1670 (1979).
- [UE80] T. Ueda, PROG. Theor. Phys. 63 (1), 195 (1980).
- [VA57] P. Vavilov, Soviet Phys. JETP 5 (4), 749 (1957).
- [WA76] M. Wade, et al., Phys. Rev. D14 (5), 1182 (1976).
- [XU85] Y. Xue, Univ. of Houston, Ph.D. Thesis, unpublished.